In Vivo Mechanical Assessment of Human Elbow Kinematics Using a Six Axis Parallel Mechanism Developed in House

A thesis Submitted for the

Degree of Doctor of Philosophy

by

Mohammad F. Alrashidi

School of Engineering and Design

Brunel University

London

June 2011

Abstract

Elbow joint laxity is a problem that normally comes with age; it increases up to critical levels due to rupture or damage to the ligaments of the elbow and affects the stability and capacities of the joint, interfering even with daily activities.

This work investigates the kinematics of the elbow through in-vivo experimental measurement. To this end, a platform based on Stewart Platform mechanism was built and used at the bioengineering labs of Brunel University in West London, the UK, to measure the six degrees of freedom of the joint.

This thesis aims to develop a method to simulate such motion which could be used for elbow implant design and manufacture.

This work contributes to both the basic science of joint movement measurement and to the clinical applications of diagnosing elbow illness. In addition this research presents the preliminary results for a design for elbow implants.

Tracking system developed in house was used to measure the degrees of freedom in healthy elbow motion. A pilot study was performed to assess the joint motion and its repeatability. A group of volunteers with normal elbow movement was used to carry out this study.

A Stewart Platform mechanism based on the tracking system was used in this study as a non-invasive tool to capture elbow joint motion and track the trajectory and pattern of the motion in three-dimensional space.

This thesis aimed to develop a method to simulate the elbow joint motion that could potentially be used for the elbow implants design and there manufacture.

The goal of this study was achieved by *in vivo* measurement of the elbow movement. It was found that the results vary from person to person, but a healthy pattern of motion can be distinguished from an abnormal pattern. To ensure the result, the motion of the right and left hand of each person was compared,

allowing the behaviour of the elbow motion to be judged and the results can help surgeons to analyze the motion of the elbow joint and follow up suspicions of abnormal behaviour in the joint or trace any possible joint laxity.

Furthermore, the errors involved with the mechanism were calculated and appropriate factors were applied to correct them.

As part of this study the manufacturing of medical implants was reviewed and discussed.

List of original publication was used in this study

1. Mohammad Alrashidi, Ibrahim Yildiz, Khaled Alrashdan, Ibrahim Esat, Evaluating elbow joint kinematics with the Stewart Platform Mechanism, Modelling in Medicine and Biology, BIOMED 2009, 8th International Conference on 26-28 May 2009, WIT Transactions on Biomedicine and Health, Vol 13, Page(s):181-189 (***A grant from the Kuwait Foundation for the Advancement of Science (KFAS) was obtained for this research study***).

2. Mohammad Alrashidi, Ibrahim Yildiz, Qureish Vanat, Khaled Alrashdan, Ibrahim Esat, Mahmoud Chizari, Evaluating the Human Joint Laxity Using Stewart Platform Mechanism, The Atlas T3 Annual Meeting Proceedings, Page(s):157-161, May 2010 (***this study was awarded a grant from KFAS***).

3. Mohammad Alrashidi, Ibrahim Yildiz, Qureish Vanat, Khaled Alrashdan, Ibrahim Esat, Mahmoud Chizari, Evaluating the Elbow Joint Laxity Using Stewart Platform Mechanism: An Experimental Study, Journal of Biomechanics, Vol:43 Supplement 1, Page S73, June 2010, doi:10.1016/S0021-9290(10)70166-4

4. Mohammad Alrashidi, Ibrahim Yildiz, Qureish Vanat, Ibrahim Esat, Mahmoud Chizari, Kinematics Analysis of the Elbow Joint; Comparison of the Kinematics of the Left and Right Elbow, World Congress on Engineering 2011 (***this study was awarded a grant from KFAS***).

Copyright

To my Mother and Father

Acknowledgments

I would like first to express my sincerest appreciation to my supervisor, Professor Ibrahim Esat, for his invaluable inspiration, notable contribution, guidance and support throughout the preparation of his research, I deeply appreciate the input which Professor Esat has had in my development as a researcher; working under his supervision was both an honour and pleasure.

Endless thanks are owed to Dr. Mahmoud Chizari for his support and guidance. His wide knowledge and his logical way of thinking have been of great value for me. His understanding, encouraging and personal guidance have provided a good basis for the present thesis.

My endless thanks are expressed also to Dr. Ibrahim Yildiz for his support and guidance during this study.

I would like to express my deepest thanks to my parents, my family, my brothers and my sisters for their unlimited support and encouragement.

My special thanks go to my friends, Nawaf Alhaifi, Khaled Alrashdan and Khaled Alhaifi for their support, valuable discussions and friendship.

I appreciate and acknowledgment the financial support for this PhD study from the Public Authority for Applied Education and Training (PAAET) in the State of Kuwait.

Chapter 1. Introduction and Motivation 1
1.1 Motivation 1
1.2 Significance of the research 3
1.2.1 Basic science significance 3
1.2.2 Clinical significance 4
1.2.3 Specific contributions of this work 4
1.3 Thesis outline 6
Chapter 2. Background 8
2.1 Introduction 8
2.2 Elbow anatomy background 9
2.2.1 Bones 10
2.2.2 Articulation 11
2.2.3 Joint capsule 12
2.2.4 Ligaments 13
2.2.5 Muscles 15
2.3 Elbow joint movement (degree of freedoms) 16
2.3.1 Flexion/Extension 16
2.3.2 Supination/Pronation 17
2.3.3 Valgus –Varus movement 18
2.4 Elbow joint kinematics 19
2.4.1 Bone kinematics 20
2.4.2 Ligaments and tendons 22
2.4.3 Main muscles of elbow joint 23
Chapter 3. Literature review 25
3.1 Introduction 25
3.2 Previous works in joint modelling 25
3.3 Elbow joint measurement - methods and devices 34
3.3.1 Motion Analysis Camera 35
3.3.2 Goniometry and Electrogoniometry 41
3.3.3 Roentgen Stereophotogrammetric Analysis 48
3.3.4 Electromagnetic Tracking System 50
3.3.5 Dynamography 51
3.3.6 Accelerometers 52
3.3.7 Modelling and simulation 52
3.4 Elbow joint injury and cure 56
3.4.1 Radial head fractures 56
3.4.2 Radial head prostheses 58
3.5 Chapter Summary 60
Chapter 4. The manufacturing process of medical implants 61
4.1 Introduction 61

4.2 Layered Manufacturing: 65
4.3 Medical Application of Rapid Prototyping (MARP) 69
4.4 Musculoskeletal Joint Modeller (MJM): 72
4.5 Laser Engineered Net Shaping (LENS) 77
4.6 The Implementation of the Stewart Mechanism to develop implants....79
Chapter 5. Design, Analysis and Simulation of Stewart Platform Mechanism.80
5.1 Introduction....80
5.2 Stewart Platform Mechanism....82
5.3 Designing a platform based on Stewart mechanism 86
5.3.1 Principles 86
5.3.2 Assembly 87
5.3.3 Wire fixation....88
5.3.4 String pot position on the base platform 89
5.3.5 Arm fixation....90
5.3.6 Initial position of the platform 91
5.3.7 Measuring device 92
5.3.8 Monitoring and recording hardware and software....94
5.4 Assessing the centre of rotation and its radius....97
5.5 Quantifying the platform 101
5.5.1 Evaluating degrees of freedom of the platform 101
5.5.2 Newton- Rephson Method....106
5.5.3 A second way to find the centre of rotation....107
5.6 Calibration of the device 109
5.7 Simmechanics Model of the Stewart Platform Mechanism 112
5.7.1 Principles 113
Chapter 6. Experimental Results and Discussion 120
6.1 Introduction....120
6.2 Measuring the Angles of Flexion-Extension and Valgus-Varus 121
6.3 Centre of Rotation (C.O. R) via angle of flexion....122
6.4 Centre of Rotation (COR) via Valgus-varus movement 124
6.5 Angle of Varus-Valgus and joint laxity 125
6.6 Centre of rotation & Stewart Platform position in 3D 126
6.7 Normal averaging....128
6.8 Comparing average results for 3 different cases....130
6.9 Comparing average results for left and right hand....132
6.10 Screw Displacement Axis (SDA) 134
6.11 Error analysis 135
6.11.1 Manufacturing errors....137
6.11.2 Uncertainty on the measuring sensors....138
6.11.3 Errors due wire length uncertainties 140

6.11.4 Errors related to the force exerted by the device 141
6.11.5 Noise and Data Acquisition errors 141
6.11.6 Calculation errors 141
6.11.7 Errors related to the fixing of the hand (skin movement) 145
6.11.8 Minimizing the experimental errors 150
6.12 Summary 153
Chapter 7. CONCLUSION AND SUGGESTIONS FOR FUTURE WORK .156
7.1 Conclusion and final remarks 156
7.2 Experimental issues 157
7.3 Future work: some recommendations 160
References 162
Appendixes 171
Appendix A 171
Appendix B 174
Data logger – Data Acquisition 174
Appendix C 180
Potentiometer 180
Appendix D 182
MATLAB Program 182
Appendix E 185
Matlab program to find the Centre of Rotation (C.o.R) 185
Appendix F 188

Figure 2-1: Bones and Articulation of an elbow joint.....10

Figure 2-2: Humerus, Ulna and Radius of the right hand 11

Figure 2-3: joint capsule of the elbow.....13

Figure 2-4: Annular ligament.....14

Figure 2-5: Radial collateral ligament.....14

Figure 2-6: Ulnar collateral ligament 15

Figure 2-7: Muscles of the hand 15

Figure 2-8 : Elbow joint movements - Flexion/Extension- schematic.....16

Figure 2-9: Elbow joint movements - Flexion/Extension- limits 17

Figure 2-10 : Elbow joint movements – supination/pronation 18

Figure 2-11 : In a varus alignment, the distal segment deviates medially with respect to the proximal segment (left). In a valgus alignment, the distal segment deviates laterally with respect to the proximal segment (right). (Source of pictures: http://moon.ouhsc.edu/dthompso/namics/valgus.htm. 19

Figure 3-1: set of five pictures on a human subject (picture 1 with 0 weights and picture 5 with maximum weight load) 33

Figure 3-2 medial and lateral epicondyles www.revolutionhealth.com.....37

Figure 3-3: Markers on the arm (lateral epicondyle, styloid process and medial epicondyle which are used to study forearm movement). 38

Figure 3-4: working out θ: The angle to be measure is the difference of these two angles, called θ (theta). 39

Figure 3-5: Example of experimental setup using a motion analysis system.....41

Figure 3-6: Device with two potentiometers 42

Figure 3-7: New device with strain gauges and straps 43

Figure 3-8: Instrumented shoulder arthrometer (Sauers et al.,2001) 45

Figure 3-9: Force-displacement curve plotted using the instrumented shoulder arthrometer (Sauers et al., 2001) 46

Figure 3-10: KT-1000 (Hatzel et al).....47

Figure 3-11: Screw-threaded shaft 48

Figure 3-12: Experimental setup 49

Figure 3-13: Experiment setup for passive elbow motion using a roller configuration. 51

Figure 3-14: Elbow simulator (Magnusen et al., 2004).....54

Figure 3-15: Custom elbow valgus laxity–testing device. It allows for 3 degrees of freedom: flexion/extension, supination/pronation and valgus/varus movement (Mihata et al., 2008) 55

Figure 4-1: LM Applications (Wohlers, 2007; Khan et al., 2007).....65

Figure 4-2: LM and CAD methodology adapted to manufacture process (taken from Khan et al., 2007).....67

Figure 4-3: LM and CAD methodology for implant design in mandibular bone based on bioceramics and new fixation (Khan et al., 2007). 68

Figure 4-4: CT-scan [http://www.ewings-sarcoma.org.uk/?page_id=212].....70

Figure 4-5: MRI [http://body-mri.com/2011/07/20/mri-scan-knee-records] 70

Figure 4-6: Standard implants (Hosni et al., 2000) 71

Figure 4-7: Customized implants (Hosni et al., 2000) 71

Figure 4-8: Snapshot from MJM software (Ozada et al., 2007) 75

Figure 4-9: Change in the centre of rotations versus forearm flexion (Ozada et al., 2007).....76

Figure 5-1: General Stewart Platform 82

Figure 5-2: Schematic of the original "Stewart Platform" by Stewart (Proc. IMechE, 1965-66).) 83

Figure 5-3: The first octahedral hexapod or the original Gough platform at birth in 1954 (Proc. IMechE, 1965-66) and shortly before retirement in 2000 (courtesy of Mike Beeson, Dunlop Tyres). 84

Figure 5-4: The first flight simulator based on an octahedral hexapod in the mid-1960s (courtesy of Klaus Cappel) 85

Figure 5-5: wires to connect platform to the base.....86

Figure 5-6: Stewart Platform Based Elbow Joint Measurement Device.....87

Figure 5-7: Platform principle 87

Figure 5-8: Schematic image of the complete assembled Stewart Platform 88

Figure 5-9: Correct arrangement of wire fixation to ensure easy manipulation for taking measurements (picture A bad fixation, Picture B and C are the correct fixation) 89

Figure 5-10: Position of the attachments.....90

Figure 5-11: String pot positioning on the platform 90

Figure 5-12: The design and the manufactured part of the arm fixations 91

Figure 5-13: Platform initialization.....91

Figure 5-14: Celesco string Pot (SPI).....92

Figure 5-15: Output signal.....93

Figure 5-16: The "Pico" data logger (adc-11) 94

Figure 5-17: Block diagram in Lab-View software (only for four out of six wires are shown in the diagram).....95

Figure 5-18: Lab-View Visualization.....96

Figure 5-19: Measurement steps of the Stewart Platform 97

Figure 5-20: Side view of the experimental setup (left) and displacement of the centre of rotation during valgus and varus motion on the YX plane (right) 98

Figure 5-21: Coordinate system.....102

Figure 5-22: Link length.....104

Figure 5-23: Newton method.....106

Figure 5-24: Centre of rotation 108

Figure 5-25: Calibration setup 110

Figure 5-26: Calibration Graphs 111

Figure 5-27: Simmechanics model of a sample pendulum system.....113

Figure 5-28: Sim-mechanics model of the Stewart Platform mechanism.....115

Figure 5-29: Inside of the "Leg" Block.....116

Figure 5-30: Simmechanics model of SPM.....117

Figure 5-31: Inside the Arm Block 118

Figure 5-32: Views from Simulation.....119

Figure 6-1: Flexion and Extension angles 121

Figure 6-2: Valgus and Varus angles 122

Figure 6-3: Centre of rotation (X, Y, Z) versus angle of flexion for both right and left arms. 123

Figure 6-4: Motions of SPM and Centre of Rotation during the Vargus and Valgus motions 124

Figure 6-5: Joint Laxity and Valgus-Varus 125

Figure 6-6: 5 samples of the centre of rotation for a case without averaging 126

Figure 6-7: Coordinate of the SP platform Position for 5 different samples of one case 127

Figure 6-8: Normal averaging for 5 samples of one left hand case (COR).....129

Figure 6-9: Normal averaging for 5 samples of one left hand case (SP) 129

Figure 6-10: Average data of COR for 3 different cases – left hand 130

Figure 6-11: Average data of SP for 3 different cases – left hand.....131

Figure 6-12: Average data of COR and SP for 3 different cases – Left hand 132

Figure 6-13: Average data of COR for 3 different cases - left and right hand 133

Figure 6-14: Average data of SP for 3 different cases left and right hand.....133

Figure 6-15: Average data-left and right hand- COR - SP- 3 cases.....134

Figure 6-16: Screw Displacement for case 1 -left hand 135

Figure 6-17: Schematic Calculation of the maximum error 140

Figure 6-18: Link Length.....142

Figure 6-19: The effect of the translational movement of the mobile platform from 1 to 10 mm along x direction to the leg's length. 146

Figure 6-20: The effect of the translational movement of the mobile platform from 1 to 10 mm along y direction to the leg's length. 147

Figure 6-21: The effect of the translational movement of the mobile platform from 1 to 10 mm along z direction to the leg's length 147

Figure 6-22: The effect of the rotational movement of the mobile platform from 0 to 60 degrees about the x axis to the leg's length. 148

Figure 6-23: effect of rotational movement of mobile platform from 0 to 60 degree about y axis to the leg's length. 148

Figure 6-24: effect of the rotational movement of the mobile platform from 0 to 60 degrees about the z axis to the leg's length. 149

Figure 6-25: Data related to the X axis - five data sets and their average, including standard deviation 151

Figure 6-26: Five data sets related to the X axis, but the average and standard deviation are excluded from data set one. 152

Figure 6-27: Five data sets related to the X axis, but the average and standard deviation are excluded from data sets one and two.....152

Figure 6-28: Five data sets for the axis and their average results, including standard deviation. 153

Figure 6-29: Five data sets for the Z axis but data set number five has been excluded from the average result and its standard deviation. 154

Nomenclature

Acromion. the outer extremity of the shoulder blade forming the bony part at the top of the shoulder.

Anconeus. Small muscle on the posterior aspect of the elbow joint.

Anterior. Towards the front, especially the front of the body

Articular. Relating to a joint

Capitulum. Less than half a sphere, it includes the anterior and inferior surfaces of the condyle seen laterally, but not its posterior surface.

Condyle. A smooth rounded projection of bone which forms part of a joint. (Waugh and Grant (2001))

Coronoid process. A projection from the front of the ulna.

Distal. Situated away from the centre of the body or some other area or from the point of attachment. The opposite of "proximal"

Epicondyle. Extension on the condyle of a long bone, the Humerus in particular.

Fossa. A triangular depression above the back part of the trochlea of the humerus in which the summit of the olecranon is received.

Glenohumeral. Relating to the shoulder joint.

Humerus/Humeral. (Relating to) A long bone in the arm which runs from the shoulder to the elbow.

Laxity. Lack of stability of a joint or joint prosthesis

Ligament. Fibrous tissue which connects bones to other bones.

Olecranon. A large, thick, curved eminence, situated at the upper and back part of the ulna.

Osteo- Relating to the bones.

Posterior. Further back in position, the back of the body in particular.

Potentiometer. An instrument for measuring or adjusting an electromotive force by balancing it against a known potential difference

Pronate. (with reference to putting or holding a hand, foot, or limb) With the palm or sole turned downwards.

Prosthesis. Artificial substitute for a missing part of the body, usually an arm or leg.

Proximal. Situated nearer to the centre of the body or an area or the point of attachment, the opposite of "distal".

Radius/Radial. (relating to) A bone of the forearm or the forelimb, in humans the thicker and shorter of two.

Sagittal. Relating to or denoting the suture on top of the skull which runs between the parietal bones in a front to back direction **or** of or in a plane parallel to this suture, especially that dividing the body into left and right halves

Scapula. Shoulder blade

Supinate. (with reference to putting or holding a hand, foot, or limb) With the palm or sole turned upwards.

Synovial joints. Joints covered by articular cartilage and with very low friction. Sliding contact is facilitated by *synovial fluid* (synovia), like a lubricant in some respects but also concerned in the maintenance of living cells in the articular

cartilages. They are also called 'freely movable joints' (Waugh and Grant (2001)) as they have characteristic features which allow a wide range of movements.

Trochlea. Like part of a pulley, occupying the anterior, inferior and posterior surfaces of the humeral condyle medially.

Ulna/Ulnar. (relating to) A long bone, placed at the medial side of the forearm, parallel with the radius

Olecranon. The posteriorly situated proximal extension of the shaft of the ulna

X .Translational displacement of SP through axis X

Y. Translational displacement of SP through axis Y

γ .Translational displacement of SP through axis Z

β .Rotational displacement of SP along axis Y

α Rotational displacement of SP along axis Z

r_n Radius of rotation

X_C. Centre of rotation in axis X

Y_C Centre of rotation in axis Y

Z_C Centre of rotation in axis Z

l_i length of the wire

Chapter 1. Introduction and Motivation

The overarching topics of this thesis are presented in Chapter 1 to set the stimulus of the work into perspective. The motives and aims of the study are introduced, and then the synopsis of the study is reviewed chapter by chapter.

The objective of this work is to facilitate and improve elbow motion measurements in *in vivo* conditions. To this end, a Stewart Platform mechanism was built at Oman University. This thesis presents three distinct topics necessary to study the functions of the elbow. The first is to summarize the elbow's anatomy and movements to find the domain of displacement and the accuracy needed to measure elbow laxity. The second is to show how the Stewart Platform mechanism based on a tracking motion is used to track small movements within a motion analysis system. Third, as a first application, the Stewart Platform, together with related software is used to compute elbow kinematics from the data collected as the elbow moves along the platform.

1.1 Motivation

The overall goal of the studies presented here was to improve and validate a Stewart Platform mechanism (Arshoy et al., 2009) and demonstrate its application to clinical research. The elbow is critical to the activities of daily living, in particular to feeding and grooming. Without proper elbow function, the hand cannot be positioned properly to interact with objects, including telephones, computers and more basic objects such as shoelaces and shirt buttons. A myriad of conditions, such as stroke or spinal cord injury, can cause an individual to lose

control of a limb, creating a serious long-term disability. Through a better understanding of the neuromuscular control required to manipulate the elbow, the long-term applications of these studies can help to understand the problems with the natural control of limbs in those who suffer from disease, injury, or other impairments. Specifically, because injuries to the elbow are common (Bain, 1999) these studies can contribute to the restoration of necessary elbow function via clearing and comparing the injured elbow functions with those of a healthy one.

Cumulative trauma disorders, including cubital tunnel syndrome, account for 56% of all occupational injuries in the United States (Melhorn, 1998). These disorders frequently compromise an individual's upper extremity control. The results of this work have the potential to advance the understanding of joint modelling and control in general through the specific study of elbow movement. Additionally, evaluations of radial head replacements become more meaningful when performed in conjunction with a physiologic elbow measurement – using this platform in a way which accurately represents the *in vivo* case, the function of the implant could be compared to a normal one.

A general approach to the study of elbow joint control is necessary to measure a particular joint which accurately recreates human motion and force capacities. This is particularly advantageous in diagnosing elbow illness in the early stages so as to reduce the likelihood of severe cases later.

The proposed elbow measurement platform offered opportunities for improvement in clinical areas. The success of this platform and of future clinical studies relies on the successful coordination and implementation of the measuring

system, including all relevant hardware, with a sufficiently accurate means of measuring the motion of the elbow. Thus the first aim of this work was to validate a theoretical aspect of the design of the platform. To this end, a theoretical study was made to show the capacity of the Stewart mechanism to measure the elbow joint's six degrees of freedom. The second goal of this work was to quantify the suitability of a motion analysis system (with the Celesco SP1 String Pot) to track the extremely fine motions of the elbow. The third aim, applicable to the clinical use of the simulator, was to develop, implement and validate software capable of computing and following the position of the forearm during pronation/supination, Valgus/Varus and Flexion/Extension movements.

1.2 Significance of the research

This work contributes to both the basic science of designing ways of measuring joint movement and to the clinical applications of diagnosing disorders of the elbow.

1.2.1 Basic science significance

The literature available still lacks an accurate and handy method of measuring elbow laxity. The design, assembly and refinement of the hardware (the Stewart Platform mechanism) represent a significant accomplishment, ensuring the long-term potential to improve medical implant design. The design and implementation of the scheme used to measure the movement of arms represents the first elbow joint measurement to operate using the Stewart mechanism concept. Techniques have been developed to accurately track the motion of the forearm as a standard

motion analysis procedure. In addition, this work contributes to the fundamental understanding of elbow joint laxity.

1.2.2 Clinical significance

The measurement of elbow moment arms *in vivo* from different angles is a new contribution to the biomechanical knowledge base and will improve the clinical understanding of elbow function. The results of this work can benefit a wide range of applications, including prosthetic limb design, the development of new rehabilitation strategies for those with compromised elbow function and the immediate benefit of clinically-oriented studies of medical implants. These applications can improve the health of individuals with compromised elbow function.

1.2.3 Specific contributions of this work

This work makes several contributions to the basic science and clinical literature. The design of the Stewart Platform mechanism advances the study of joints in general and the elbow in particular. However, concern exists between the engineering measurement of laxity and its clinical evaluation in an elbow joint. That is because the divergence could be the inequality among medical protocols and engineering aims. For instance, the effect of acquired knowledge on treatment protocol may be the interest of surgeons, but the engineer may concentrate on the method of measurement and evaluating mechanical parameters of the joints (Kupper et al., 2007).

The objectives of this research are to measure with this sophisticated proposed tracking mechanism the degrees of freedom of the joint, the kinematics movements of elbow joint and its possible laxity. This device will use Stewart-type parallel mechanism concepts.

With this system it is possible to measure the position of the centre of rotation during flexion. The device is thus better than the existing model, with additional capacities. Some problems were, however, associated with it such as inaccuracy, invasiveness or in most cases non-practicability for live human subjects, since most methods have been designed for cadaveric studies.

The study focused on flexion, extension, valgus and varus motions and all the experimental data were taken from an experimental setup. The centre of rotation and motion of the angles of the forearm were found by the kinematics of the Stewart Platform Mechanism with a matlab-simmechanics based program algorithm. The motions of the joint were measured and the results of these measurements were validated by experimental measurements. Comparisons of the results demonstrate that the Stewart Platform based measurement device sufficiently measures all motions of the elbow with six degrees of freedom, together with its centre of rotation

In this study, a platform based on the Stewart mechanism was developed for measuring the elbow kinematics. The Stewart Platform includes a fixed table and a moving plate connected to the table using six wires, the lengths of which can be changed. Since there are six legs, the Stewart Platform can be used to position the platform for six degrees of freedom (discussed in chapter 5). In other words, with this

mechanism any position of the platform can be inferred by measuring the length of the legs. The legs consist of wires between the base and the platform (see Chapter 5)

1.3 Thesis outline

The research to achieve the stated objective is reported in six chapters, followed by appendices containing supporting information and results. Following the present chapter, which presents a general overview of the research, motivation and significance, are six chapters which are briefly outlined below.

Chapter Two: Background.

Reviews the background of the biomechanics of the human elbow and the way in which it moves. This chapter covers the kinematics of the elbow joint and functional motion of the elbow.

Chapter Three: Literature Review.

Contains a comprehensive review of the literature as the foundation of the research. It covers various methods which have been used so far to measure elbow movements generally and elbow laxity in particular. In addition it covers elbow joint injuries and remedies for them.

Chapter Four: Manufacturing process

Describes how the study of kinematic and kinetics of parts of the body may help to manufacture an implant which could mimic as far as possible the function of the original joint in the body. We show how the increasing use of medical implants in the recent years has encouraged manufacturers all over the world to invent and develop new methods in answer to the high demand for medical

implants, reduce their cost and improve their accuracy as applied to human requirements.

Chapter Five: Stewart Platform design.

Illustrates and describes in detail the basis of measurement of the Stewart mechanism used in this research. In addition, it covers the different parts of the hardware and software of the mechanism. The calibration of the device is also explained in full.

Chapter Six: Result and Error Analysis.

Shows the application and capacity of the new Stewart Platform to make possible some experiments in different cases. The device tested a number of volunteers and successfully measured a full range of motion at the elbow, giving data on the centre of rotation.

The chapter also describes the process of data averaging to reduce random errors. Moreover, there is a full discussion about the sources of error and how to minimize them.

Chapter Seven: Findings and Discussion.

The chapter will close the work by reviewing the carried out study. It then highlights the suggestions and conclusions over the reviewed work. Finally, future researches which may take place are discussed.

Chapter 2. Background

2.1 Introduction

Joint laxity in elbows is a problem which normally comes with age, and can increase up to a critical level if the ligaments of the elbow are ruptured or damaged; it affects the stability and capacities of the joint, interfering even with daily activities.

Joint laxity is defined as excessive joint movement in the presence of external force applied to the joint. The laxity depends on the bony surface, soft tissues such as capsules, ligaments and other supporting structures, such as menisci. In biomechanical research much effort has been made to measure human joint laxity by the development of various techniques, most of which have been used to measure knee and shoulder laxity. Although relatively little effort has gone into measuring elbow laxity, there is a substantial body of work on elbow mobility measurement techniques. In addition, only a few works have been reported on non-invasive devices to measure elbow joint laxity. Moreover, the flexion-extension and varus-valgus movements which are both made possible principally by articulation of the humerus and ulna are important if one is designing a prosthesis which mimics healthy elbow movements.

2.2 Elbow anatomy background

The human elbow is the most important joint to perform the daily activities. It plays a key role in hand positioning and also load transfer. With an elbow injury, daily activities can be severely limited.

Research shows the elbow prostheses is like a simple hinge, while the motion of a healthy elbow is more complex than a simple fixed axis joint. Its multiple contact points and cam action make its kinematics difficult to understand. As the observed joint kinematics are inherently coupled with those of the shoulder, it is not easy to model or experiment in *in vivo* conditions. Such limitations of restricted movements can be experienced by patients for whom an artificial joint replaces their natural elbow. In order to design a prosthesis which mimics the natural elbow joint, researchers should learn the exact kinematics measurements of the elbow which allow six degrees of freedom.

A joint or articulation is a combination of two or more bones. It is a contact point between bones or between cartilage and bone. Arthrology is a term for the scientific study of joints; its terms of reference include the connective tissues which relate to joints. The two functions of joints are to:

- permit motion
- provide stability

These functions of mobility and stability tend to be competing requirements which differ according to the structure of each joint and necessarily involve compromise.

The strength and flexibility of a joint is determined by it structure. The closer the joints fit at the contact point, the stronger the joint is. However, a tight-fitting joint can restrict movement.

The movement of the joints is determined by:

- the shape of the articulation bones
- the flexibility of the ligaments which bind the bones together
- the tension of the related muscles and tendons

The structure of the elbow joint includes three bones which are attached by numerous ligaments and tendons and are actuated by several muscles which cross the joint. These structures act in concert to control the position of the forearm and also to transfer loads from the hand and forearm to the upper arm.

2.2.1 Bones

The elbow consists of three bones, as shown in figure 2-1: the humerus, radius and ulna. To define them:

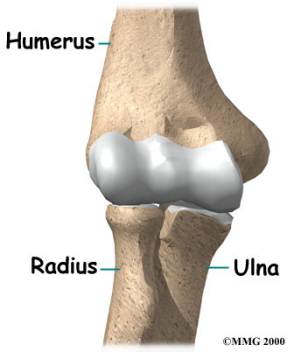

Figure 2-1: Bones and Articulation of an elbow joint
(source: http://www.wephysio.co.uk/article.php?aid=248)

Humerus: a long asymmetrical bone which makes up the skeleton of the arm. It articulates with the shoulder blade at the proximal part and with the radius and ulna at the distal part.

Ulna: the larger bone of the forearm. It is made up of a long main part and two extremities. The proximal one is bulky and is part of the elbow joint. The distal extremity is part of the wrist joint.

Radius: The smaller bone of the forearm. This bone goes from the inside of the elbow to the thumb base of the wrist.

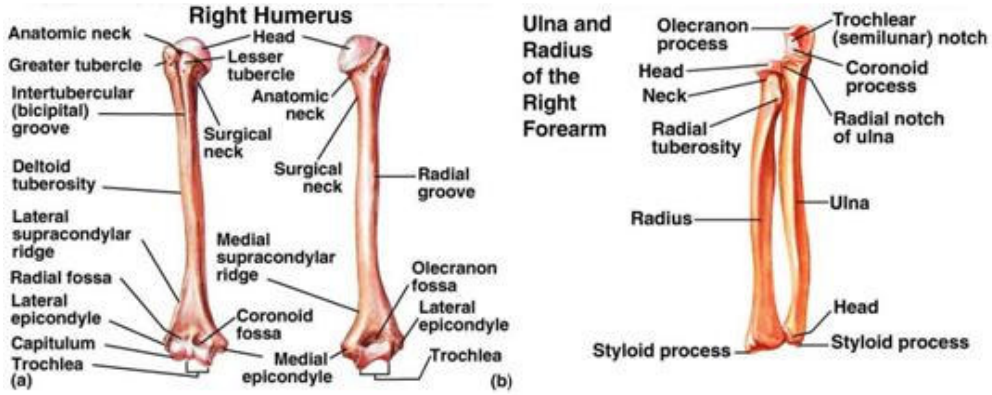

Figure 2-2: Humerus, Ulna and Radius of the right hand
(source: http://www.sweethaven.com/sweethaven/MedTech/Anatomy)

2.2.2 Articulation

The elbow is the joint which unites the arm to the forearm. It consists of three articulations:

Humerus-ulna articulation: This is essentially a hinge joint, that is to say, it enables the flexion and extension of the elbow to take place. It links the distal part of the humerus with the proximal part of the ulna.

Humerus-radius articulation: It links the distal part of the humerus with the proximal part of the radius.

Radius-ulna articulation: It links the two proximal parts of the ulna and the radius. It enables the movements of supination and pronation. These are further discussed in the section on elbow movements.

2.2.3 Joint capsule

There is only one capsule enclosing the three articulations. This capsule is inserted around the articulations and is mixed with annular ligament.

The joint capsule is fundamental to the role of the synovial joints. The capsule seals the joint space, supplies inactive stability by restricting motion and provides active stability via its proprioceptive nerve endings; which could possibly form articular surfaces for the elbow joint. The capsule is a dense fibrous tissue which is attached to the bones and creates an insulating cover around the joint. It differs in size based on the stresses which act upon it. The capsule may be torn, causing laxity, or damage surrounding tissues.

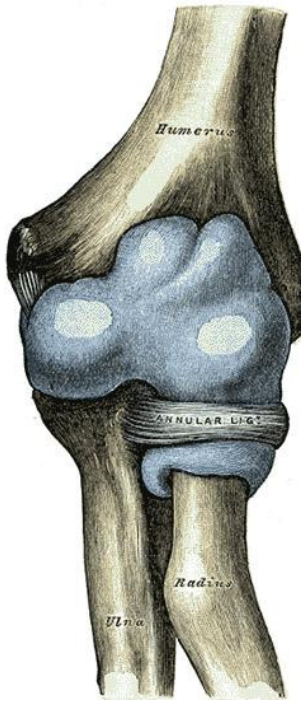

Figure 2-3: joint capsule of the elbow
(source: http://www.theodora.com/anatomy/elbow_joint.html)

2.2.4 Ligaments

A ligament is generally defined as a bundle of strong, flexible, dense fibrous connective tissue constructed with collagenous fibres. Ligaments attach onto bones, and link them together to establish a joint. Unlike tendons, they do not link up muscles to bones. Some ligaments restrict the movement of articulations. They enable stability of the joint to be maintained and they keep the functional surfaces of the different bones in opposition.

The annular ligament: this stabilizes radius-ulnar articulation. It is attached to the front and back of the ulna. It is a U-shaped ligament and which encircle the head of the radius to keep the radius in contact with ulna.

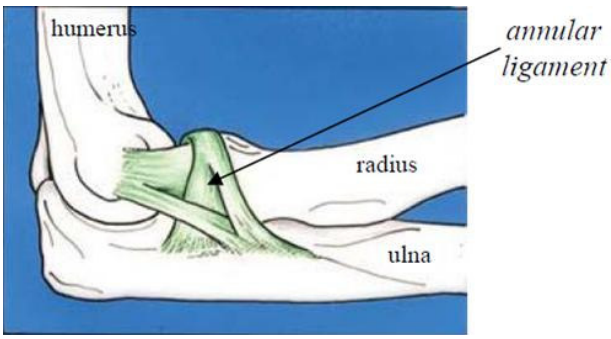

Figure 2-4: Annular ligament (source : http://www.maitrise-orthop.com/corpusmaitri/orthopaedic/mo77_dumontier/index_us.shtml)

The radial collateral ligament: this is made of three parts. From the lateral epicondyle of the humerus to the annular ligament have two parts of them. Third one goes from the epicondyle to the lateral olecranon of the ulna. It allows flexion and extension movements but prevents any lateral movement of the elbow.

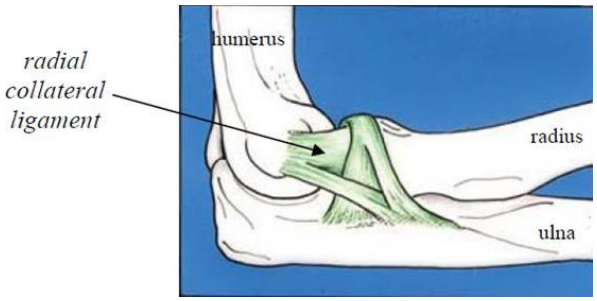

Figure 2-5: Radial collateral ligament (source : http://www.maitrise-orthop.com/corpusmaitri/orthopaedic/mo77_dumontier/index_us.shtml)

The ulnar collateral ligament: this is linked to on the humerus bone (on the medial epicondyle) and to the medial coronoid process and olecranon on the ulna. Like radial collateral ligament, it allows flexion and extension movements but prevents any lateral movement of the elbow.

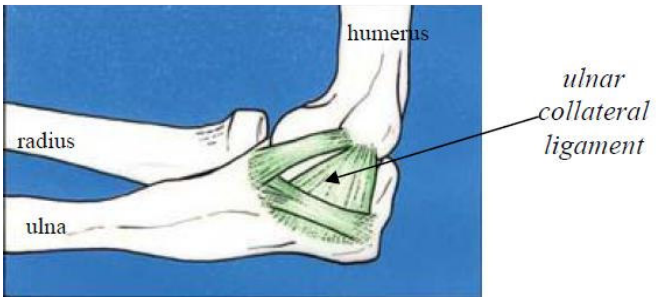

Figure 2-6: Ulnar collateral ligament (source : http://www.maitrise-orthop.com/corpusmaitri/orthopaedic/mo77_dumontier/index_us.shtml)

2.2.5 Muscles

The main muscles of the elbow joint are the biceps brachia, of which the most important functions are simply to flex the elbow and to rotate the forearm; the triceps brachia, which extends to the ulna through the triceps tendon; and the main muscle of the forearm, the brachioradialis, is a muscle which performs flexing on the forearm, at the elbow joint. Depending on the position of the forearm, it can also peroform both pronation and supination,.

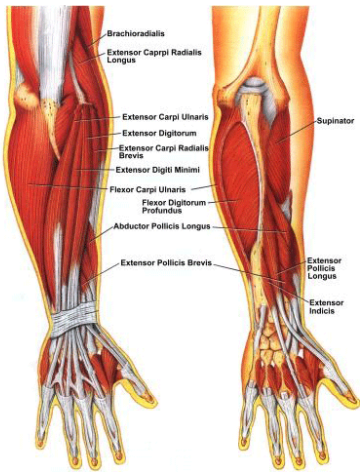

Figure 2-7: Muscles of the hand (source: http://www.illpumpyouup.com/articles/forearm-training.htm)

2.3 Elbow joint movement (degree of freedoms)

The elbow joint has two main functions: flexion/extension and supination/Pronation. In reality, there is another movement: the valgus-varus which is a very small movement.

2.3.1 Flexion/Extension

This is the movement which consists in bending and straightening the arm.

Flexion: In extreme flexion, the radial head and coronoid process are in contact with the corresponding fossa of the humerus; and the angle between the arm and the forearm is approximately 30°.

Extension: In extreme extension, the olecranon process is in contact with the corresponding fossa of the humerus; and the angle between the arm and the forearm is approximately 180°.

The axis of the trochlea is oriented obliquely. This is why the axis of the humerus and the ulna are not permanently parallel.

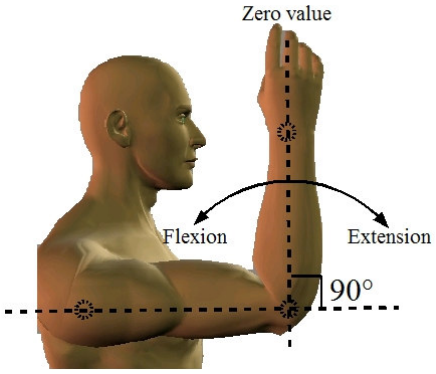

Figure 2-8 : Elbow joint movements - Flexion/Extension
(source: http://www.dh.aist.go.jp/bodyDB/a/Xu-99-01e.html)

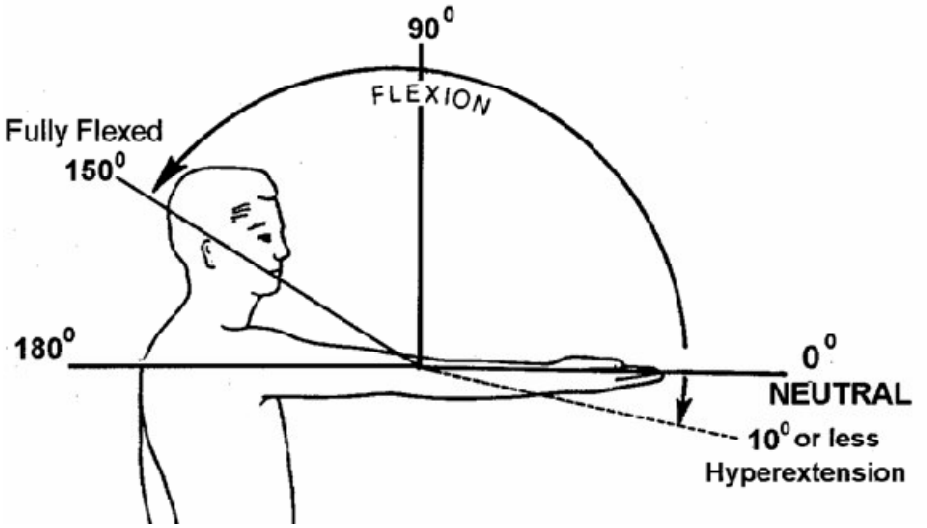

Figure 2-9: Elbow joint movements - Flexion/Extension- limits
(source: American Academy of Orthopaedic Surgeons)

2.3.2 Supination/Pronation

This movement consists of rotating the forearm around its axis (Torsion).

Supination is the movement which makes the forearm rotate to the exterior, that is to say, with the thumb at the exterior. The maximal angle of supination is about 85°.

Pronation is the movement which makes the forearm rotate to the interior, that is to say, with the thumb at the interior. The maximal angle of pronation is about 80°.

During pronation-supination the axis of rotation is around the distal radioulnar joint and the forearm is rotating similarly to a revolute joint (Hollister et al., 1994). An image of a pronated and supinated arm is shown below in Figure 2-10.

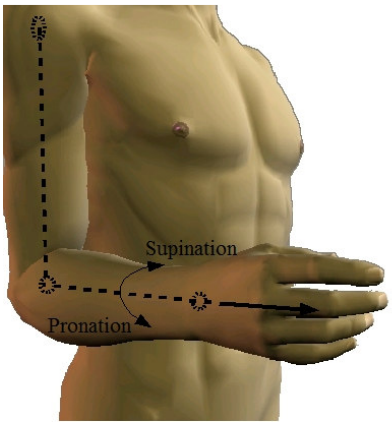

Figure 2-10 : Elbow joint movements – supination/pronation
(source: http://www.dh.aist.go.jp/bodyDB/a/Xu-99-01e.html)

2.3.3 Valgus –Varus movement

So far, two movements in the elbow joint have been outlined: flexion/extension and pronation/supination. There is also another movement: the valgus-varus. This is a very little movement, less important than the other ones, but it exists. Unfortunately, existing prostheses do not allow this movement.

The adjectives Valgus–varus refer to the pattern among two anatomical sectors. To picture the pattern, a line was drawn to show the axis of the proximal segment. A second line was drawn to illustrate the axis of the distal segment. The two lines then compared, focusing on the distal segment's alignment with respect to the proximal segment.

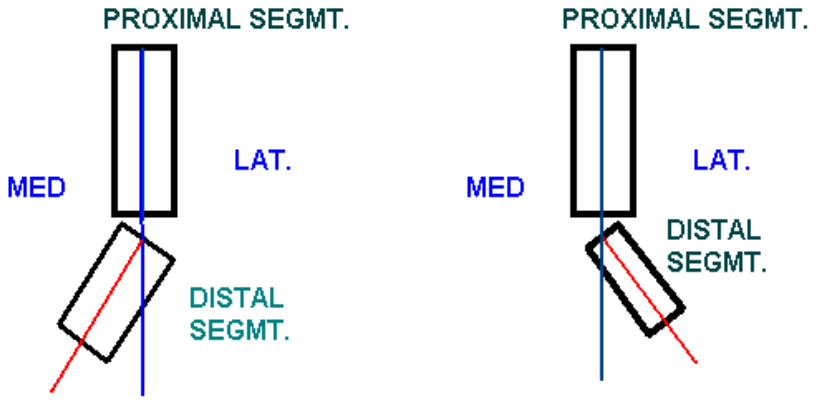

Figure 2-11 : In a Valgus/Varus motion
(Source : http://moon.ouhsc.edu/dthompso/namics/valgus.htm)

Valgus means turned towards the outside. For the elbow, the movement of valgus corresponds to a deviation of the forearm about the axis of the humerus outwards. Conversely, **Varus** means turned towards the inside. For the elbow, the movement of varus corresponds to a deviation of the forearm about the axis of the humerus inwards.

2.4 Elbow joint kinematics

It is vital to identify the exact kinematics of the elbow to be able to construct prostheses which imitate the natural elbow joint. The elbow joint cannot be epitomized by a simple hinge, for it actually allows six degrees of freedom.

2.4.1 Bone kinematics

As mentioned above, the elbow joint is made up of three bones: the ulna (little finger side of the forearm), radius (thumb side of the forearm) and humerus (upper arm bone) (Figure 2-1). Thus there are three bony articulations at the joint: radiohumeral, unlohumeral and radioulnar. Though three articulations comprise the elbow joint, it is widely considered to have only two degrees of kinematic freedom: flexion/extension (f/e) and pronation/supination (p/s), as shown in Figure 2-9 and Figure 2-10 respectively. Full extension is defined as 0° of flexion (i.e. the flexion angle is measured with respect to the vertical and is not the angle included between the forearm and the upper arm). Neutral (0° of pronation or supination) is defined as having the radial styloid directly over the ulnar styloid with the elbow at 90° of flexion.

The elbow is one of the most intricately constructed joints of the human body and, as such, is one of the most stable (Morrey et al. 1981). The entire elbow joint complex is constrained anteriorly by the coronoid process and radial head and posteriorly by the olecranon (Bain, 1999). The entire joint complex is enclosed in a single capsule and stabilized by both medial and lateral ligaments.

Constrained by the shape of the proximal end of the ulna, the flexion/extension axis of the elbow is nearly constant, like a perfect hinge (An and Morrey, 2003). Elbow laxity can create up to 3°-4° of variation in the axis (Duck et al., 2003). The centre of rotation has been found to be in an area 2-3mm in diameter at the centre of the trochlea (An and Morrey, 2003), though others have since found this locus to be larger (Ewald, 1975). Morrey et al.(1981) have suggested that the f/e

axis is internally rotated from 3°-8°. It is also important to note that, when fully extended, the long axis of the ulna is not aligned with the long axis of the humerus. The acute angle between the two is referred to as the *carrying angle*. For the moving elbow, a precise definition of the angle is controversial, despite agreement on the concept. In An and Morrey measurement (2003), the typical elbow range of motion includes 150° of flexion (from 0° to 150°) (see Figures 2-8 and 2-9) and the carrying angle for men is 10° -15°. For women, the carrying angle is about 5° greater.

During p/s movement, the radius rotates in a circular motion around the long axis of the ulna. Translation of the radius at the proximal end is considered insignificant and movement at the distal end is sliding in nature. The distal end of the radius, at the radioulnar joint, rotates around the ulnar styloid, at the proximal end, while the radial head is more constrained. Thus this axis of rotation is generally thought to pass from the centre of the radial head (the proximal end of the radius) through the tip of the ulnar styloid (An and Morrey, 2003). The axis remains constant, regardless of elbow position (Hollister et al.,1994). The axis of forearm rotation has been shown to pass approximately 4 mm from the centre of the capitellum and 8 mm from the ulnar styloid (Hollister et al.,1994, Duck et al.,2001, Veeger et al.1997). Note that this axis is oblique to the long axes of both the radius and the ulna. This motion is critical for wrist and hand positioning. The full range of p/s motion is about 160° (from 75° pronation to 85° supination) (An and Morrey, 2003).

The radial head plays a key role in elbow joint stability and load transfer. The radial head is a stabilizer against valgus load and aids the coronoid in providing an anterior buttress for the humerus (Hotchkiss and Weiland, 1987, Morrey and An, 1983, Morrey et al., 1991, Ring et al., 2002). Captier et al., (2002) describe the biometry of the radial head and find that in most cases 57% of the cross-sectional radial heads were elliptical in shape, which implies adaptation of the radial neck to accommodate the differences in kinematics between the radial heads of circular and elliptical cross-section. This adaptation also affects the load transfer across the joint. Morrey et al., (1991) have shown that up to 90% of body weight can be transferred across the radial head.

2.4.2 Ligaments and tendons

Morrey and An (1983) explained that the elbow's stability is due in part to the congruity of the bony articulations and in part to the soft tissue constraints. For example, at 90° flexion, the bony articulations are mostly responsible for stability. However, in full extension, the anterior capsule is taut and thus plays a role in varus and valgus stability. The collateral ligament complexes and the anterior capsule serve as stabilizers (Morrey et al., 1991). The multi-bundle structure of these complexes has been documented (Beckett et al., 2000). The lateral collateral ligament helps stabilize the lateral ulnohumeral joint (Morrey et al., 1991), specifically by preventing supination of the ulna (Bain, 1999). Sojbjerg et al., (1987) have shown that the annular ligament plays a role in varus and valgus elbow stability, both with and without the radial head in place. The medial collateral ligament is the main valgus stabilizer for the flexed elbow (Morrey et

al., 1991). The posterior band of this ligament prevents pronation of the ulna in conjunction with the bony articulations (Bain, 1999). Coleman et al., (1987) and Morrey et al., (19790 note that the interosseous membrane and triangular fibrocartilage complex contribute to the axial stability of the forearm. In fact, these structures may be responsible for preserving radial head length, even in the absence of a radial head.

2.4.3 Main muscles of elbow joint

The major muscles crossing the elbow joint are the biceps brachii, brachialis, brachioradialis, extensor carpi radialis longus, triceps, flexor carpi radialis and anconeus (Bain, 1999). Other forearm muscles, such as the flexor carpi ulnaris, cross the elbow, but do not notably contribute to elbow motion (Bain, 1999). Muscle forces and force directions have been reported as having muscle tensions and potential excursions (Brand et al.,1981, Gonzalez et al., 1996; Nijhof and Gabriel, 2006; Van Zuylen et al., 1988). Muscle moment arms have also been measured and reported.

The biceps brachii originates on the scapula with two heads and anteriorly covers the brachialis as it continues down the arm. The long head originates on the superior glenoid labrum in nearly 50% of the population, otherwise from the supraglenoid tubercule (Vangsness et al., 1994). It inserts onto the radial tuberosity and thus wraps around the radius during pronation. Mechanically, it acts as an elbow flexor and a strong supinator (Morrey and An, 1985).

The brachialis originates on the anterior distal half of the humerus and inserts onto the ulnar tuberosity. It acts as a flexor. While large in cross-sectional area, its position relative to the elbow joint gives it poor mechanical advantage and thus limits moment-generating capacity. However, since it inserts into the ulna, the insertion site is unaffected by pronation or supination movements (Morrey and An, 1985).

The triceps brachii has three heads at its origin, the outer two, which originate on the posterior side of the humerus and the long head, which initiates from the infraglenoid tubercule of the scapula. The lateral head initiates on the humerus just lateral and superior to the radial groove. The medial head originates on the humerus medial and is inferior to the radial groove. The insertion site is on the posterior surface of the olecranon. Functionally, it is the elbow's main extensor. It is also interesting that, although two of the origin heads are not affected by shoulder position, the long head does cross the glenohumeral joint and can aid in humerus extension and adduction (Morrey and An, 1985).

The pronator teres initiates on the medial epicondyle of the humerus and inserts onto the mid-radius. This geometry gives it function as both a strong pronator and a weak flexor. During extreme supination, it will wrap around the radius (Morrey and An, 1985).

Chapter 3. Literature review

3.1 Introduction

Sauers et al., (2001) state that the translational laxity of the joint is often measured through physical investigation. Clinicians use the information which is derived from this type of testing, including the magnitude and direction of the laxity, to decide whether surgery or rehabilitation is needed. However, not much is known about the degree of laxity of the shoulder and elbow in healthy and unhealthy (injured) subjects.

This assessment is made through tests such as the anterior-posterior drawer, load and shift and sulcus. These tests are individually carried out, and the surgeon has to rely on his/her "belief" to measure the magnitude and orientation of the laxity and diagnose any possible injuries. Obviously, the output data of these tests are not reliable. They have poor reproducibility and diagnostic value. Their poor reproducibility is due to various factors, including experience of the examiner, out-of-range force application and patient positioning. In addition, the observed magnitude may change significantly when muscular tension occurs around the joint.

3.2 Previous works in joint modelling

The kinematics of the elbow joint occupies a considerable place in orthopedic surgery. Morrey et al., (1981) studied the motions of the elbow joint. They measure elbow flexion and forearm rotation by using an electronic goniometer.

Another study was published by Morrey and Chao in 1976, for calculating elbow joint motion with the help of biplanar roentgenograms. In their research, they obtain three-dimensional kinematics of the joint. Tanaka et al., (1998) used electromagnetic motion tracking data and describe the first three-dimensional elbow kinematic.

The rotary flexibility of the elbow joint has been investigated in orthopaedic research. Wagner et al., (1977) sought to develop a method of determining the rotatory flexibility of the elbow joint. They developed a measuring apparatus for determining active and passive rotatory flexibility. Further, Hotchkiss et al., (1987) indicated the quantification of relative contributions to valgus stability of the posterior and anterior portions of the medial collateral ligament (MCL), the radial head and silicon rubber radial head replacement. It was believed that the excision of the radial head was part of the surgical treatment for rheumatoid arthritis, some fractures and other conditions where fractures of the radial head and dislocations of ulnahumeral joint were the cause of elbow instability. The work reported by Morrey et al., (1988) comprises an investigation of the role of the radial head in transmitting loads and maintaining the stability of the elbow joint. They find that the greatest force occurs with the elbow extended, where greater radiohumeral force is transmitted in pronation than in supination at the flexion of the elbow. In 1991 O`Driscoll et al. devised a method to demonstrate the posterolateral rotatory instability of the elbow. It was then emphasized in the study of O`Driscoll and Horii et al., (1992) that the lateral collateral ligament of the ulnar part is a discrete part of the lateral collateral ligament complex (LCLC),

whereas the function of the lateral ulnar collateral ligament (LUCL) is a way of preventing the posterolateral rotatory instability of the elbow, as well as promoting varus stability. Another study was reported by Nestor and O`Driscoll et al., (1992) to explore and diagnose posterolateral rotatory instability; following an application of the test which was presented by O`Driscoll et al., (1991). In this, Nestor and O`Driscoll et al. pointed out that posterolateral rotatory instability in adults is the result of injury to the ulnar part of the radial collateral ligament secondary to varus extension stress without dislocation.

Further, Olsen and Jens et al., (1996) investigated how the elbow joint laxity is prevented by the LCL, when forced varus and external rotatory stress is applied to the forearm. However, because the LCL is always transacted as the last structure and AL lesion included the LUCL fibres distally, the isolated stabilizing effect of the LCL or the annular ligament (AL) may not be assessed. In their study, it is pointed out that the LCL prevents laxity during external rotational stress. This is the first step in the dislocation of the elbow component. The measured magnitude result of the joint laxity by the different ligament dissections was comparable with those measured by Olsen et al., (1996). Hannouche et al. (1999) found it hard to diagnose postero-lateral rotatory instability with the performed test as described by O`Driscoll et al., (1991), where the position of maximal displacement in cases of rotatory instability is performed with elbow extension and flexion movements. Further studies have been made by several authors to investigate elbow sublaxation, dislocation and valgus laxity during the pivot shift test (PST) associated with lesions in the LCLC (O`Driscoll and Horii et al., 1992). while the

lateral ulnar collateral ligament (LUCL) is only a secondary constraint, Olsen et al. (1998) suggest that the LCL is the primary soft tissue constraint to PST stress and the annular ligament (AL). The radial head contributes an important role in the kinematics of the elbow joint. The radial head has a minor effect to valgus stability, while the medial collateral ligament (MCL) is the main valgus stabilizer. This was previously reported in the literature by Hotchkiss et al. (1987) and Morrey et al. (1983). The radial head fracture which is not complicated by medial collateral ligament injury may be treated using excision without altering the kinematics of an intact elbow joint (Morrey et al., 1983). Nevertheless, Jensen et al., (1999) assert that the radial head's influence on the kinematics of the elbow joint must have been known but was not investigated adequately in previous studies. Some studies, moreover, have failed to indicate which approach was used (Hotchkiss et al., 1987; Sojbjerjg et al., 1987) to diagnose a severance of ligaments, which affects the validity of the results (Morrey et al., 1991).

The general view in several papers is that rotation of the forearm may not significantly affect the laxity and stability of the joint (Morrey et al., 1991; Olsen et al., 1996). In fact, little is known about the influence of forearm rotation on the laxity and stability of the elbow joint. In order to determine whether or not forearm rotation influences the varus-valgus laxity of the elbow joint with deficiency of the MCL and the radial head, Pomianowski et al., (2001) developed a device which allowed the forearm to be kept in the desired position of rotation in order to evaluate varus-valgus elbow laxity in different forearm rotations. However, they found that varus-valgus laxity of the elbow is greatest in pronation

and least in supination throughout the range of flexion, regardless of the integrity of the radial head. Only a few studies, such as Olsen et al., (1998) have assessed the ligaments and capsule practically considering pathological external forearm rotation (PEFR); however in only one research (O`Driscoll and Morrey et al (1992)) that has evaluated the joint compression forces given during the experiment. Therefore, to evaluate the joint compression loads *in vivo*, Deutch et al., (2003) anticipated to assess the ligaments as being controlled eventually to posterior elbow dislocation and pathological external forearm rotation (PEFR). They identify that in a strong axial load in line with the forearm, for example the fall of the outstretched arm, or an external torque, in about 30 degrees of elbow flexion may be the best circumstances to start the tearing of ligaments and capsule, causing the joint dislocation. In a previous study, Morrey et al., (1991) showed that the removal of the radial head may not affect valgus laxity in a normal joint, but after the MCL has been divided, excision increases the valgus laxity. Hence, Pominowski et al., (2001) and King et al., (1999) mention that replacing the radial head with a metallic prosthesis greatly change and reduces valgus laxity, and may completely substitute for the valgus constraint provided using relative radial head. Then, in order to examine elbow pain and laxity, MRI and sonography were performed by De Smet et al., (2002) on basketball pitchers. The MRI technique was able to diagnose UCL injury, but could not clarify whether these injuries were partial or complete tears. As an alternative method, the sonography supplied extra information which was not available on MRI. Therefore, De Smet et al., 2002 were able to enumerate the degree of joint laxity,

by measuring the amount of joint enlargement (with sonography) which took place during valgus stressing. It was also noted that the use of stress sonography may be useful for evaluating the importance of medial elbow laxity due to UCL injury. Jensen et al., (2004) was aimed to study the phenomenon such as cut when it takes place on the radial head and effect of LCL division on the elbow laxity. It also was under consideration to know how radial head prosthetic replacement with LCL repair may affect the stability of the joint.

Jensen et al., (2004) explained that when the LCL is disrupted, the radial head changes the rotary and varus laxity. They also suggested that the radial head replacement is not necessary, as the repaired ligament can provide the lost tension when a excision occurred at the radial head. Some experienced researchers have studied the diagnosis of injury to the UCL and the degree of laxity; however there has been insufficient evaluation. In the biomechanical study of Sojberjg et al. (1987), it was confirmed that valgus laxity is most obviously seen at 70 degrees of flexion when the UCL is cut, which evidently proves that the degree of elbow flexion has an effect on valgus laxity. In the above literature, it was not possible to assess the effect of forearm rotation on stability as the position of the forearm was ignored during the test of valgus stability. Furthermore, as an effective study, Safran et al. (2005) proposed with the hypothesis that if the insertion of muscles which cross the elbow joint remained intact, at different degrees of elbow flexion, the valgus laxity may be affected by forearm rotation. The effect of forearm rotation and elbow flexion on valgus laxity was their aim. More recently Safran (2007) has presented a paper about elbow valgus laxity measurement using

radiographic and nonradiographic techniques. He suggests that a nonradiographic (non-invasive) device is more sensitive in detecting valgus elbow laxity than a stress radiograph. It is claimed that this device could increase a clinician's ability to accurately diagnose UCL laxity non-invasively.

Researchers in Oman University (Zolfograniah, 2008) have used a camera and image processing to measure elbow kinematics. In their first round, they tested 18 subjects, both male and female of different ethnic origins and of various ages. Three pictures were taken from each marked (Zolfograniah, 2008) arm: one while the elbow was at rest; one when a load of 1 kg was held in the hand and the subject was asked to try to hold the elbow still in space and let the load pull the forearm downward; and finally one the same as the second with a load of 2 Kg instead of 1 Kg. Therefore, the first readings are comparison results between the first and second pictures and the second readings are the results of comparing the second and third pictures.

In most cases of this population, comparing the first and second pictures showed an angle of deformity of around 1 degree, which mostly increased by over 50% in the 2Kg set of data. Most of the data for the 1-Kg load are scattered around 1 degree of laxity and for the 2-Kg load around 1.5-2 degrees.

In the second round of the test, they used a wooden stand. This time all the movement of the forearm came from the elbow, whereas in the first round much of it came from the shoulder joint; hence, this wooden stand was designed to fix the upper part of the arm in space. 5 different pictures were taken of each subject's arm. The first picture was taken when no load was applied to the arm

and the arm was in a resting position. The subjects were asked to hold their arms parallel to the ground and maintain a 90-degree angle at the elbow. Then the upper part of the arm (between the elbow and the shoulder) was placed on the wooden stand to stabilize it and create more robust results.

The subjects were next asked to hold a 1-kg load in their hands but still try to keep their hands parallel to the ground. In the third picture the same load was applied but the subjects were asked not to engage their arm muscles in order to let the arm drop down under the pull of the load. All this downward movement came from the elbow and no longer from the shoulder (unlike the first-round trials).

Finally, the same two pictures as before were repeated, the only difference being that a 2-kg load was instead of a 1-kg load. One set of the five different pictures with a human subject is reproduced below:

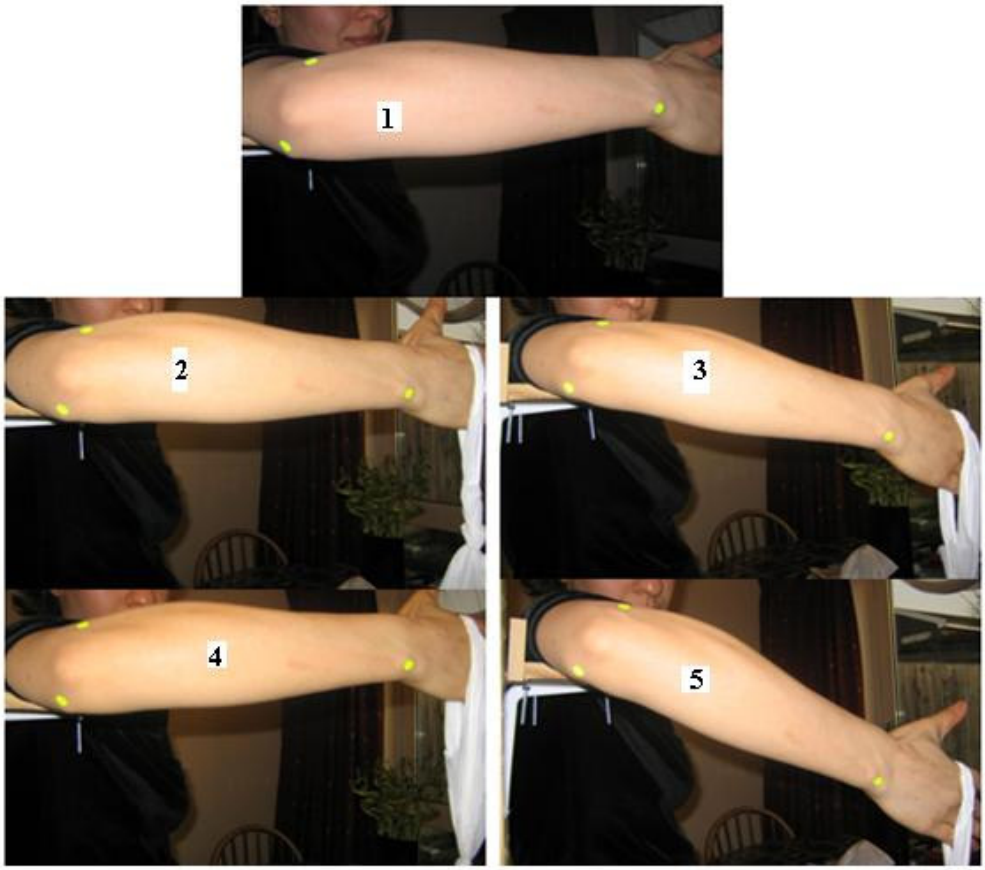

Figure 3-1: set of five pictures on a human subject (picture 1 with 0 weights and picture 5 with maximum weight load)

The presence and effect of the wooden stand in the pictures it noticeable.

Another thing to notice is the remarkable increase in the laxity values - up to 8 or 9 degrees. This is a pure result of using a wooden stand to stabilize the arm which makes the readings more robust, accurate and immediate.

Another point is that, in most extreme cases, there is no more than a 20 % increase between the second reading and the fourth, when the load is doubled. It is understood from the results that in these cases, the laxity of the elbow joint

probably does not necessarily increase in a **linear pattern**, meaning that if the load in increased from 1 kg to 2 kgs, the laxity will not be doubled, but will merely increase by 10%-30 %. This probably means more instability in the elbow joint, which leads to the maximum laxity being reaching when even a light load is applied. The consistency in their results is remarkable and again confirms the accuracy of the results and robustness of the technique.

Mihata et al., (2008) use a customised device (Figure 3-15) to measure elbow valgus laxity. With an applied varus torque of 1.0 N.m and an applied valgus torque of 1.5N.m the elbow valgus laxity was measured as the angle of the forearm between the varus and valgus positions. A 1.0 N.m varus torque was utilized as the starting position, because the neutral varus/valgus position of the elbow is intricate to identify. With the varus and valgus torques, 3D position of the forearm using a Microscribe 3DLX (Immersion Corp, San Jose, Calif) was digitized. Then the position data was used to calculate the varus/valgus angle (Mihata et al., 2008).

3.3 Elbow joint measurement - methods and devices

A number of devices and methods were used to measure the elbow joint's kinematics. Some of the existing devices and methods are listed below:

Motion Analysis Camera

Goniometry and Electrogoniometry

Dynamography

Roentgen Stereophotogrammetric Analysis

Electromagnetic system

Sonography Imaging

Accelerometers

Modelling and simulation

These different devices and methods are appropriate to one specific kind of measurement. Before using a device it is essential to ensure that it is appropriate to the measured movement. For example, a system with cameras and markers will be used to measure the general movement of the body during an exercise, whereas a joint angle sensor will be used to measure only the rotation of a particular joint. The system of measurement must be chosen not only according to what movement is measured, but also to the desired accuracy. These devices do not all offer the same level of accuracy. Therefore, researchers must understand be the limitations of their results.

3.3.1 Motion Analysis Camera

Currently, most researchers prefer to use a motion analysis camera to study the kinematics and kinetics of movements. The device used is 3-D, infrared, high-speed, Motion Analysis System (with eight-camera) which picks up reflective markers on a computer. To reflect infrared light from the camera flashes, a number of reflective markers are positioned on the body. Only this type of marker is displayed in the computer image. The images will produce X, Y and Z coordinate data from all the calculated movements in turn. The data are then transferred to data acquisition software for analysis.

However, users must beware of the problems which these different devices present. Indeed, these systems of measurement are never perfect. For example, the system using video is not very accurate for some movements, because it records the movement of markers placed on the skin. Hence, the measured movements are those of the skin but not the underlying movements of the bones. Indeed, during movement, the skin moves around the bones. Thus, it is difficult to measure the movement of a bone with such a device and it would not be appropriate for measuring elbow movement, since the displacement of the skin at the elbow is not negligible. The skin movement around the bone would prevent the results from being accurate. To follow the movement of the elbow joint itself, it is essential to know the movement of the bones in order to understand the displacement of each one. The main purpose in knowing the displacement of the bones is to design prostheses which match as far as possible the undamaged elbow.

Researchers from the American Sports Medicine Institute (ASMI) in their study use Engle, a device with a digital system from the Motion Analysis Corporation in Santa Rosa, California. This system comes complete with a computer program which is then used to calculate the kinematics and kinetics measurements. The measurements which are normally collected are body angles, joint velocities, timing mechanisms, joint forces and torques. (American Sports Medicine Institute, 2007).

Researchers from Sweden use a 3-D motion analysis performed with a ProReflex Motion Capture System (Qualisys, Sweden). This system includes an advanced optolectronic camera system which produces clean and accurate 3-D data. The

data analysis was performed using special programme written in MATLAB (The Mathworks, Inc.)

Researchers at Oman Orthopaedic Research and Learning Centre have investigated elbow joint kinematics using image analysis based on marker positions. They stick three different markers to three different positions on the forearm (Figure 3-3). One of them sticks to the bony area at the back of the wrist, while the other two are stuck onto the epicondyles which are located on the distal of the humerus near the joint. The third marker sticks to the styloid process which is a bony trajectory on the distal end of the ulna, immediately before the wrist joint. All these three points are shown in the picture below:

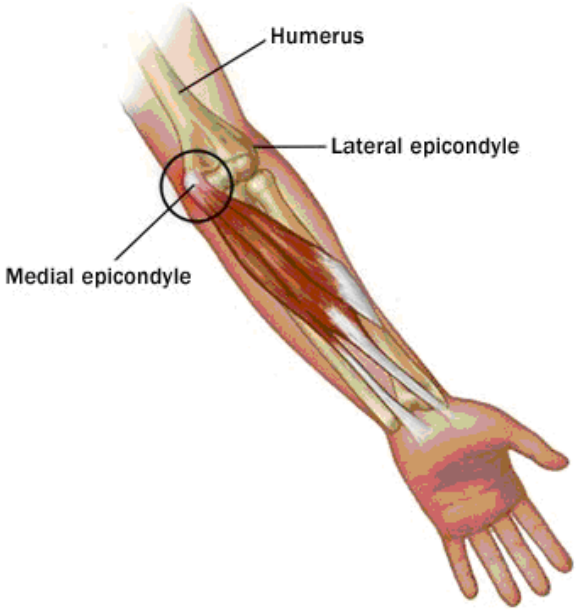

Figure 3-2 medial and lateral epicondyles www.revolutionhealth.com

Figure 3-3: Markers on the arm (lateral epicondyle, styloid process and medial epicondyle which are used to study forearm movement).

As discussed above, a big proportion of the movement of the elbow joint in the varus-valgus plane originates from the glenohumeral joint. As we move our arm in varus and valgus directions, the humerus is not fixed and by virtue of this we can use the valgus and varus motions. The disadvantage of such a possibility of movement is that it makes it much more difficult to measure the actual varus and valgus movement which comes from the elbow itself.

By attaching two markers on the Epicondyles onto the skin (at the distal end of the humerus) researchers gain an almost exact sense of how far the humerus has rotated when the arm was moved in the desired plane; hence, by measuring the amount of displacement of the hand compared to these two points, researchers can figure out the alteration in the angle of direction of the arm caused by the varus and valgus movements (Morrey and Chao, 1976).

As a first step, this procedure was simulated by using as markers three tiny squares of paper, located on a dark surface so as to minimize unwanted noise at this level. The position of the markers was changed and an attempt was made to

detect them in the pictures. The procedure for detecting them was a simple code generated by MatLab.

In the next step, the coordinates of the middle-points of each marker are calculated by a simple algorithm and then a triangle is drawn on each binary image which connects the three points together.

Finally, as

Figure 3-4 shows, two triangles are drawn, made up of the line drawn from the wrist to the mid-point of the line connecting the two epicondyles and the angles **alpha & beta** which are the angles between these lines.

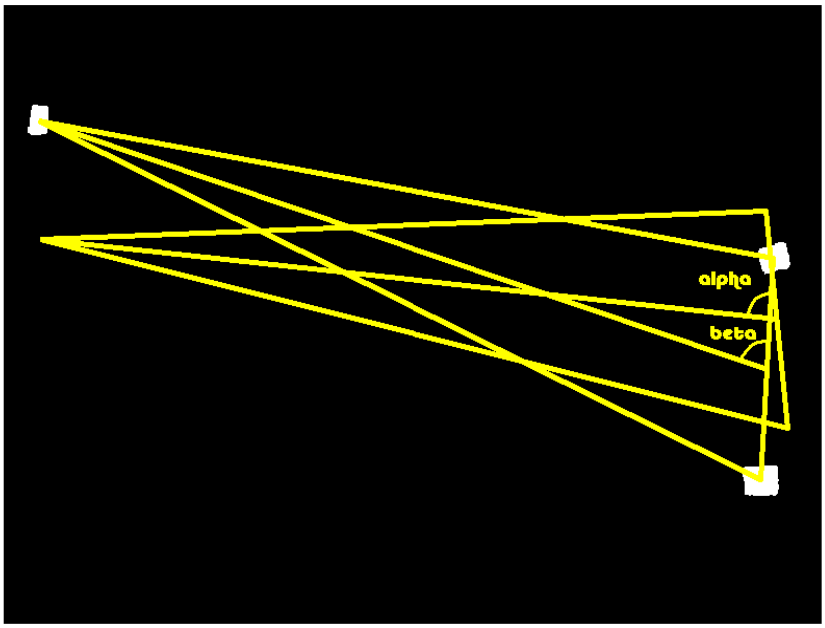

Figure 3-4: working out θ: The angle to be measure is the difference of these two angles, called θ (theta).

In the first step, no load was applied on the forearm, the arm or the elbow in their resting positions. In the second step, a load of 1 kg was applied to the arm when held parallel to the ground and then the subjects were told to let the load pull the arm down; finally, a load of 2 kg was exerted. Three pictures were taken and then they were compared on a MatLab platform to detect any elbow deformity.

As two of the markers are located on the humerus and the last one is on the ulna, it is possible to analyse the movement of the forearm in relation to the humerus. This analysis leads to information about the kinetics of the elbow joint, which is the intersection of these two parts of the upper limb.

These three points form a triangle with the base consisting of the markers on the epicondyles and the apex on the ulnar process. This triangle was used in image processing techniques. As load is exerted on the elbow, this triangle deforms and the outcome will depend on the size of the angles calculated through the image processing procedures.

In addition, a wooden stand was used to fix the upper part of the arm in space. The wooden stand is a very simple device with adjustable height, consisting of a long pillar to which the main plate sticks. The main plate is the one on which the upper arm rests. This plate also has lateral edges to prevent the arm from slipping off.

Instead of this, movement can be captured by a high speed video, using a Vision Research high-speed video camera. This camera can record motion at 450 frames per second, in contrast to standard video, which is only 30 frames per second.

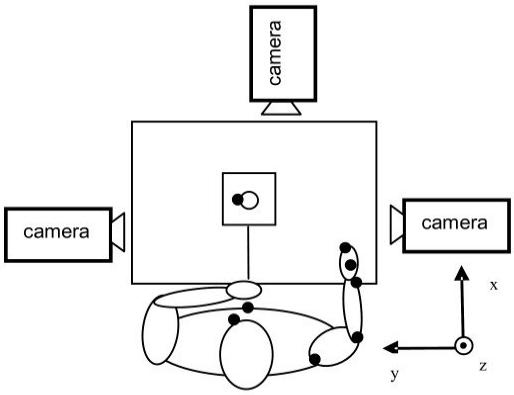

Figure 3-5: Example of experimental setup using a motion analysis system

3.3.2 Goniometry and Electrogoniometry

Goniometers usually measure the static positions of limb segments with respect to the ROM at a joint. These devices are based on the concept of a protractor and the effect of gravity. Their size varies according to the sizes of the body segments to be measured.

An electrogoniometer is a device to measure angles; it consists of a potentiometer placed at the centre of a joint with two extensions attached to the body parts forming the joint. The degrees of movement in the joint attached to the device can be read from an oscilloscope, a recording paper, or a computer. The advantage of using electrogoniometry is its ability to record the action of a joint when it is not visible to the observer. In addition, it can record instantaneous angular displacement with the respect to time (Adrian & Cooper, 1987).

Regarding the joint angle sensor, this device has the practical advantage that it can rapidly be fixed to a joint. However, it is not very accurate, because human joints

are complex and often allow motion in more than one plane. Moreover, the centre of rotation moves when a joint moves. In the case of the elbow, the centre of rotation moves during flexion. Therefore, this system is not very good for capturing the complexity of human movement. It would be adequate for simple rotations in one plane about one fixed axis of rotation. It provides good approximations but not very accurate results.

A former Oman student, Garnier designed and made the prototype of the first device of its kind for measuring the movements of the elbow joint and analysing its kinematics. He wrote his project under the supervision of Prof. Esat (Garnier 2005-6).

In the device which preceded that of Garnier, a potentiometer was deployed to measure the motions of the elbow joint, but it was always open to three major problems; insufficient accuracy, the problem of skin fixing and the movement of the shoulder joint (Garnier 2005-2006). Garnier in his new design accepted the challenge of these problems.

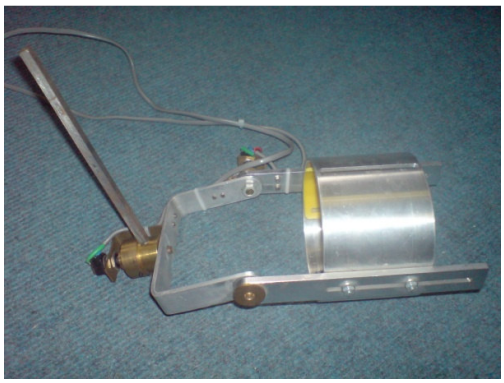

Figure 3-6: Device with two potentiometers

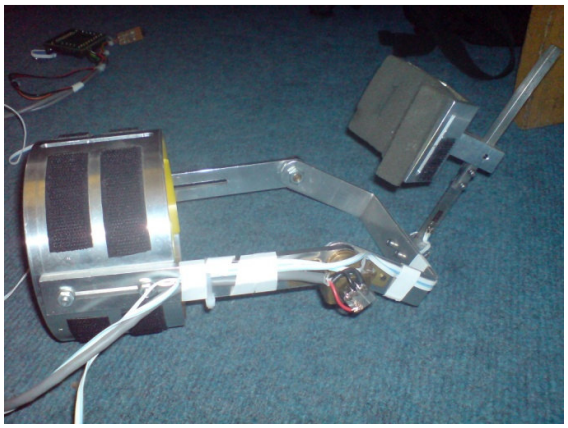

Figure 3-7: New device with strain gauges and straps

The potentiometer in current use can measure angles between 0º and 270º. Since extension and flexion cover a range of almost 180º, such a potentiometer can cover 66% of its range. But using the same element to measure the varus and valgus motions resulted in a very weak output signal. The angle range for these motions is 30º, which is 11% of the potentiometer's range. Therefore the output signal is not precise, is susceptible to noise and also has to be amplified (Garnier S. 2005-2006).

At the same time, fixing the device on the arm is a major problem. No matter how much fixative is applied, the skin will move in relation to the bones and this movement will badly distort the measurement of the valgus and varus motions.

In addition, a big percentage of the elbow movement in the varus/valgus plane comes from the rotation of the shoulder joint, which is very difficult to avoid or block. Garnier, however, came up with a new device to deal with these problems.

The first step was to add some straps to the device to raise the level of fixation on the upper arm. To some extent, these straps also solve the problem of skin movement.

The major problem with the predecessor was its precision, but this was to a great extent solved by using strain gauges instead of the potentiometer which measures the valgus and varus motions (Garnier, 2005-6). As Garnier states, strain gauges are the most common measuring sensors. They consist of a thin wire printed or stuck on an insulating plate.

When the object on which the strain gauge is stuck is distorted, the length of the gauge is extended by having to stretch and its resistance changes accordingly.

A half bridge chosen for Garnier's project had two active gauges and two resistances. Its main advantages were that the output signal was doubled and the thermal effects were automatically cancelled.

A full bridge is normally used as a torque or force sensor. It is high in sensitivity. It consists of four active gauges and its signal is amplified by four. But it is expensive and unsuitable for the present project.

The potentiometer which is mounted on the device measures the flexion and extension of the elbow while the strain gauges measure the valgus-varus movements.

Sauers et al use an instrumented arthrometer (Figure 3-8) to measure the laxity of the glenohumeral joint. A custom-designed test chair equipped with nylon strapping was used to position the patient. Using a custom force applicator, load was applied to the glenohumeral joint. A load cell which had a mounted plastic

handle (Omega Engineering, Stamford, Conn., USA) was creating the force applicator. A metal hook was attached for securing the force applicator to an arm cuff at the opposite end of it. The arm cuff was made of padded nylon with dimension of 3x18 in. It was wrapping around the proximal humerus and secured with strips fastened by hooks and looping strips. The load cell was regularly calibrated to ensure accuracy, with a known force (Sauers et al., 2001).

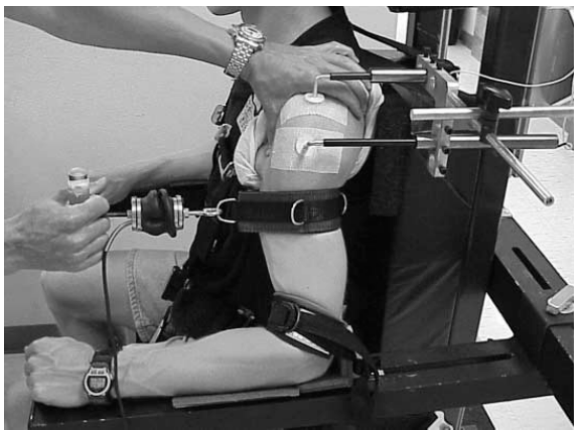

Figure 3-8: Instrumented shoulder arthrometer (Sauers et al.,2001)

The linear displacement of the humeral head and acromion process were calculated using two linear transducers (LDTs; Davis Instruments, Baltimore, Md., USA). The LDTs can calculate linear displacement to the nearest tenth of a millimetre and consist of a retractable, high-grade aluminium strip inside an aluminium cylinder. The first LDT used to measure the displacement of the humeral head, and the second one used to measure the movement of the acromion process of the scapula.

One adapter was attached to the skin surface over the lateral portion of the proximal humerus, and the other was attached to the skin surface during the acromion process. A standard analogue calliper was used to calibrate the LDTs

regularly. The humeral head displacement then recorded by tracing the scapulothoracic motion and then the possible laxity of the glenohumeral joint was calculated.

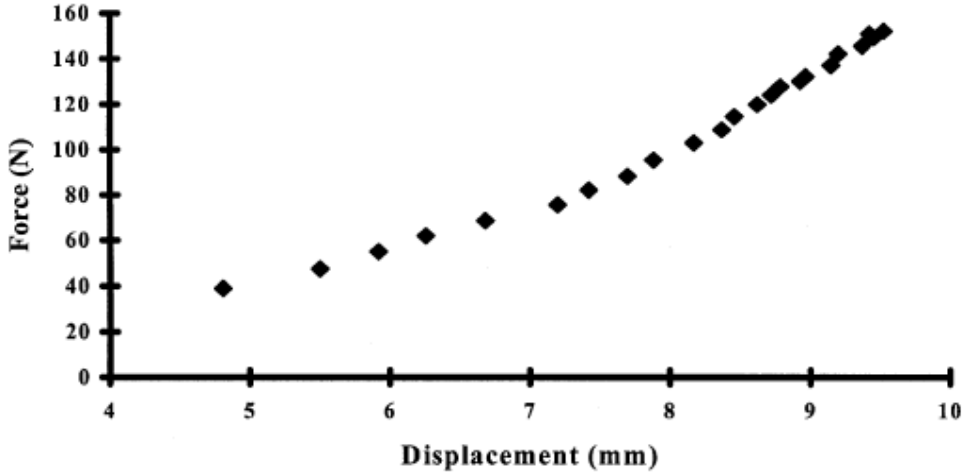

Figure 3-9: Force-displacement curve plotted using the instrumented shoulder arthrometer (Sauers et al., 2001)

Evaluating joint laxity using a KT-2000 knee ligament arthrometer was studied by Hatzel et al. (2006). As indicated in all the relevant articles, the glenohumeral joint is a potentially unstable joint is vulnerable to injury, particularly in sports where high-speed movement or big momentum is required and the joint undergoes instant stresses.

Figure 3-10: KT-1000 (Hatzel et al., 2006)

Hatzel et al believe that, although the GH joint allows great movements in different directions, a very tiny translation occurs in the humeral head as motions are made. In addition, the malfunctioning of the joint is a result of either an increase or a decrease in the translation of the humeral head on the glenoid. This is why it is essential to quantify the amount of translation of the humeral head. So Hatzel et al., adapted the KT-2000 knee arthrometer which was already to hand and used it to measure the laxity of the shoulder joint (Hatzel et al., 2006)

Basically, the KT-2000 knee ligament arthrometer has two sensors which are horizontally fixed on the main frame and should be inspected beforehand to make sure that they are parallel.

The amount of GH motion in the sagittal plane records in a KT-2000 method using a dial which records displacement in millimetres (Hatzel et al.,2006).

The patient is placed supine on the bed and the hand is fixed to a custom-built stabilization device. A thermoplastic mould forms a gutter in which the arm and shoulder rest and, at the same time, the GH positioning is maintained. During the testing the motion of the arm and shoulder is restricted, due to the moulded structure which ensures the stability. In addition, the patient's supine position on the bed which prevent the movements of the scapula and in turn scapulothoracic articulation

3.3.3 Roentgen Stereophotogrammetric Analysis

Roentgen stereophotogrammetric analysis can be used to determine the motion between the humerus and ulna under valgus load and between the humerus and radius during the maximal pronation of the forearm after various dimensions. This analysis will detect motion after a selective transsection of the medial collateral ligament complex. It is proven to be an accurate way of measuring the micromation of prosthetic implants with respect to the surrounding bone.

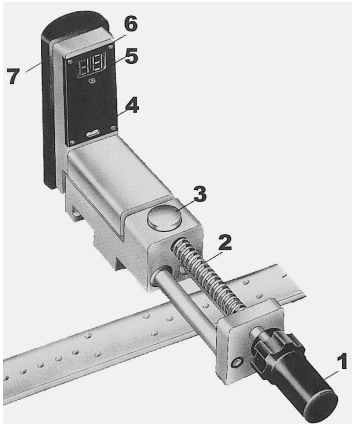

Figure 3-11: Screw-threaded shaft

Figure 3-11 shows the type of screw-threaded shaft used. In the illustration:

1. Indicates turning grip.
2. Treaded spindle.
3. Release button for free motion.
4. Charging indicator lamp.
5. Socket for charging equipment.
6. Digital readout.
7. Front cushion pad.

The analysis made with this shaft is used to calculate the 3D motions of bone structures. In a study by researchers from Denmark, a Plexiglas disk (Medis, Leiden, the Netherlands) was used with metal screw-threaded pins containing 8 tantalum beads as artificial landmarks for specimens of bony elements. The disk was fixed to the medial epicondyle, the proximal radial shaft and the coronoid process of the ulna. The analysis as set up consists of two roentgen tubes which are placed above the Plexiglas calibration cage and an x-ray cassette placed underneath.

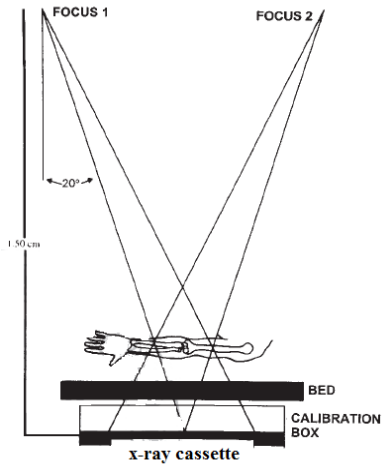

Figure 3-12: Experimental setup

(source: Medis, Leiden, the Netherlands)

As shown in Figure 3-12, the elbow is positioned above the calibration cage underneath which the x-ray cassette can be inserted. Two synchronized roentgen tubes are positioned about 1.5m above the cage.

The translation data were determined using the roentgen stereophotogrammetric analysis software from Medis, which automatically detects markers and gives accurate measurement for digitized radiographs.

3.3.4 Electromagnetic Tracking System

Researchers from the Biomechanics Lab in the USA use an electromagnetic motion tracking system in their research to assess elbow joint kinematics in passive motion. Kinematic rotations of the elbow joints were recorded using the D.C. electromagnetic tracking system, which is a Flock of Birds product of Ascension Technology. This motion is traced by the receiver, which is connected to the humerus of the patient and corresponds with the transmitter, which is connected to the ulna. The experimental setup, as shown in Figure 3-13, must be built of non magnetic materials to prevent any distortion of the recording by ferromagnetic objects (Bottlang et al. (2000).

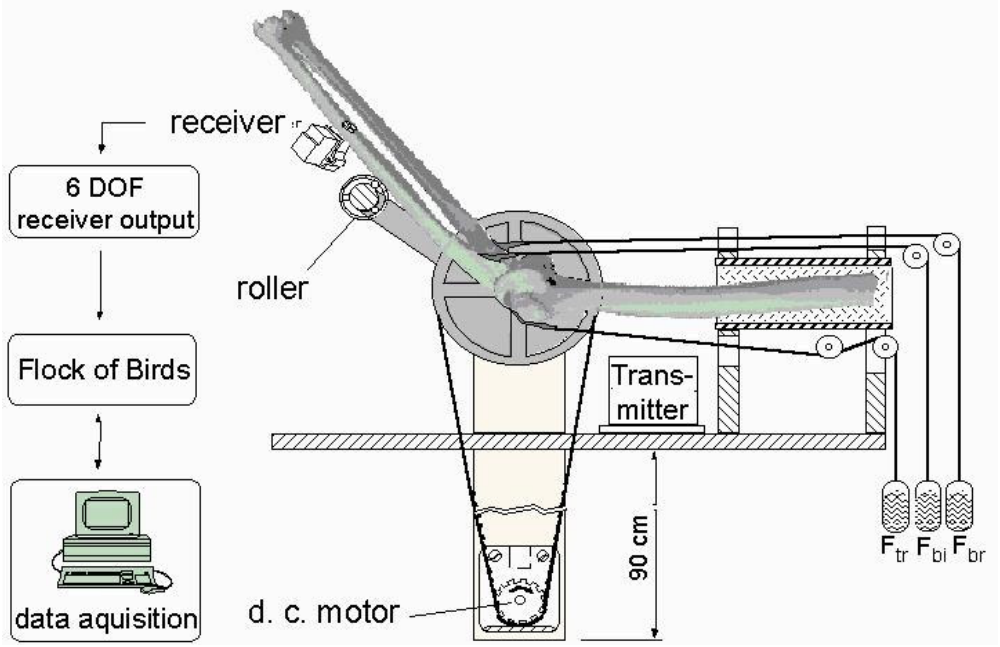

Figure 3-13: Experiment setup for passive elbow motion using a roller configuration. (Bottlang et al. (2000).

The best-fit screw displacement axis (SDA) was found by averaging all the screw displacement axes obtained over the entire range of motion. The SDA was marked on the specimens. Another method used to locate the SDA is radiographic. However, this method has the disadvantage that it is difficult to locate the landmarks which form the centre of the shadows cast by the parts of the elbow (Bottlang et al.,2000).

3.3.5 Dynamography

Dynamography is a technique for measuring the forces produced during an activity. It consists of spring devices and cable tensiometers. Resistance sensors, strain gauges and pressure sensors have been placed on devices to determine the effectiveness of the force produced. Strain gauges are considered force

transducers, since, having been attached to a recorder they receive power from the power supply and change it into force (Adrian & Cooper 1987).

3.3.6 Accelerometers

An accelerometer is a device to measure acceleration, which indirectly measures force. It functions by multiplying the mass which is accelerated by the acceleration value to yield the force being produced. To supply measurements, it can be attached to the human body or to another device. The disadvantage of this device is that the placement and charting of the device position are crucial to the interpretation of the data (Adrian & Cooper 1987) and the results are severely affected by the least drift or system inaccuracy. In fact, these errors are integrated and continue to affect the data. Another of its problems, as with the electromagnetic system, is the securing of the accelerometers on the skin and the problem of the skin movement around the bones.

3.3.7 Modelling and simulation

A greater need for the understanding of elbow functions is caused due to uncertainty and a lack of knowledge regarding the restoration of the proper functions, following an elbow injury. Researchers have combined mathematical modelling of the anatomical characteristics of a living body with simulation techniques for the purpose of predicting performance achievements and developing new performance techniques. Expertise in mathematics, anatomy, physics and computers is required to fully exploit these theoretical tools (Adrian & Cooper, 1987).

Experimental data collected with the tools of cinematography, videography, dynamography, electrogoniometry, electromyography and accelerometry are the foundation for the development of the model. Researchers enter on a computer the values for the relevant parameters and their boundaries. Algorithms of motion, forming the equations for calculation, are used in the simulation, where the movement can be varied with respect to speed, timing and ROM. The movement pattern can then be simulated with changes in variables, to determine if the performance is enhanced or if safe limits have been exceeded (Adrian & Cooper, 1987).

There are many software packages available to perform simulations and derive the best biomechanical mode. In addition, CAD/CAM, CAEDS and other available computer-aided design programs can perform stress analysis.

An elbow motion simulator which is capable of producing motion in a cadaver forearm has been designed and developed. Magnusen at the University of Pittsburgh 2004 improved a model of an elbow simulator. This device advances the capacities of previous similar devices by simulating the range of movement and force-loading conditions in the elbow. To simulate the muscles electric cylinders are used, (in this case, the biceps, brachialis, triceps, brachioradialis and pronator teres). A braided cable is attached to the cylinders and is then inserted in the arm at the tendonous insertion of each muscle. The muscles maintain an accurate line of action within the cable by preserving a physiological moment arm about the joint of rotation, which is done using custom-designed pulley systems. The humeral shaft is held securely during experimentation by a humeral clamp. The

device can be rotated to test movement in either a varus or a valgus orientation. Preliminary testing was performed with a wooden arm model by its inventor to verify the simulator's capacities (Magnusen et al. 2004).

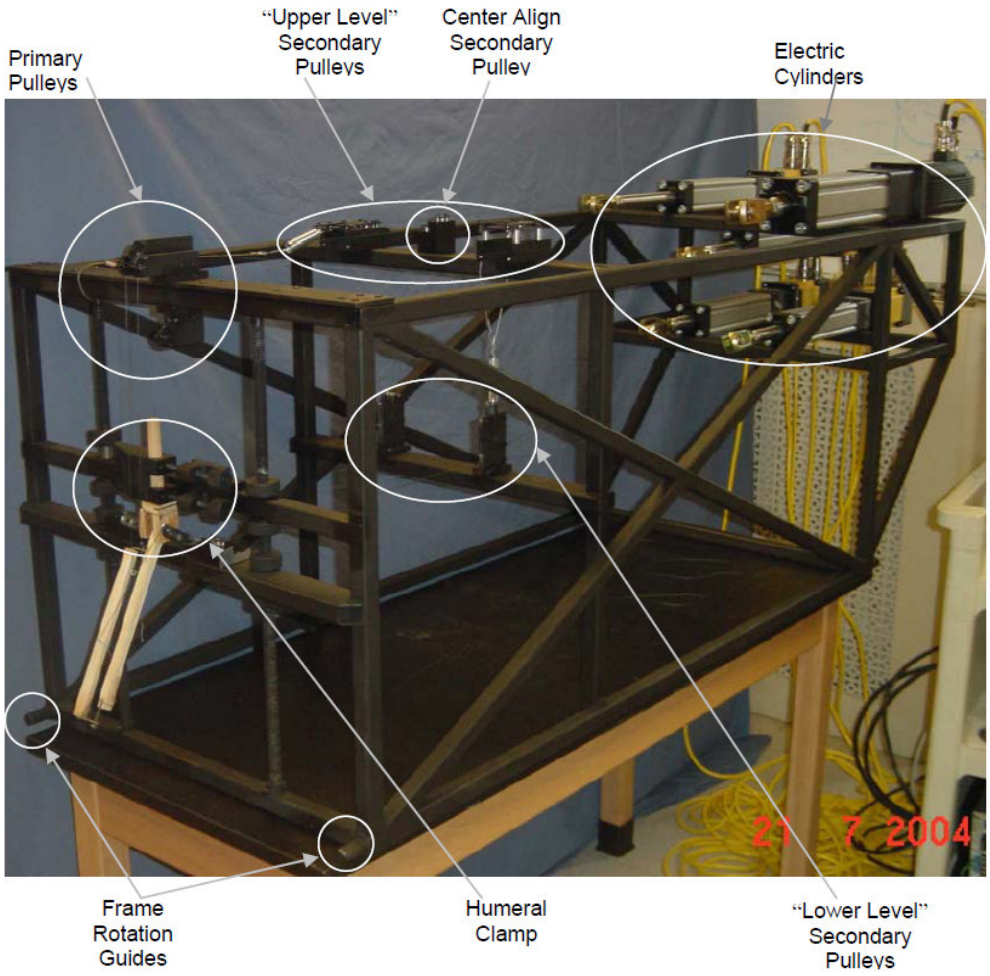

Figure 3-14: Elbow simulator (Magnusen et al., 2004).

Without considering the effect of humeral external rotation Mihata et al., (2008) measure elbow valgus laxity in *in vitro* conditions for 7 cadavers utilizing a

testing device shown in Figure 3-15. The specimen was preconditioned by loading with a force of 0.5 Nm in both valgus and varus directions 10 times each, before measuring the valgus laxity. While the forearm was loaded with the varus and valgus torques, a Microscribe 3DLX (Immersion Corp, San Jose, Calif) was used to digitize the 3D position of the forearm. The varus/valgus angle was calculated from this data. The accuracy of the Microscribe (Immersion Corp) has been determined at 0.30 mm (Mihata et al., 2008).

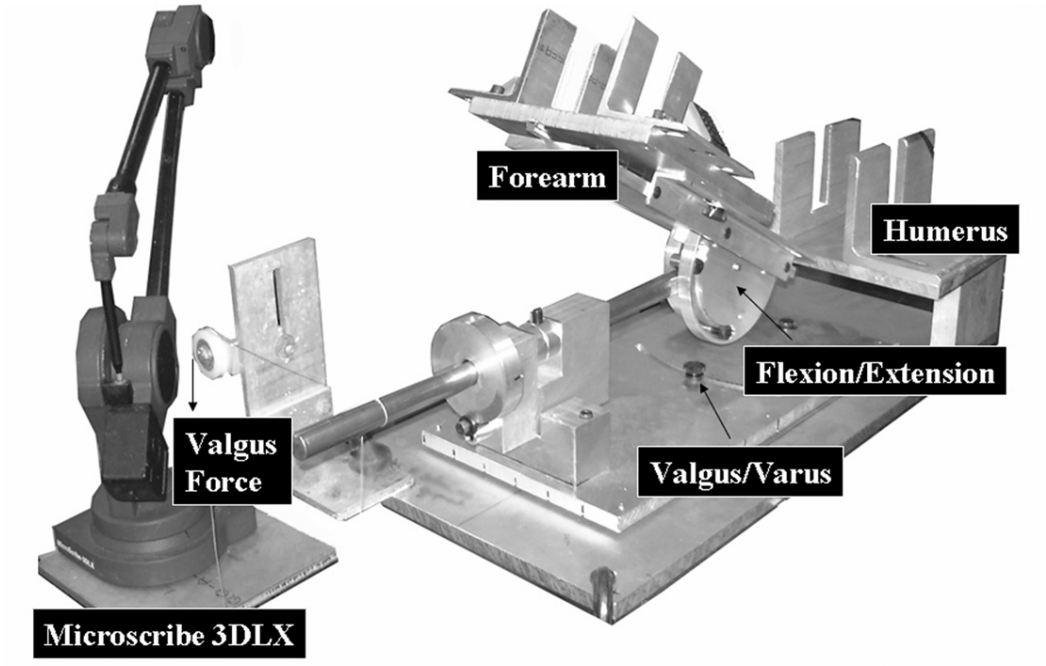

Figure 3-15: Custom elbow valgus laxity–testing device. It allows for 3 degrees of freedom: flexion/extension, supination/pronation and valgus/varus movement (Mihata et al., 2008)

3.4 Elbow joint injury and cure

The elbow joint is one of the most active joints in the human body. We use it for almost every movement of the hand. Complete elbow function is critical to such daily functions as feeding, grooming and hygiene. Elbow function can be impaired through both acute and chronic injury and trauma. In the case of extreme injury, the radial head may be replaced with an implant.

It often happens that we involve this joint in a movement of the upper limb without any awareness of doing so; the use of this hinge joint is quite unintentional. When we hold our hands in a particular position in space, a great deal of their stability comes from the elbow. It is the elbow that enables the forearm to perform smooth and precise movements when combined with other joints of the arm.

3.4.1 Radial head fractures

Radial head fracture is the most common adult elbow injury, occurring in 17%-19% of elbow trauma cases and accounting for 33% of elbow fractures (Morrey, 2000). Radial head fractures alone account for 5.4% of all adult fractures (Morrey 2000, Conn and Wade 1961, Johnson 1952). About 15%-20% of these fractures involve the neck (Thomas, 1905, Arner et al.1957) and radial head fracture is twice as common in women as in men (Castberg et al.,1953, Ring et al.,2002). Comorbidities may include fractures of the olecranon and/or coronoid and disruptions of the medial collateral ligament, triangular fibrocartilage complex and/or interosseous membrane. Treatment varies accordingly (Trousdale et al.,

1992, King et al., 1991, Ring et al., 2002) and can include excision, surgical reconstruction and complete radial head replacement.

Clinicians have, however, been disappointed with treatment outcomes (Morrey 2000). As the radial head also aids the triangular fibrocartilage complex and the interosseous membrane in preventing proximal migration of the radius with respect to the ulna (Hotchkiss 1997), displaced radial head fractures are routinely reduced and internally stabilized (Hotchkiss 1997, Mikic & Vukadinovic 1983, Ring et al., 2002). This treatment sometimes, however, produces unsatisfactory clinical results (Mikic & Vukadinovic 1983, Ring et al., 2002). Radial head excision has been advocated for comminuted fractures, but complications can occur, such as an unstable elbow or chronic wrist pain (Tomaino et al., 2003, Kinght et al., 1993). In an extreme case, the radial head may be replaced. In short-term clinical follow-ups, metallic radial head implants have performed acceptably in cases of unreconstructable fractures (Moro et al., 2001, King et al., 1999). However, one radiographic review has suggested that a metallic radial head implant did not restore physiological load transfer across the elbow (King et al., 1999). In another study, two out of thirty-six metallic implants were removed because of painful loosening (Moro et al., 2001). At the same time, it has also been shown that metallic radial head arthroplasty can offer improved valgus stability, approaching that of the native radial head and far superior to that offered by silicone implants (Pribyl et al., 1986).

3.4.2 Radial head prostheses

Radial head prostheses have had increasing levels of success. In the mid-1970s, 55% of patients receiving radial head implants had complications. Nonetheless, overall, the results were good in sixty percent of patients (Morrey et al., 1981) Radial head prostheses should prevent the complications of radial head excision, transfer normal loads and re-establish the original elbow kinematics (Cherry 1953, Swanson 1981). A number of studies have examined the transfer of loads of prostheses by measuring elbow stability and laxity (Pomianowski et al., 2001, Pribyl et al., 1986, Van Riet et al., 2004, Gordon et al., 1982, Liew et al., 2003, Sojbjerg et al., 1987). Silicone radial head prostheses were popular for a while but caused a reactive synovitis and did not re-establish normal ulnar-humeral load transmission (Gorden and Bullough, 1982; King et al., 1999; Pribyl et al., 1986). In cadaveric studies, metallic radial head replacements restored the axial forearm stiffness to almost normal (Jensen et al., 2003; King, 1999; Pomianowski et al., 2001), but reduced the humero-radial contact area by 68% (Liew et al., 2003).

The kinematics of the native and replaced radial head have been studied much less than the issue of load transfer. Excessive relative motion between the radial head and capitellum may lead to wear on the capitular cartilage and may cause other soft tissue damage and distal radial-ulnar joint pathologies. Studies have shown that the contact between the noncircular shape of the native radial head and the radial fossa of the ulna causes translation of the radial head during pronation-supination (Van Riet et al., 2004; Van Riet et al., 2003; Weiss et al., 1992). It has been observed that the radial head may translate anteriorly with pronation and

posteriorly with supination (Weiss et al., 1992). Due to the noncircular shape of the radial head, it has been speculated (Van Riet et al., 2003) that the radial head should translate predominantly in the medial-lateral direction. Note that all three experiments above were qualitative, providing no quantitative measures (Galik et al., 2007).

Preservation of the original kinematics also requires preservation of the normal axis of forearm rotation (i.e., the pronation-supination axis, the helical axis and the screw displacement axis). The location of axis rotation as a function of prosthetic alignment and orientation remains unknown.

There is controversy with radial head replacement whether the annular ligament should be reconstructed. Sojbjerg et al., (1987) concluded that this ligament is the major stabilizer of the lateral side of the elbow. However, the experiment was performed amidst confusion about the nomenclature of the lateral collateral ligament (LCL) and the research team inadvertently cut the lateral collateral complex. To confirm this, a subsequent study (Olsen et al., 1996) showed that it was the LCL ligament that was the important stabilizer of the lateral side of the elbow. The annular ligament did not have any effect on valgus laxity, but was responsible for 2.3° of varus laxity, or about 20% of the laxity achieved by transaction of the medial collateral ligament. Weiss and Hastings (1992) applied force to the radial head to study radioulnar divergence. They concluded that the main contributors to the proximal radioulnar stability were the annular ligament and the middle third of the interosseous membrane.

3.5 Chapter Summary

The engineering outputs and surgical point of view to measure the laxity is different. This is could be because of the differences between clinical and engineering goals. As an example the engineer may focus on measurement techniques, while the surgeon may be interested in the effect of acquired knowledge on the entire treatment protocol. However reviewing a clinical problem may establish a need for collaboration to create new methods which can enhance the treatment of the patients who suffering from joint problems such as joint laxity. Hence, developing an experimental and theoretical method which can evaluate the mechanical behaviour of the joints is a real challenge. However, ease of use and clear interpretation of the data required for clinical evaluation and maintaining the safety (Mihata et al., 2008) is the demand for the new methods.

In Chapter one background proposed to elbow joint anatomy and showed different degrees of freedom and movement in elbow joints. We also discussed kinematics of elbow joint.

In this chapter categorised elbow movement and laxity measurement are discussed in particular different measuring tools and instruments. The overviewed the work which has so far been done on elbow kinematics. Discussion of elbow joint injuries and cures which make the measurement of laxity necessary.

Chapter 4. The manufacturing process of medical implants

4.1 Introduction

The increasing use of medical implants in recent years has encouraged many manufacturers around the world to invent and develop new methods in response to the high demand for medical implants as applied in the human body, reduce their cost and improve their accuracy. In general, the manufacturing process of a proposed medical implant follows a similar pattern, comprising:

Kinematics modelling of the segment

Implant design

Data analysis

Experiment *in vitro*

Experiment *in vivo*

Clinical use of the implant

The first step calls for a deeper understanding of the kinematics of the segment, to allow a general schematic of the implant to be drawn. At this stage, the segment must be studied and analyzed biologically and physically. Almost all input information required for the next stages comes from physical and biological analysis. Therefore, all the medical information about the segment is combined with physical principles to make an observational structure of the proposed

implant. Analyzing the kinematics and dynamics of human segments and joints is very important for understanding the tensioning of tissues such as ligaments and tendons, cartilage compression and the range of joint motion, as well as the interaction between tissues and bones during joint articulation.

In the second step, the structure derived from experimental observations and physical concepts is converted to a software design. Nowadays, many applications have been created to give a primary schematic of implants, before modifying the design in the light of data from kinematics analysis. In this chapter some medical software is introduced, such as MJM, Computer Cad Design (CAD), MIMICS, Rapid Prototype (PR) and LENS, together with a short overview of the process involved in implant design. In spite of the variety of design applications, almost all the graphical data input in the design application comes from two major methods, namely, MRI and CT-scan, because the high resolution and adequate accuracy of these methods satisfy the quality requirements of such applications.

In recent years, in parallel to development of computational power, it has become popular in many scientific areas use of computational tools to simulate a product in the virtual environment. In the medical area, by means of computational tools the kinematics and dynamics information on all normal, abnormal and prosthetic joint articulations can be simulated and has been extremely helpful for researchers seeking to understand the situation of the joint. The purpose of software design is to modify models in the virtual environment and analyze the effect of possible

implants. Usually, Finite Element Analysis is applied so that the effect of external factors on the implant can be observed. By means of numerical analysis, the problems of an implant design are demonstrated, enabling the designer to modify and test the model in the virtual environment. FEA divides the object in geometrical terms, such as triangles, edges and points, through which the performance and functionality of the model can be tested repeatedly without additional cost. The use of FEA allows almost any abnormal behaviour of the model to be inspected and in addition these abnormalities are shown by small geometrical shapes which can signify the increasing accuracy of the test.

It should be mentioned that the situation and condition are assumed in the software to be ideal; therefore, by use of computer software simulates only the gross motion of the implant is simulated. In other words, the outcomes of computer software should not be considered the precise in their analysis of the segment. In fact, all the simulated segments are seen as ideal engineering sections, in which the input constraints can improve the situation to the point where, as far as possible, it represents reality.

Although the test is virtual, the implant must be observed *in vitro* to ensure safety and effectiveness for patients. Generally in laboratory and ideal situations, the test is carried out on animals or segments of human cadavers and different characteristics of the implant are examined, including the biocompatibility, biomechanics, metallurgy, biofunctionality and bioadhesion of the implants.

Implants are generally made of titanium because of the specific characteristics of this metal.

The surface of titanium is covered by a layer of titanium oxide, which is resistant to the chemical environment and provides many desirable characteristics such as biocompatibility, immunity to corrosion, osseointegration, density and shear strength. Osseointegration is very important, because the metal allows the surrounding tissue to grow and osseointegrate with the molecular structure of the implant. The titanium alloy which is used in the biomedical implants is Ti6Al4V due to its range of desired characteristics (Tengvall et al., 1992).

However, virtual testing and experimentation *in vitro* do not provide much information about the dynamics of joints and their surrounding tissues in practice. From a biomedical point of view, it is much more important to precisely understand the dynamics of human segments. In biomedical science, all the diagnostic devices, treatments and surgery can be performed when the device has been tested and improved according to sufficiently precise biomechanical or dynamic knowledge. After the reliability of the implant is proved in the laboratory, it must be tested on real patients, because the situation *in vitro* is ideal and there is always a difference between the real and the ideal. Clinical professionals apply the implants to volunteers to observe the effects of these external objects on them patients. This is the latest step before implants mass production, so it must be assured that the qualification of the object meets the necessary requirements.

Finally, the improved design goes to manufacture for mass production. However, for some cases the implants must be modified before it has been applied for the patients.

4.2 Layered Manufacturing:

Layered manufacturing (LM) is a name of production based on additive method. By use of CAD system a 3D model of the object is generated. Then LM machine add these sliced layers on the previous layer which is now platform for the new layer (Bibb R, Eggbeer D et. al. 2006).

The LM technologies because of its unique ability can be used for fabricating and manufacturing of almost any complicated geometrical shapes. This technology does not require much technical expertise, as well as reduction in minimal tooling cost and time (Giannatsis J et. al. 2007 and Milovanović J et. al. 2007).

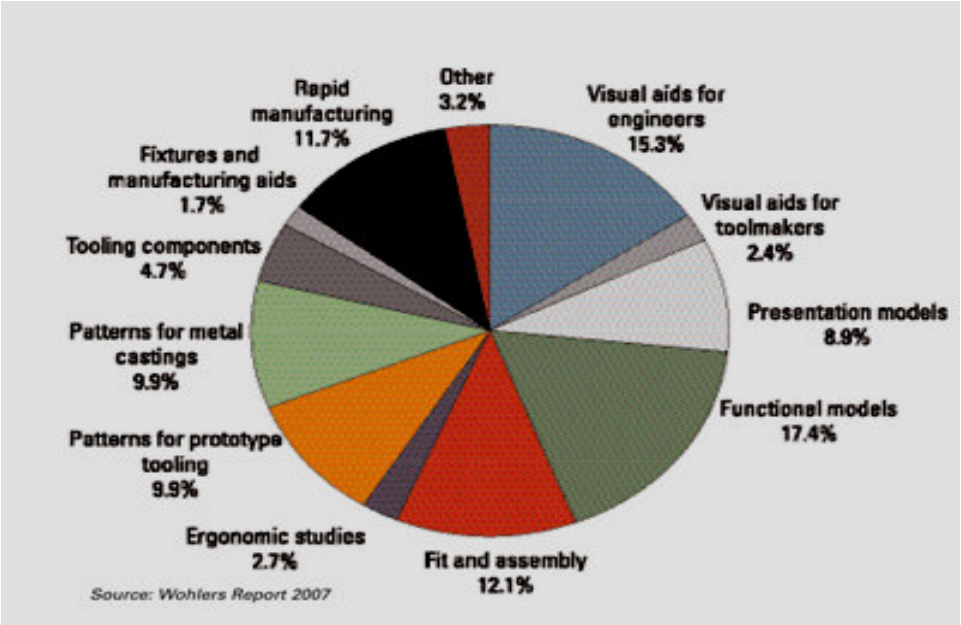

Figure 4-1: LM Applications (Wohlers, 2007; Khan et al., 2007)

In this chapter only the medical application of LM will be studied which is customized orthoses and protheses implant and replacement, but in general other applications of LM are visualisation and surgical planning, tissue engineering, drug delivery, micron-scale medical devices and scaffoldings (Khan et al., 2007).

LM technology is used for fabricating customized implants for reconstructive and plastic surgery. Because of the specific ability of LM technologies to manufacture complicated geometry, it is applied to the making of custom implants. Experience with LM shows that its use can reduce operating time at reasonable cost. One of the unique advantages of LM technologies is the quick fitting of the custom implant to the patient's size, as applied to hip sockets, knee joints and spinal implants. Different experiments of the LM technologies demonstrate the tolerance of this system to be around 0.2 mm, which is considered an acceptable degree of error which allows the implant to fit and match very well with the surrounding tissues (Khan et al., 2007).

3D medical imaging, such as MRI and CT-scan produce can yield for the LM system valuable data and useful information regarding the body structure of patients. The image data can be used as the input for the software. They are visualized, segmented and finally constructed in three dimensions. The three dimensional constructed model can be used as the input data for the CAD modelling system. At this stage, the generated models can be exported to CAE

software for a finite element analysis. LM technologies are used in the last stage in order to produce the physical medical models (Khan et al., 2007).

The integration of different software, including CAD, FEA and LM in conjunction with medical imaging is considered a realistic method for modelling different body structures in medical applications. The generated image file from the CAD model is in STL forma, which in integration with the LM machine could be used to build up a physical model (Khan et al., 2007).

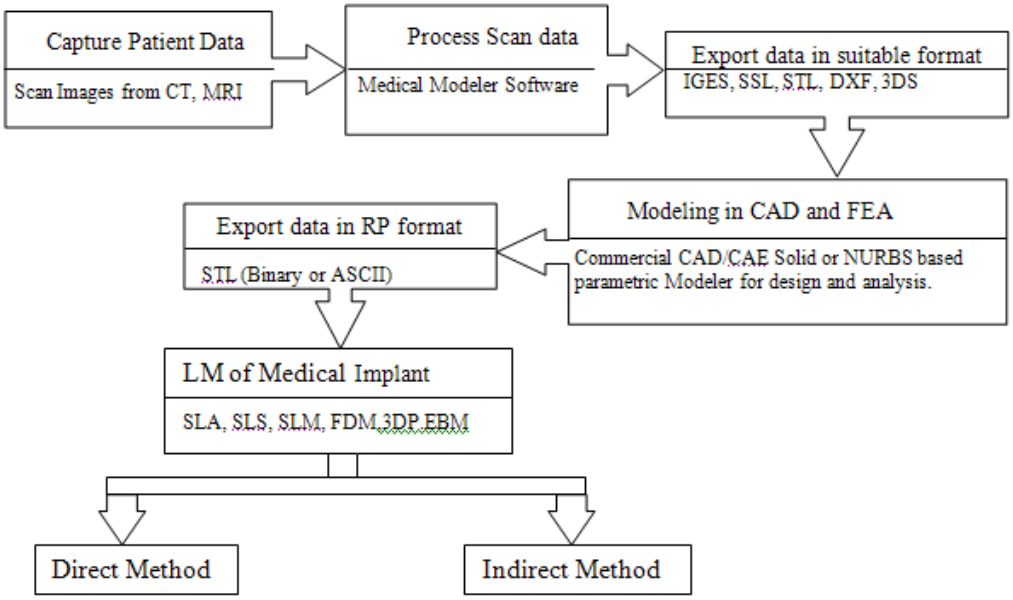

Figure 4-2: LM and CAD methodology adapted to manufacture process (taken from Khan et al., 2007).

The above flow chart in Figure 4-2 chart demonstrates the different steps of the design and manufacturing process of medical implants (Khan et al., 2007).

Another major application of the LM technologies is in manufacturing the scaffold and bones by the use of bioceramics. These types of biomaterial have a specific chemical composition that can be used as a bone substitute.

The following flow-chart presents the different steps of the design and manufacturing process of customized bioceramic implants.

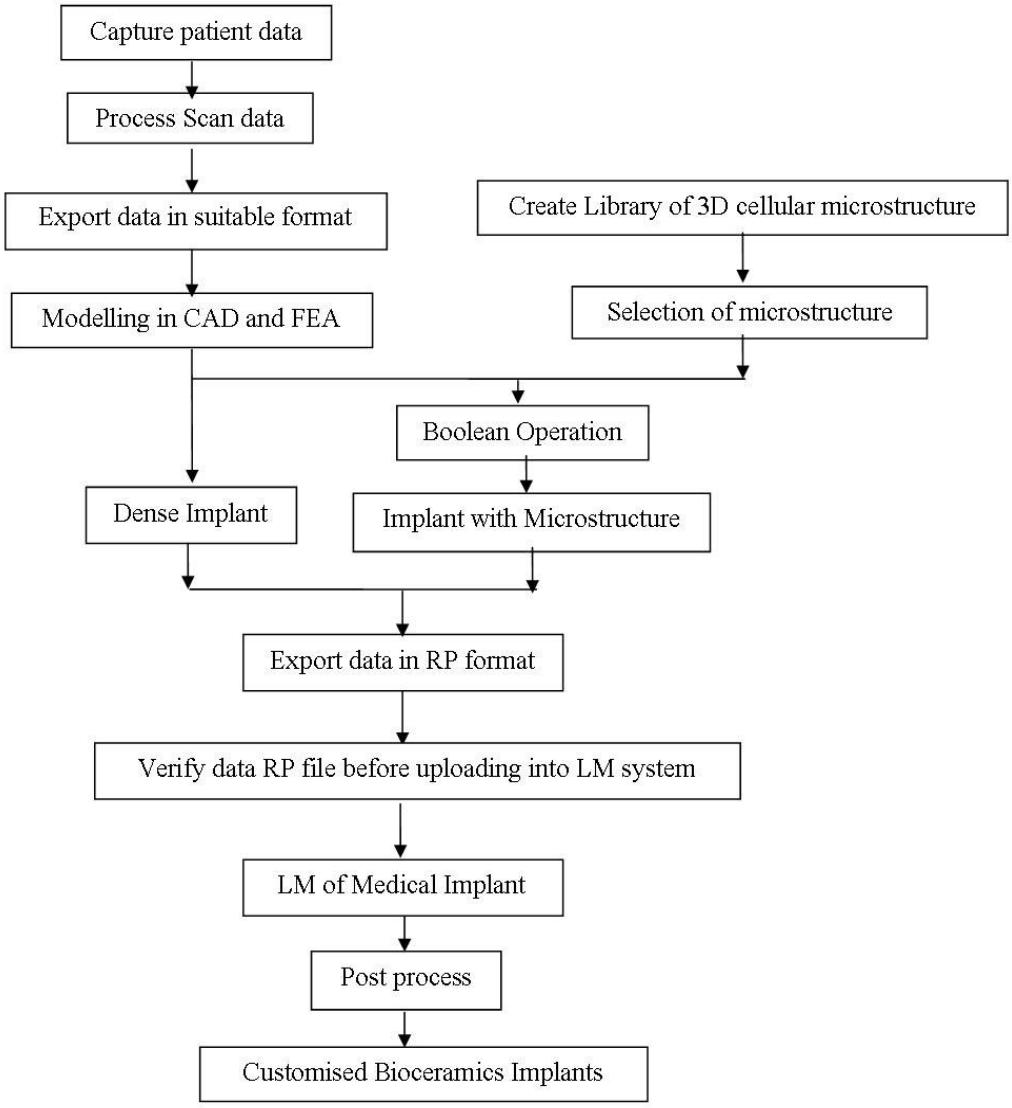

Figure 4-3: LM and CAD methodology for implant design in mandibular bone based on bioceramics and new fixation (Khan et al., 2007).

4.3 Medical Application of Rapid Prototyping (MARP)

By advancements and improvements in the areas of Rapid Prototyping, Reverse Engineering and Image Processing, the combination of the above technologies enables manufacturers to create a highly accurate physical model directly from a Computed Tomography scan or Magnetic Resonance Image.

This chapter provides an overview of procedures for the optimal design of implants by means of Medical Applications of Rapid Prototyping. Two techniques are normally applied to capture internal medical data: Computed Tomography (CT) (Figure 4-4) and Magnetic Resonance Imaging (MRI) (Figure 4-5). These techniques provide cross- sectional images of a scanned part of the human body, but are different in that CT scanners use radiation while MRI does not. However, the quality of the captured data depends on the accuracy of the scanning machine and the resolution data, together with the time of the scanning period (Hosni, 2000).

Usually, a CT scan is applied in modelling bone structures and MRI is suited for soft tissues. It should be mentioned that in both these technologies, the final model is in the same format: cross sectional data images.

Figure 4-4: CT-scan [http://www.ewings-sarcoma.org.uk/?page_id=212]

Figure 4-5: MRI [http://body-mri.com/2011/07/20/mri-scan-knee-records]

The three steps in converting the acquired data from CT-scans and MRI to the final model are:

1. The CT/MRI equipments usually supply the scanned data on magnetic tapes or optical disks. The data obtained are read from the appropriate medium.

2. The readable data are converted into manipulable format. In this stage, the CT/MRI format is translated into an image format specific to the conversion software.

In creating a 3D-model from the 2 dimensional scan images, contours have to be identified for the targeted element of the target region, using statistical analysis and gray scale. Once selected the different layers have to be connected to enable the generation of the CAD model as a solid object (Figure 4-6) and (Figure 4-7) (Yasser A. Hosni1 et al., 2000).

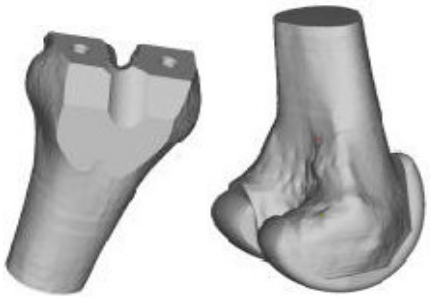

Figure 4-6: Standard implants (Hosni et al., 2000)

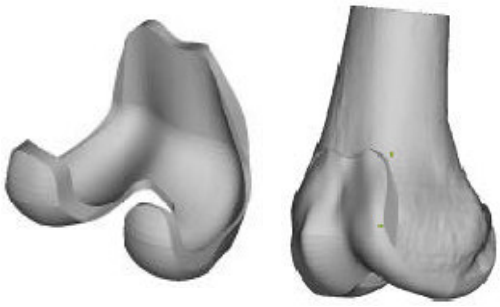

Figure 4-7: Customized implants (Hosni et al., 2000)

Once a 3-dimensional model has been created, using different tools and the patient's data, the implant can be manufactured. Depending on the design and performance of the implant, these data, including the patient's age, weight, degree

of activity, etc. are required. Customized implants are superior to standard implants because the demand less natural bone to be removed than standard ones do.

The process of custom designing implants for each patient on the basis of CT-data has proven feasible and promising. If the process of custom designing and manufacturing implants based on patient-specific data can be further streamlined and the cost reduced to an acceptable level, this could become the common process in future. With the ability to design and produce any type of implant at a low cost, no further mass production of implants would be necessary. By combining custom-designed implants with newly developed orthopedic surgical robots, their advantages could be extended even further.

In addition, the proposed procedure would reduce bone removal by an estimated 40%; meanwhile increased and faster bone ingrowths will reduce the rehabilitation period for patients and prevent related problems such as muscle and joint stiffness (Hosni et al., 2000).

4.4 Musculoskeletal Joint Modeller (MJM):

The MJM is design software for analyzing anatomical joints, without simplifying their kinematics and mobility, tissue deformation or the anatomic line of their actions. With MJM software, joints are simulated as unconstrained joints with 6 degrees of freedom and tissues are modelled without any simplification in their anatomic morphology. MJM software applies a collision detection and collision response algorithm, based on the trajectory of movement of the targeted bone with

the aim of avoiding penetration between the virtual bodies. The developed collision detection algorithm is more efficient than the collision detection algorithm and exhaustive search method (Esat et al., 2010).

As noted above, in developing human joint models, some obstacles must first be tackled:

1) Kinematics modelling and joint mobility

2) Modelling of tissue deformation

3) Collision response and detection

4) Dynamics motion equations

In order to achieve enough accuracy in measuring the dynamic motion of the joints, inverse and forward dynamic analysis is applied. In one study of human elbow joint modelling, the analysis was focused on flexion movement of the forearm and measuring the relative change in the centre of rotations and in the varus-valgus movement.

Although the biological conditions for this modelling are *in vivo*, some assumptions must be considered in order to enable the software to simulate the segment. For the elbow specifically, the joint is considered first to have 6 degrees of freedom and second that its ligaments, tendons and cartilage are modelled as viscoelastic materials (Ozada et al., 2007).

The elbow joint is here seen as a hinge joint with only one degree of freedom and the major movements of the joints, including flexion and extension, are analyzed; hence, small movements such as varus and valgus, must be ignored.

The following equations demonstrate the linear and nonlinear movement equations of the elbow joint:

$$\ddot{x}_i = \frac{F_{xi}}{m_i}, \ddot{y}_i = \frac{F_{y_i}}{m_i}, \ddot{z}_i = \frac{F_{z_i}}{m_i}, \ddot{\theta}_{xi} = \frac{T_{x_i}}{I_{xx_i}}, \ddot{\theta}_{y_i} = \frac{T_{y_i}}{I_{yy_i}}, \ddot{\theta}_{z_i} = \frac{T_{z_i}}{I_{zz_i}}$$

$$\begin{bmatrix} \mathbf{m}_i & 0 \\ 0 & \mathbf{J}_i \end{bmatrix} \begin{Bmatrix} \ddot{\mathbf{x}}_i \\ \ddot{\boldsymbol{\theta}}_i \end{Bmatrix} - \begin{bmatrix} \mathbf{k}_p & \mathbf{k}_p \mathbf{R}_{pi} \\ \mathbf{R}_{pi}^{\mathrm{T}} \mathbf{k}_p & \mathbf{R}_{pi}^{\mathrm{T}} \mathbf{k}_p \mathbf{R}_{pi} \end{bmatrix} \begin{Bmatrix} \mathbf{x}_i \\ \boldsymbol{\theta}_i \end{Bmatrix} + \begin{bmatrix} \mathbf{k}_p & \mathbf{k}_p \mathbf{R}_{pj} \\ \mathbf{R}_{pi}^{\mathrm{T}} \mathbf{k}_p & \mathbf{R}_{pi}^{\mathrm{T}} \mathbf{k}_p \mathbf{R}_{pj} \end{bmatrix} \begin{Bmatrix} \mathbf{x}_j \\ \boldsymbol{\theta}_j \end{Bmatrix} = \begin{Bmatrix} \mathbf{F}_i \\ \mathbf{M}_i \end{Bmatrix}$$

The first step of the preparation for simulating the object is digitalizing the bone for mesh data by applying the Faro Arm which is plugged into the Geometric software. The digitized data are a mixture of points described by triangles, edges and points which need to be converted into mesh data by the use of functionalities of geometric software. In addition, the holes and any surface defects are smoothed to achieve the appropriate mesh surface data.

The mesh data object is then ready to be imported to the MJM software. Other parts attached to the bone, such as ligaments, tendons and cartilage are added to the model. The mechanical properties of each of the segments can be selected from the database table

.

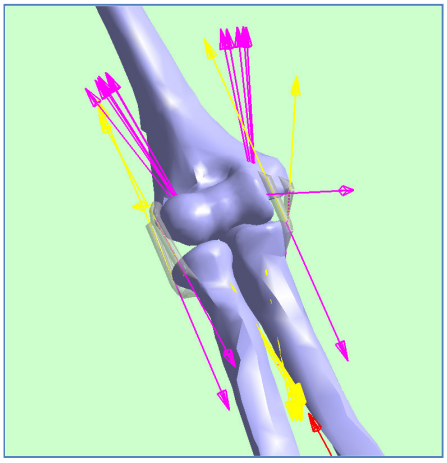

Figure 4-8: Snapshot from MJM software (Ozada et al., 2007)

When the primary assumptions of the simulation have been allowed for, the model is ready for dynamic analysis to run, using inverse and forward dynamic analysis. The following figure is a snapshot of the MJM software during the running of the program.

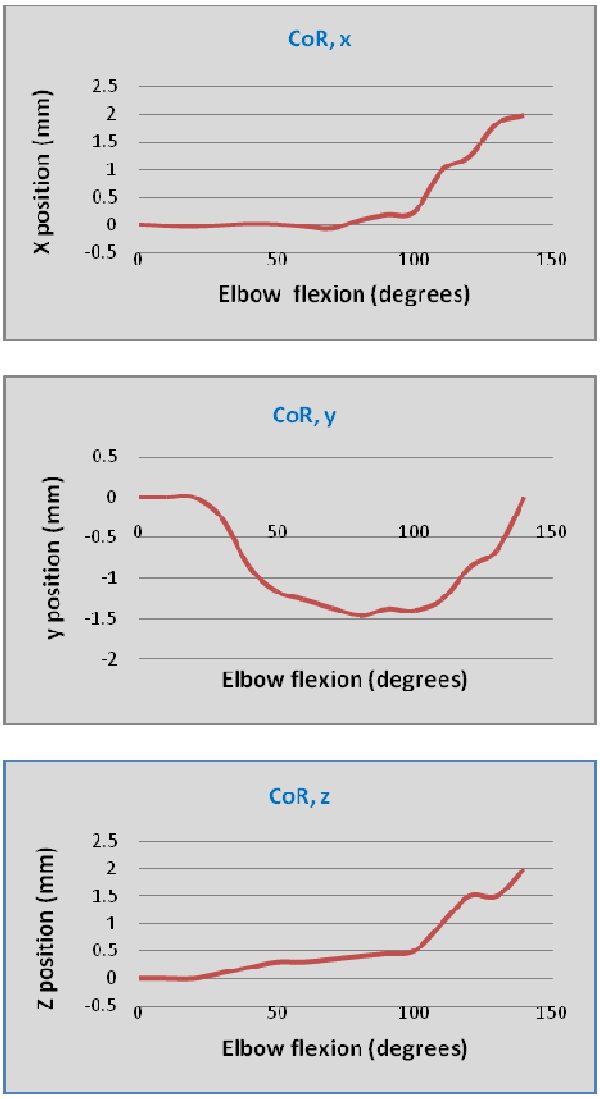

Figure 4-9: Change in the centre of rotations versus forearm flexion (Ozada et al., 2007)

This study demonstrates the importance of accurate measurements, otherwise the result is the incorrect design of the implant. Moreover, since the elbow has translational and rotational movements in 3 directions, any reduction in the degrees of freedom would yield inaccurate measurements of tissue tensions,

moment arms, changes in the centre of rotations and contact forces (Ozada et al., 2007).

4.5 Laser Engineered Net Shaping (LENS)

As noted above, the development of medical implants is being modernized. Beside the classical machinery methods and technologies, new advanced Rapid Prototyping technologies can produce more accurate and complex medical implants. A good example of the available technologies is the highly targeted metal deposition technology named LENS. This technology enables rapid and agile manufacturing and improved design flexibility, repair and remanufacturing. LENS technology also improves the mechanical and material properties of the manufactured implants.

This chapter studies the process of manufacturing modern medical implants by use of LENS technology and focuses on material quality and quality benefits of the implants (Balažic et al., 2008).

Rapid Prototype is considered a high-quality alternative to the classical manufacturing technologies for medical implants which are made of titanium and other biomaterials. RP includes a group of technologies in which the 3-dimensional model of the implant is built from a CAD file without any mediating action. The RP has two categories: technologies adding the material during the prototype building and technologies removing the material during the prototype manufacture (Hollander et al., 2006).

Laser Engineered Net Shaping (LENS) is a laser fabricated technique. Laser technology is widely used and is known for its precise performance. It can be used

for cutting, welding and drilling the implants and provides higher quality and accuracy within a range of 10 μm which increases the efficiency and accuracy of machining (Balažic et al., 2008).

This type of technology produces a fine weld bead and exposes the component to far less heat than conventional techniques without damage to the fundamental layers, due to its smaller and more controlled heat-affected region. Once a geometry and material or material combination has been identified, LENS can rapidly produce a three dimensional prototype with good properties (Griffith et al., 2005).

The 3D CAD model is the basis of the manufacturing process of the modern medical implants. These files are converted to an STL file and, depending on the model, metallic powder is delivered to the melted spot by a nozzle and the shape of the implant is built up [http://www.optomec.com].

In LENS technology the metal is melted by the use of a powerful laser supplied coaxially to the focus of the laser beam through a deposition head. The laser goes through the centre of the head and is focused on a small spot by a couple of lenses. Once one layer is built up, the implant moves vertically and a fresh layer is added on the completed layer(s).

LENS technology has great potential for the design and production of different metal parts. In addition, by using LENS many applications become possible, such as rapid prototyping and the joining of unlike metals. Different materials such as steels can be successfully used for production. Although, the laser source uses

requires a big energy but the high cost of the process is a drawback (Lacalle et al., 2002).

4.6 The Implementation of the Stewart Mechanism to develop implants

The first step in developing an implant is to fully understand the kinematics and kinetics of the elements and the joints. Our new mechanism will be very helpful in this regard. With it, mechanism the range of joint movements in different directions can be measured and the centre of rotation of the joint can be repeatedly calculated. In the second step, it is possible with these results to design a primary schematic of implants, thanks to design software.

Finally after prototyping the first model, the new mechanism can be used to measure the capacity and range of movement of the implant in *in vivo* as well as *in vitro* conditions. With this method we can measure how the designed implant will mimic the normal joint. With this mechanism we can also improve the designed implants so as to find their limitations on movement and their range, in comparison to that of normal joints.

Chapter 5. Design, Analysis and Simulation of Stewart Platform Mechanism

5.1 Introduction

Different devices are appropriate to different kinds of measurement. Before using a device one must make sure that it is appropriate to the measuring the desired movement. For example, a system with cameras and markers will be used to measure the general movement of the body during an exercise, whereas a joint angle sensor will be used to measure the rotation of one particular joint. The system of measurement must be chosen not only according to what movement should be measured, but also to the level of accuracy required. Moreover not all devices offer the same accuracy. Therefore, one must be aware of results with limitations.

Furthermore, one must be aware of the problems presented by different devices. For example, a system with video does not record some movements very accurately. Since it needs markers placed on the skin, the measurement detects the movements of the skin but not the underlying movements of the bones. Consequently, this system would not measure elbow movements well, elbow laxity in particular.

The joint angle sensor is a practical device which can quickly be fixed to the joint, but is not very accurate. Not only are human joints complex and often capable of motion in more than one plane, but also because in movement the centre of rotation moves. The elbow, for example, has a centre of rotation which

moves during flexion. Therefore, the joint angle sensor cannot deal well with elbow movement, but would suit only simple rotations in one plane about one fixed axis of rotation. It provides good approximations but not very accurate results.

Moreover the method used by Mihata et al. (2008) was applied only to cadavers (in *in vitro* conditions) unlike the case in this paper (requiring *in vivo* conditions). This method could be used for clinical purposes to diagnose joint laxity and other diseases which limit joint movements.

To follow the movement of the elbow joint, one must know the movement of the bones in order to understand the displacement of each bone. In addition, the device used should measure all the possible movement for a joint, not only that in a specific plane. Knowledge about the displacement of the bones is needed to design prostheses which match as far as possible the actions of a healthy elbow.

To overcome these difficulties we used the Stewart Platform mechanism. With this mechanism, on the one hand, all six degrees of freedom in the elbow joint can be measured and, on the other hand, we can use it to gain reliable data about the movement of the bones by attaching the arm as securely as possible.

The first part of this chapter introduces the Stewart mechanism, while the second part introduces the system which we designed to measure the movements of the elbow joint. In the next step, we show how this mechanism can measure all six degrees of freedom for this joint and to end with, we discuss the calibration of the mechanism.

5.2 Stewart Platform Mechanism

The Stewart Platform originally intended to be used as a flight simulator in 1965, is a simple device to track a motion (Stewart, 1965). A schematic of a Stewart Platform is shown in Figure 5-1.

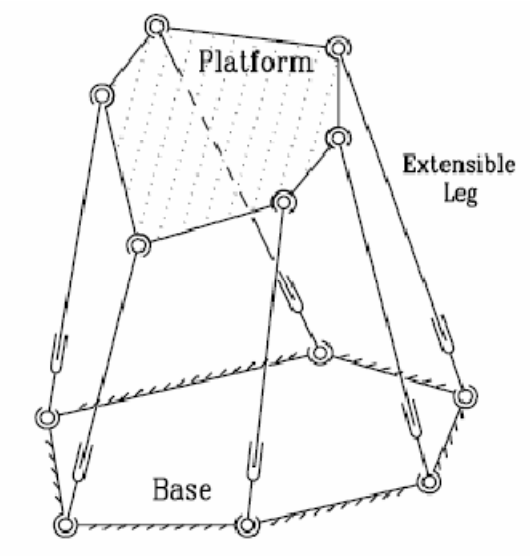

Figure 5-1: General Stewart Platform

The Stewart Platform is one of the most popular manipulator devices. It is a six degree-of-freedom positioning system which consists of a moveable plate, a fixed plate and six wires linking the plates.

Gough (1962) had earlier suggested a structure similar to Stewart's model, as a machine for testing tyres. In his system there are six actuators in parallel resulting in a fully parallel actuated mechanism, as shown in Figure 5-2. Gough was the first one to realize the benefits of this kind of manipulator structure; however, the present research began with a paper by Stewart. The traditional name of this

structure is the Stewart Platform, but it is sometimes also referred to as the Stewart-Gough Platform (Dasgua and Mruthyunjaya 2000).

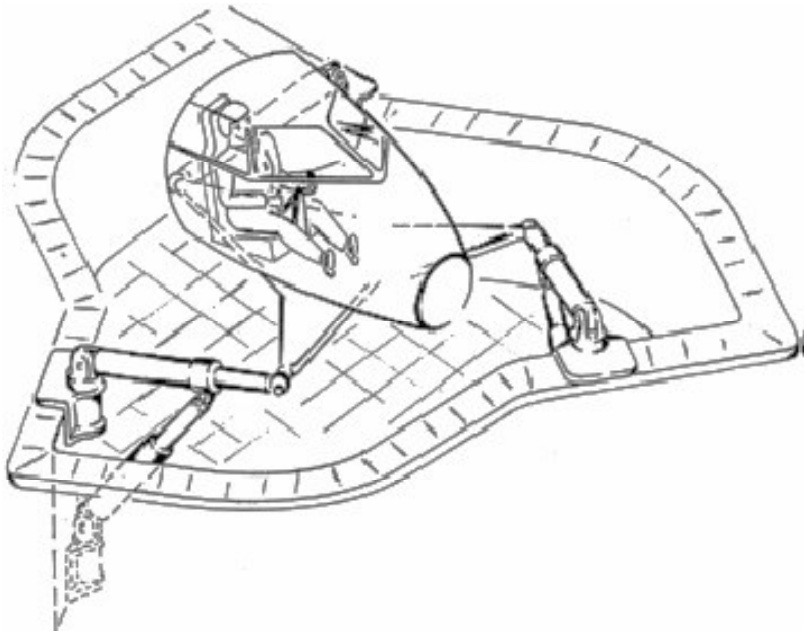

Figure 5-2: Schematic of the original "Stewart Platform" by Stewart (Proc. IMechE, 1965-66).)

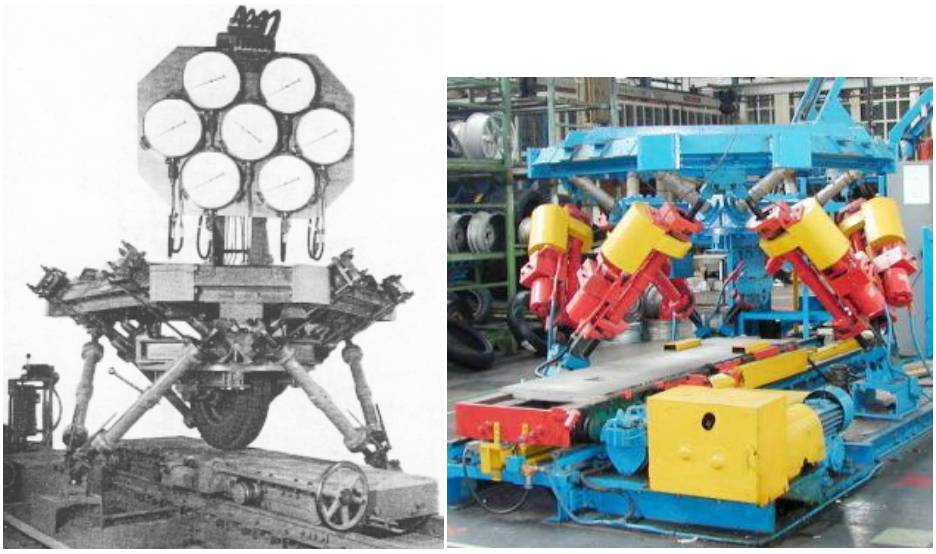

Figure 5-3: The first octahedral hexapod or the original Gough platform at birth in 1954 (Proc. IMechE, 1965-66) and shortly before retirement in 2000 (courtesy of Mike Beeson, Dunlop Tyres).

For about 15 years from the time it was proposed, no interest was shown in this mechanism, until Hunt described the advantages of using parallel manipulators. After 1983, researchers acknowledged its high load capacity and precise positioning capabilities and started to make detailed analyses of its structure. Today's popular parallel manipulator, known as the Stewart Platform, has reached a generalized form which consists of six linear actuators connected to the base with spherical or universal joints and to the moving platform with spherical joints (Hunt, 1983). From the 1980s, the Stewart Platform gained popularity, mainly because of the advantages of parallel manipulators over serial ones (Dasgua and Mruthyunjaya 2000).

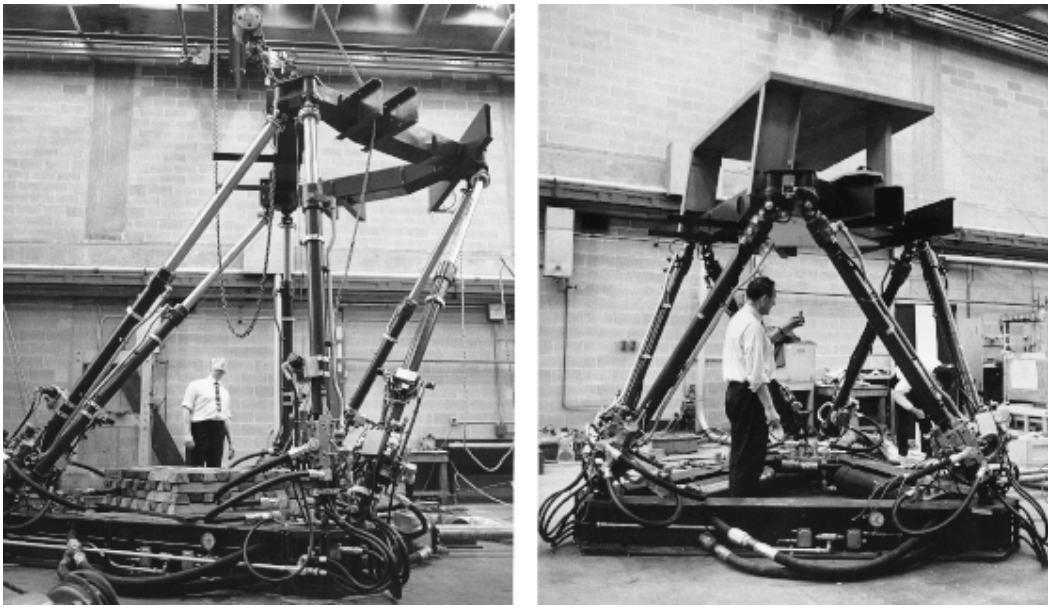

Figure 5-4: The first flight simulator based on an octahedral hexapod in the mid-1960s (courtesy of Klaus Cappel)

Parallel manipulators have been used since the 1980s wherever high load carrying and precise positioning capability are needed. Since its inception, it has been used as a flight simulator, but a wide range of applications has also benefited from using it. As well as the industries listed above, the platform has recently been used in medical applications because of its precise positioning capability. A history and description of the uses of this device followed by a discussion of different designs and commercial products has been written by du Plessis (1999).

5.3 Designing a platform based on Stewart mechanism

5.3.1 Principles

In this study, a platform based on the Stewart mechanism was developed for measuring the elbow kinematics. The Stewart Platform includes a fixed table and a moving plat linked to the fixed table by six legs, the lengths of which can be changed. Since there are six legs, the Stewart Platform can be used to position the platform for six degrees of freedom (discussed below). In other words, with this mechanism any position of the platform can be inferred by measuring the length of the legs. The legs consist of wires between the base and the platform (see Figure 5-5).

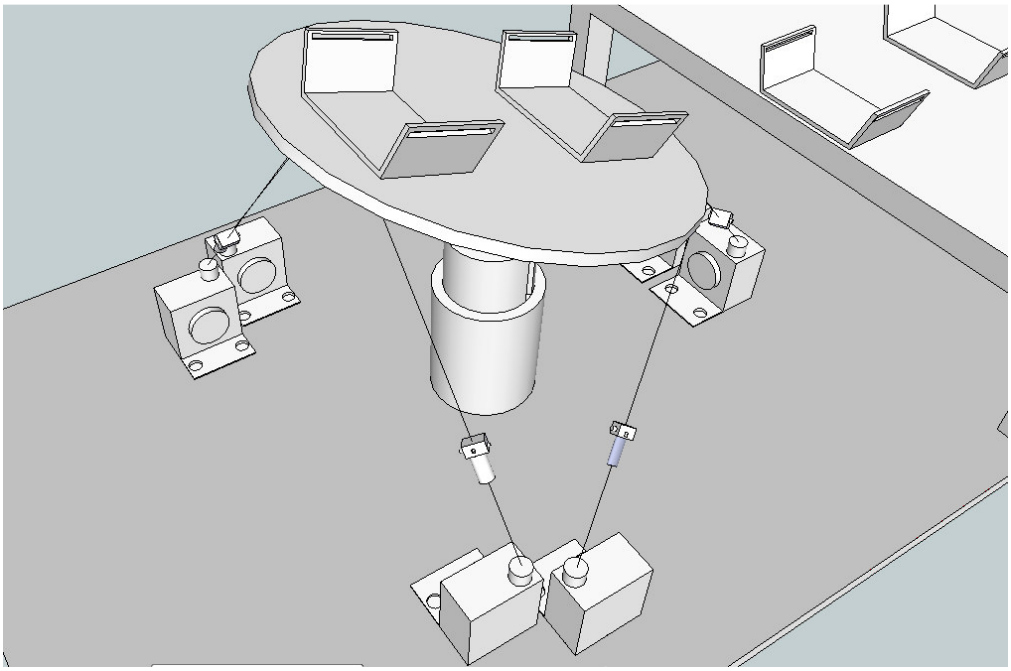

Figure 5-5: wires to connect platform to the base

To measure elbow joint movements, this system controls the position of the forearm in relation to the position of the arm. The arm is fixed to a plate linked to

the base and the forearm is fixed to the platform. Six degrees of freedom of the forearm can be defined by knowing the position and the orientation of the forearm at six different points on the platform related to a fixed base.

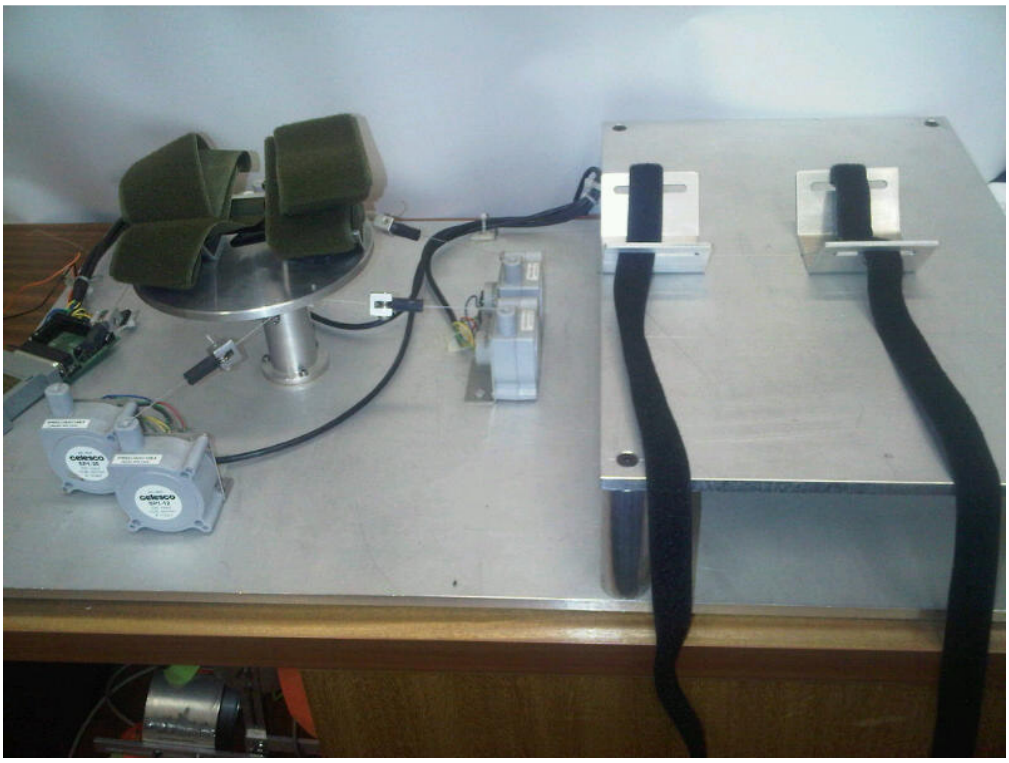

Figure 5-6: Stewart Platform Based Elbow Joint Measurement Device

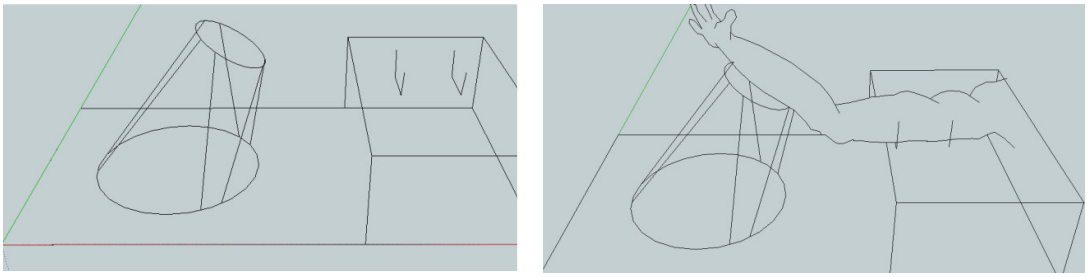

Figure 5-7: Platform principle

5.3.2 Assembly

Figure 5-8 shows the complete assembly of the Stewart Platform. To ensure optimum accuracy and ease of manipulation in obtaining the measurements,

several major precaution should be taken as the platform is assembled, namely, a) the fixing of the wire; b) the positioning of the string pot; c) the securing of the arm; and d) the initialization of the platform positioning.

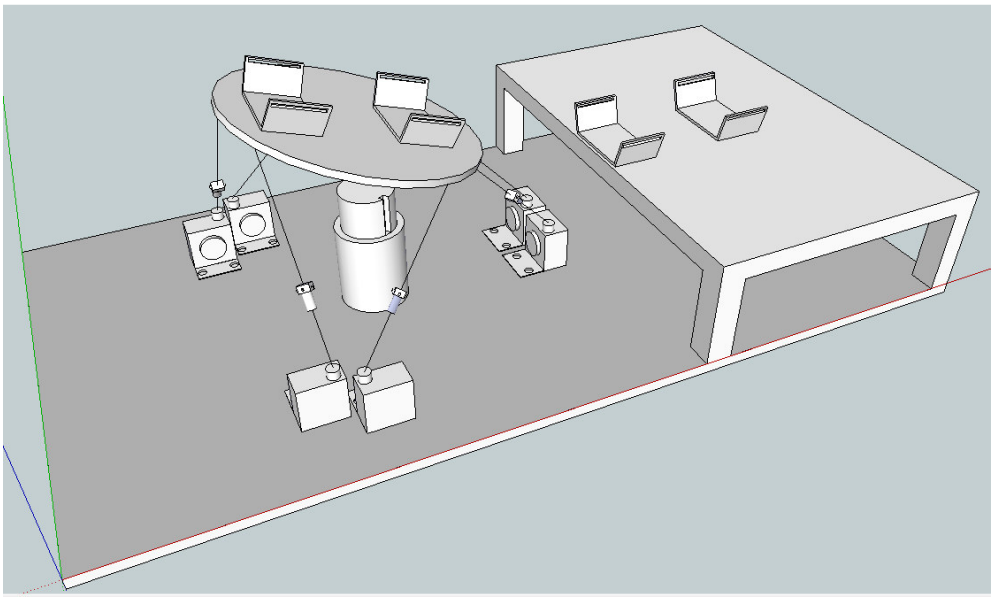

Figure 5-8: Schematic image of the complete assembled Stewart Platform

5.3.3 Wire fixation

The wires on the platform must be fixed to allow free rotation. If the attachment on the platform is not in line with the position of the string pot on the base, the attachment will inevitably rotate. To solve this problem, a part is added at the end of the wire.

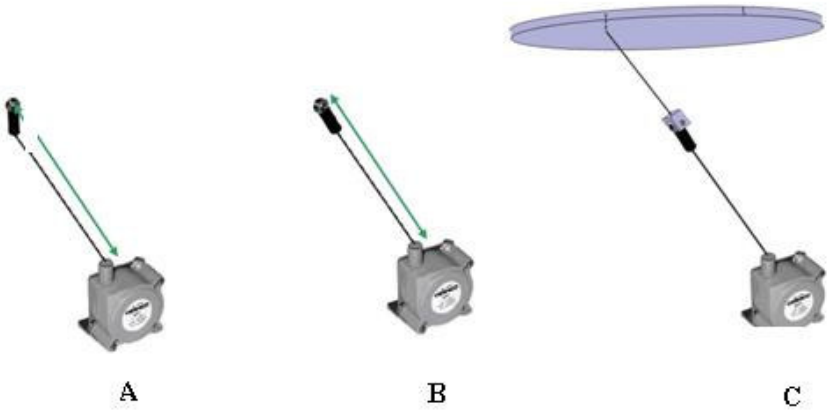

Figure 5-9: Correct arrangement of wire fixation to ensure easy manipulation for taking measurements (picture A bad fixation, Picture B and C are the correct fixation)

5.3.4 String pot position on the base platform

As shown above, the attachments of the six wires (on the base and on the platform) must be positioned around two circles Cb and Cp. Therefore, the position of the fixed string pots must be calculated precisely.

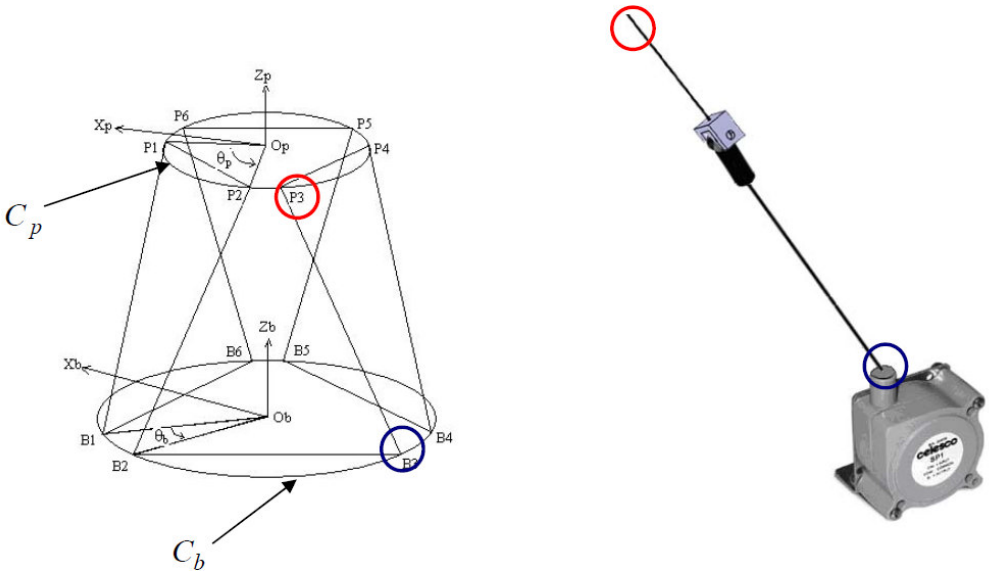

Figure 5-10: Position of the attachments

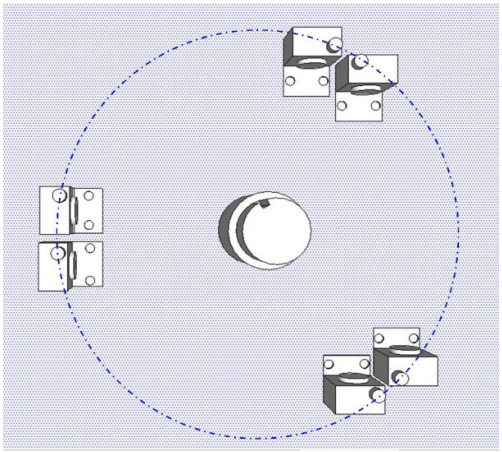

Figure 5-11: String pot positioning on the platform

5.3.5 Arm fixation

This is a most important point. Errors in the results of most measurement systems are mainly caused by lack of care here. The arm should be fixed securely to ensure that as far as possible the skin must not move around bones. A V-shaped

device with straps is used. Two are used to secure the arms and two others are used for the forearm.

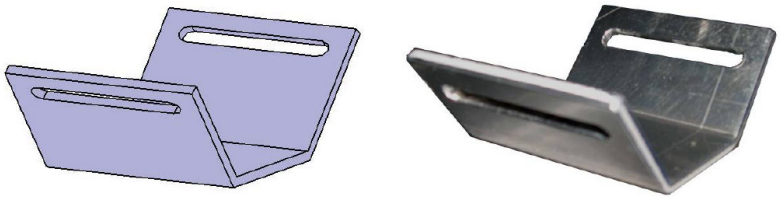

Figure 5-12: The design and the manufactured part of the arm fixations

5.3.6 Initial position of the platform

If our measurements are to be repeatable, we should have a reference point for all measurements. In other words, before taking any measurements, the platform must be in a known position. Therefore a system is designed to fix the platform in the same position before starting every test. Once the first set of data are measured, we can translate the top of the stand inside the bottom part to make our movements with no obstacles.

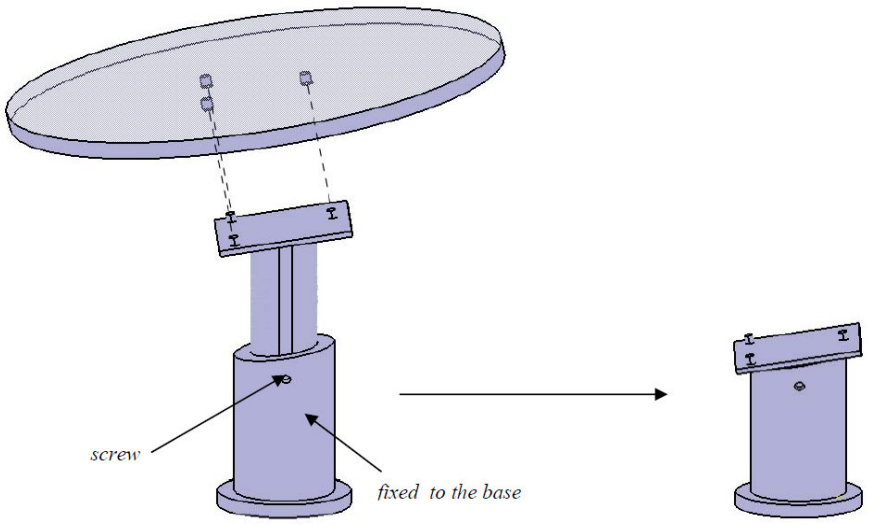

Figure 5-13: Platform initialization

5.3.7 Measuring device

To measure elbow movements, the position of the platform needs to be determined with a knowledge of the length of the six wires. With this, thanks to a system of equations, the position and the orientation of the platform can be determined.

Figure 5-14: Celesco string Pot (SPI)

An important part of this system is a device, which, must be very accurate, to enable us to measure the length of the wires. Because almost all the precision of the system depends on the measurement of the wires, a system which will offer good accuracy must be chosen and the Celesco SP1 String Pot was chosen. This device uses flexible cable, a spring-loaded spool and a potentiometer to measure linear position.

The SP1 offers different ranges of measurement. Three different SP1s are used according to the length that they must measure. The SP1 near the elbow will measure short displacements, whereas those far from the elbow (thus, nearer the

hand) will measure bigger displacements. Table 5-1 shows the Celesco information

Table 5-1: Celesco information

Item Number	SP1-4	SP1-12	SP1-25
Full stroke range	4.75 in	12.5 in	25 in
Accuracy (% of f.s.t)	1.00 %	0.25 %	0.25 %
Potentiometer cycle life	2.5 M cycles	500 K cycles	500 K cycles
Cable tension (+/- 25 %	7 oz	7 oz	7 oz

This potentiometer will give an output voltage proportional to the length of the cable. The calibration of the device will enable the wire length to be directly inferred from the output voltage, as shown in Figure 5-15.

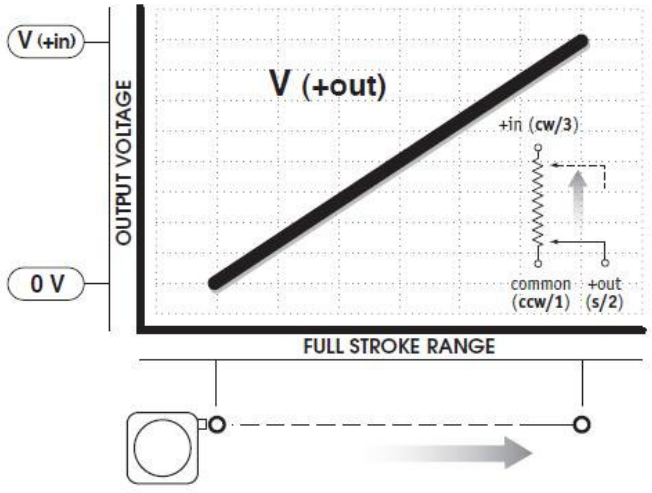

Figure 5-15: Output signal

The forearm and the upper arm are placed on either the mobile or the fixed platforms and firmly anchored by belts. The mobile platform consists of a metal

plate with six cords attached to it. When the forearm is moved, the length of the cords changes and this is registered by the sensors by the relationship of the cords to the fixed platform. Therefore the positions of the forearm are compared in relation to those of the upper arm. One cord-senor unit allows one degree of freedom and hence six cords can measure six. The data from the sensors are measured as the lengths of cords vary in motion in relation to a reference length. These devices are effectively rotational potentiometers.

5.3.8 Monitoring and recording hardware and software

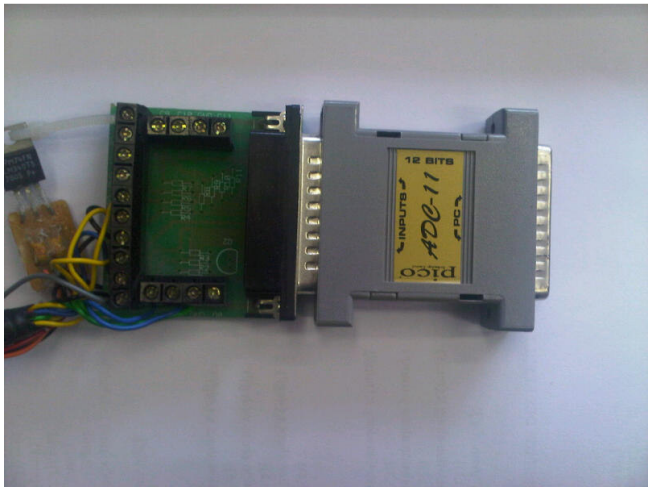

Figure 5-16: The "Pico" data logger (adc-11)

Thanks to the Pico data logger and Lab-View as data acquisition hardware and software respectively, the output voltage of each device can be read directly. During measurement, the data for each device can be visualized. The output voltage and length of the wires are shown for each device on the six diagrams, as shown in Figure 5-17. The Block-Diagram in Lab-View as follows.

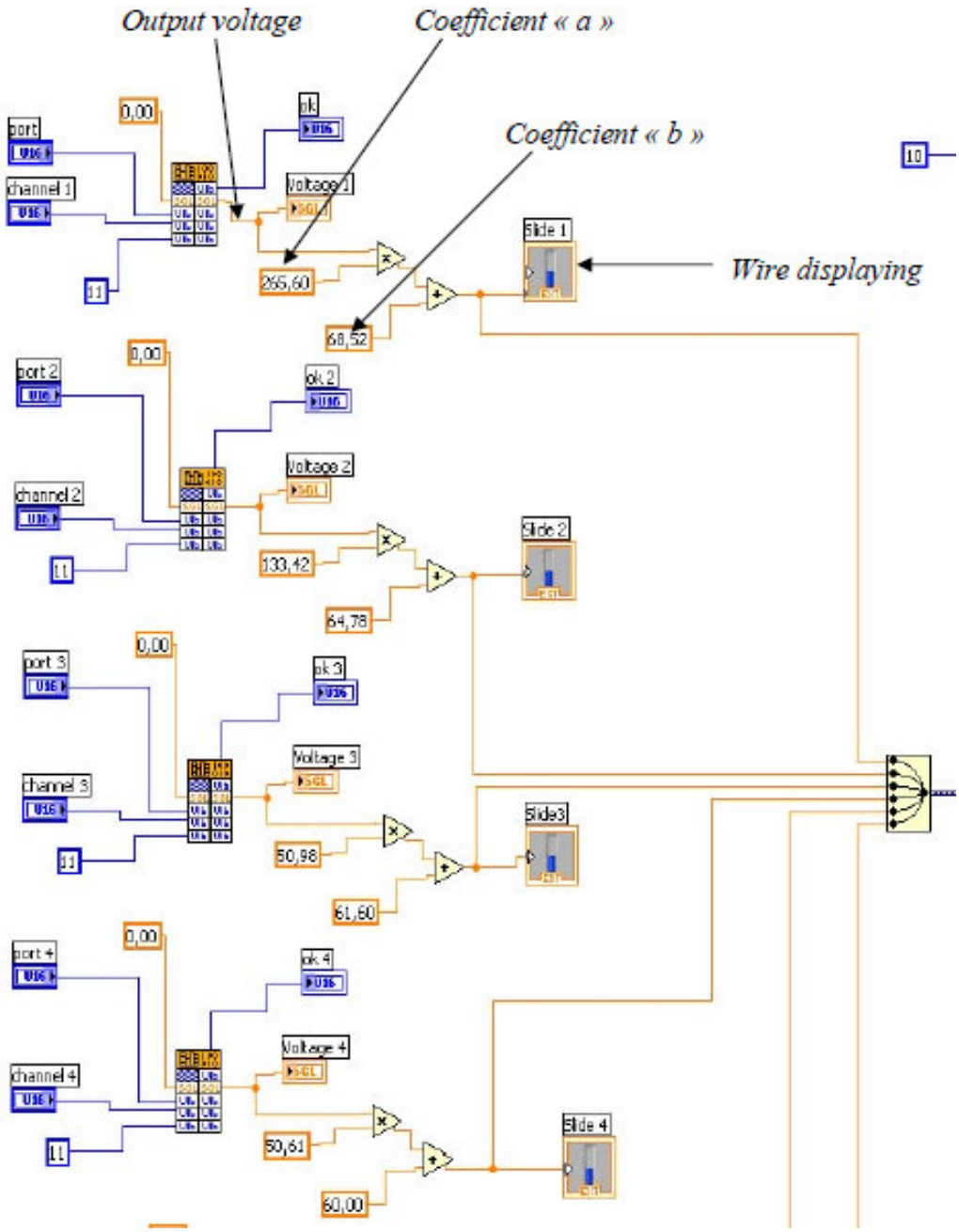

Figure 5-17: Block diagram in Lab-View software (only for four out of six wires are shown in the diagram)

As can be seen, in the bock diagram, the voltages from our sensors convert to elongation by receiving a related coefficient which we calculated in the

calibration process. Then these results are saved in Excel software for further calculation.

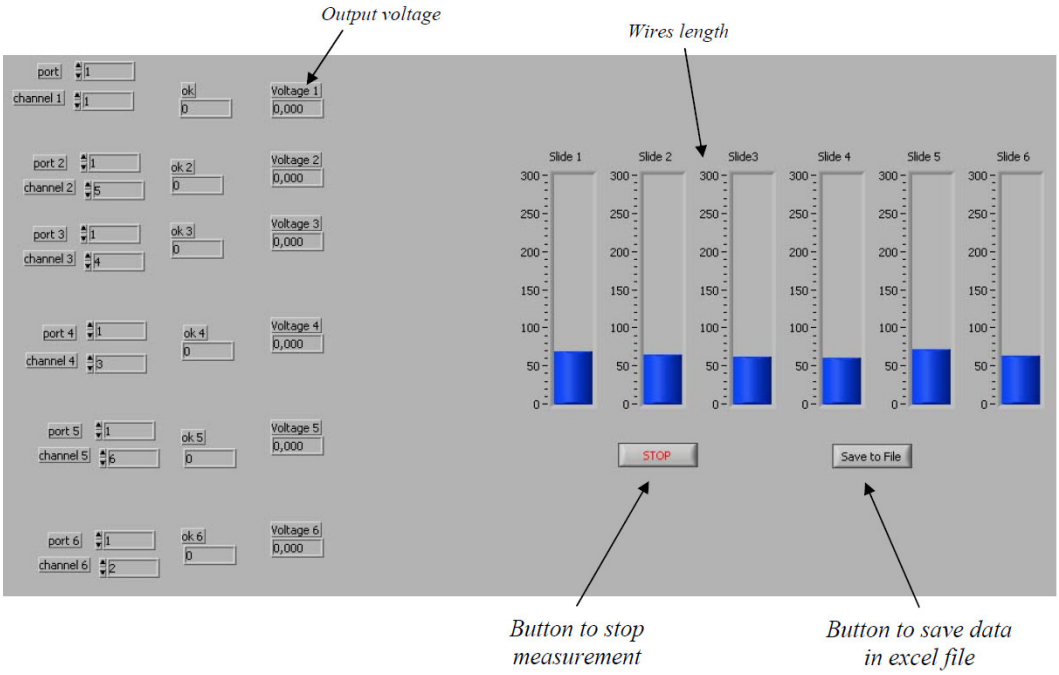

Figure 5-18: Lab-View Visualization

In the next step, the saved data are transferred to Matlab Simmechanics (Mathworks, Natick, MA, USA) to calculate the centre of rotation of the joint. This program can simulate the dynamics and kinematics of the joint. That is to say, during any movement of the elbow, all the lengths of each wire are saved in a file. Labview is programmed to take measurements every 10ms. Figure 5-20 illustrates the block diagram of measurements of the elbow kinematics using the Stewart Platform.

Another interest of this device is to measure the centre of rotation of the elbow joint during flexion. The centre of rotation is assumed to move during flexion,

with respect to the platform. The pattern of the centre of rotation can be measured using the SP

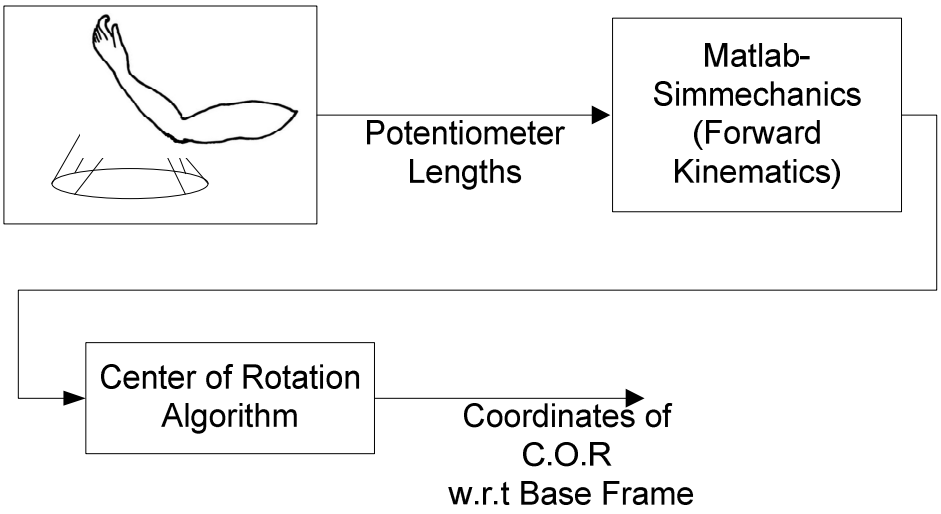

Figure 5-19: Measurement steps of the Stewart Platform

5.4 Assessing the centre of rotation and its radius

Three displacement and rotational parameters of SP are listed in Table 5-2.

Table 5-2: Three displacement and rotational parameters of SP

X	Translational displacement of SP through axis X
Y	Translational displacement of SP through axis Y
Z	Translational displacement of SP through axis Z
γ	Rotational displacement of SP along axis X
β	Rotational displacement of SP along axis Y
α	Rotational displacement of SP along axis Z

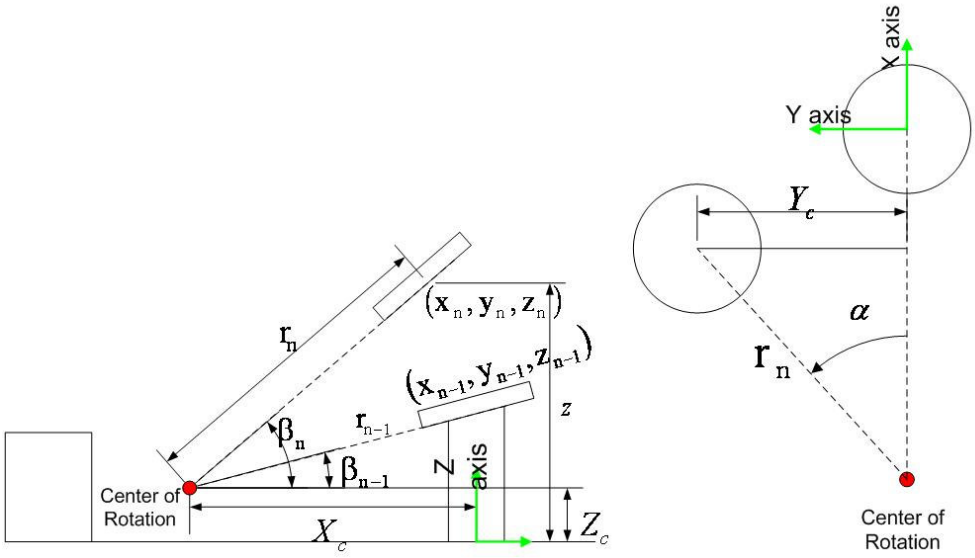

Figure 5-20: Side view of the experimental setup (left) and displacement of the centre of rotation during valgus and varus motion on the YX plane (right)

In the side view of the experimental setup (Figure 5-20), subscript "n" illustrates the nth position of the mobile plate of the SP and subscript "n-1" shows the previous position of the SP. Assuming a displacement with β angle (see Figure 5-20), the relation between displacement and the angle of motion can be given as:

$$r_n \sin(\beta_n) = z_n - Z_c$$
$$r_{n-1} \sin(\beta_{n-1}) = z_{n-1} - Z_c$$
$$r_n \cos(\beta_n) = x_n - X_c$$
$$r_{n-1} \cos(\beta_{n-1}) = x_{n-1} - X_c$$

In this equation system, there are 4 unknown variables (r_n, r_{n-1}, X_c, Z_c) and 4 equations. From these systems of equations a radius of rotation can be calculated.

First, eliminate the unknown

$$z_c = z_n - r_n \sin\beta_n \tag{5.1}$$

$$z_c = z_{n-1} - r_{n-1} \sin\beta_{n-1} \tag{5.2}$$

$$x_c = x_n - r_n \cos\beta_n \tag{5.3}$$

$$x_c = x_{n-1} - r_{n-1} \cos\beta_{n-1} \tag{5.4}$$

$$z_n - r_n \sin\beta_n = z_{n-1} - r_{n-1} \sin\beta_{n-1} \tag{5.5}$$

$$x_n - r_n \cos\beta_n = x_{n-1} - r_{n-1} \cos\beta_{n-1} \tag{5.6}$$

From Equation (5.6) we can obtain r_{n-1} as;

$$\frac{-x_n + r_n \cos\beta_n + x_{n-1}}{\cos\beta_{n-1}} = r_{n-1} \tag{5.7}$$

Import r_{n-1} to Equation (5.5)

$$z_n - r_n \sin\beta_n = z_{n-1} - \left(\frac{-x_n + r_n \cos\beta_n + x_{n-1}}{\cos\beta_{n-1}}\right).\sin\beta_{n-1} \tag{5.8}$$

Expand this equation;

$$z_n - r_n \sin\beta_n = z_{n-1} - \frac{-x_n.\sin\beta_{n-1} + r_n \cos\beta_n.\sin\beta_{n-1} + x_{n-1}.\sin\beta_{n-1}}{\cos\beta_{n-1}} \tag{5.9}$$

Multiplying two sides by $(\cos\beta_{n-1})$;

$$\begin{aligned} &z_n.\cos\beta_{n-1} - r_n \sin\beta_n.\cos\beta_{n-1} = z_{n-1}.\cos\beta_{n-1} + x_n.\sin\beta_{n-1} \\ &- r_n \cos\beta_n.\sin\beta_{n-1} - x_{n-1}.\sin\beta_{n-1} \end{aligned} \tag{5.10}$$

$$r_n \cos\beta_n . \sin\beta_{n-1} - r_{n-1} . \sin\beta_{n-1} . \cos\beta_{n-1} = z_{n-1} \cos\beta_{n-1} + x_n \sin\beta_{n-1} - x_{n-1} \sin\beta_{n-1} - z_n \cos\beta_{bn-1} \quad (5.11)$$

$$r_n(\cos\beta_n . \sin\beta_{n-1} - \sin\beta_n . \cos\beta_{n-1}) = \cos\beta_{n-1}(z_{n-1} - z_n) + \sin\beta_{n-1}(x_n - x_{n-1}) \quad (5.12)$$

Finally, the radius of rotation r_n can be shown as

$$r_n = \frac{\sin(\beta_{n-1})(x_n - x_{n-1}) + \cos(\beta_{n-1})(z_{n-1} - z_n)}{\cos(\beta_n)\sin(\beta_{n-1}) - \sin(\beta_n)\cos(\beta_{n-1})} \quad (5.13)$$

The displacement of the centre of rotation (COR) is related to joint anatomy. In living organisms, the centre of joint rotation cannot be determined easily because of the varying tissue dynamics caused by the skin, subcutaneous fat and muscle surrounding the bony architecture. However, it is possible to get information about the joint laxity of the human elbow joint from the valgus-varus motion of the forearm. The motions of flexion and extension cannot give significant information about joint laxity because of the degree of freedom allowed by the elbow. Valgus-varus motion is more discriminative and relates clinically to laxity. Other rotational motion, such as postero-lateral motion, which is an important component of the postero-lateral instability seen in lateral elbow ligamentous injury, can be obtained by the SP.

Valgus-varus motion is related to the position of the SP in XY plane. As shown in Figure 5-20, α describes the range of motion. The displacement of COR in axis X can be calculated from the geometric relations in the triangle:

$$X_c = x_n - r_n \cos(\beta_n) \quad (5.14)$$

From the same geometric relations, it is possible to find COR in axis Y and Z.

$$Y_c = y_n - r_n \sin(\alpha_n) \quad (5.15)$$

$$Z_c = z_n - r_n \sin(\beta_n) \tag{5.16}$$

5.5 Quantifying the platform

It was mentioned that, with this system, the position and orientation of the platform can be controlled by measuring the length of the legs. In other words, with this mechanism it is possible to know any position of the platform at random by measuring the length of the legs.

5.5.1 Evaluating degrees of freedom of the platform

To know the six degrees of freedom of the platform at any time, we must formulate equations which enable to find the position of the platform from the length of the wires.

First, we must the problem from the other side. That is to say, we must set up equations which enable us to calculate the length of the wires for any given position and orientation of the platform.

In this case, there are six unknowns' l_i (l_1, l_2, l_3, l_4, l_5, l_6). The purpose is to find l_i for a given position and orientation of the platform $(x, y, z, \alpha, \beta, \gamma)$.

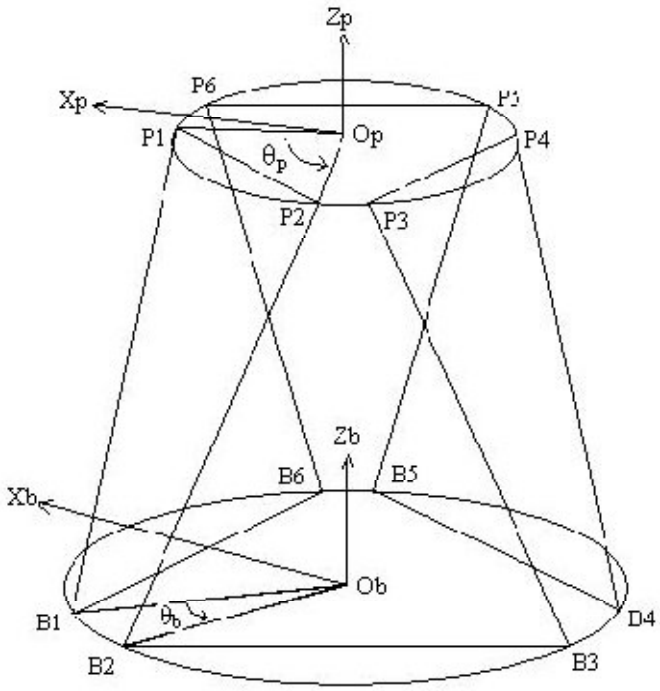

Figure 5-21: Coordinate system

In figure 5-21 B stants to Base of the platform and P stants to moving platform >First, two coordinate frames {P} and {B} are created. They are each linked to the base and to the platform. The origin of frame {P} is located at the centre of the platform, the Z_p axis is pointing upward and the X_p axis is the bisecting line of the angle, (O_P P_6-O_P p_1). The origin of frame {B} is located at the centre of the base, the Z_b axis is pointing upward and the X_b axis is the bisecting line of the angle (O_b B_6-O_b B_1).

These two coordinate frames will enable us to determine the position of the links attachments on the base (B_1, B_2, B_3, B_4, B_5, B_6) and on the platform (P_1, P_2, P_3, P_4,

P_5, P_6). Angle (O_pP_1, O_pP_2) is denoted by θ_p. Angles (O_pP_1, O_pP_3), (O_pP_3, O_pP_5) and (O_pP_5, O_pP_1) are each equal to 120°.

Similarly, angle (O_bP_1, O_bP_2) is denoted by θ_b. Angles (O_bB_1, O_bB_3), (ObB3, ObB5) and (OpP5, OpP1) are equal to 120°.

Angle (X_p, O_pP_i) is denoted λ_i and angle (X_b, O_bB_i) is denoted as Λ_i for i = 1,2,…,6.

Therefore we have:

$\Lambda_i = 60i - \theta_b/2$ and $\lambda_i = 60i - \theta_p/2$ i = 1, 3, 5

$\Lambda_i = \Lambda_{i-1} + \theta_b$ and $\lambda_i = \lambda_{i-1} + \theta_p$ i = 2, 4, 6

Furthermore:

$^{P}p_i = \{p_{ix}, p_{iy}, p_{iz}\}^T = \{r_p*\cos(\lambda_i), r_p*\sin(\lambda_i), 0\}^T$ for i = 1, 2, …, 6

→ describes the position of the point Pi with respect to frame {P}.

$^{B}b_i = \{b_{ix}, b_{iy}, b_{iz}\}^T = \{r_b*\cos(\Lambda_i), r_b*\sin(\Lambda_i), 0\}^T$ for i = 1, 2, …, 6

→ describes the position of the point Bi with respect to frame {B}.

where r_b and r_p represent respectively the radius of the base and the radius of the platform. Now, the length l_i of one wire *i* can be calculated:

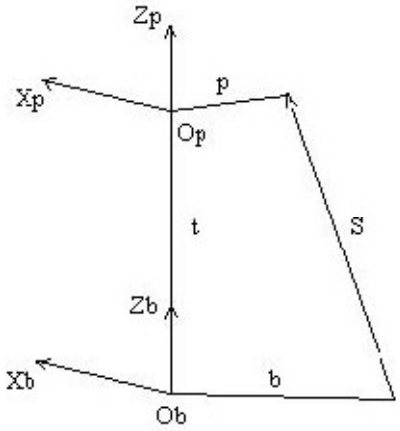

Figure 5-22: Link length

The length l_i of vector ${}^{B}S_i$ can be expressed by $l_i = \sqrt{(S_{ix}^2 + S_{iy}^2 + S_{iz}^2)}$.

The length of vector ${}^{B}S_i = \{S_{ix}, S_{iy}, S_{iz}\}^T$ with respect to frame {B} can be broken down into:

$${}^{B}S_i = -{}^{B}b_i + {}^{B}t + {}^{B}p_i$$

- ${}^{B}b_i = \{b_{ix}, b_{iy}, b_{iz}\}^T = \{r_b * \cos(\Lambda_i), r_b * \sin(\Lambda_i), 0\}^T$
- ${}^{B}t = \{x, y, z\}^T$ represents the position of the origin of frame {P} with respect to frame {B}. That is to say, it represents the position of the centre of the platform with respect to frame {B}.
- ${}^{B}p_i = . R_{BP} {}^{P}p_i .$ It is the orientation matrix representing the rotation of frame {P} with respect to frame {B}.

$$ {}^{B}_{R}R = \begin{bmatrix} \cos\alpha\cos\beta & \cos\alpha\cos\beta\sin\gamma - \sin\alpha\cos\gamma & \cos\alpha\sin\beta\cos\gamma + \sin\alpha\sin\gamma \\ \sin\alpha\cos\beta & \sin\alpha\sin\beta\sin\gamma + \cos\alpha\cos\gamma & \sin\alpha\sin\beta\cos\gamma - \cos\alpha\sin\gamma \\ -\sin\beta & \cos\beta\sin\gamma & \cos\beta\cos\gamma \end{bmatrix} $$

(5.17)

where

- α is the rotation of frame {P} with respect to frame {B} about the Z_b.
- β is the rotation of frame {P} with respect to frame {B} about the Y_b.
- γ is the rotation of frame {P} with respect to frame {B} about the X_b.

Therefore:

$$B_{P_i} = \begin{bmatrix} \cos\alpha\cos\beta * rp * \cos(\lambda_i) + (\cos\alpha\sin\beta\sin\gamma - \sin\alpha\cos\gamma) * rp * \sin(\lambda_i) \\ \sin\alpha\cos\beta * rp * \cos(\lambda_i) + (\sin\alpha\sin\beta\sin\gamma + \cos\alpha\cos\gamma) * rp * \sin(\lambda_i) \\ -sin\beta * rp * \cos(\lambda_i) + cos\beta\sin\gamma * rp * \sin(\lambda_i) \end{bmatrix}$$

(5.18)

The length of the wire can be calculated as follows:

$$l_i = \sqrt{S_{ix}^2 + S_{iy}^2 + S_{iz}^2} \quad \text{or} \quad l_i^2 = S_{ix}^2 + S_{iy}^2 + S_{iz}^2 \tag{5.19}$$

If we replace ${}^{B}S_i$ by $-{}^{B}b_i + {}^{B}t + {}^{B}p_i$ the following expression can be found:

$$l_i^2 = x^2 + y^2 + z^2 + r_p^2 + r_b^2 + 2\left(r_{11}p_{ix} + r_{12}p_{iy}\right)(x - b_{ix}) + 2\left(r_{21}p_{ix} + r_{22}p_{iy}\right)\left(y - b_{iy}\right) + 2\left(r_{31}p_{ix} + r_{32}p_{iy}\right)(z) - 2\left(xb_{ix} + yb_{iy}\right) \text{ for } i=1,,,,6 \tag{5.20}$$

It is a system of equations which gives the lengths of the six wires l_i from the position and orientation of the platform *(x, y, z, α, β, γ)*. However, regarding the project, the opposite is required. That is to say, it is the position and orientation of the platform *(x, y, z, α, β, γ)* which must be found from the lengths of the six wires l_i. Therefore a set of six simultaneous non-linear equations must be solved. To work out the solution, the Newton method is used.

5.5.2 Newton- Rephson Method

A simple equation with the form F(X) = 0 can be solved by the Newton method:

X_0 is chosen as the start point.

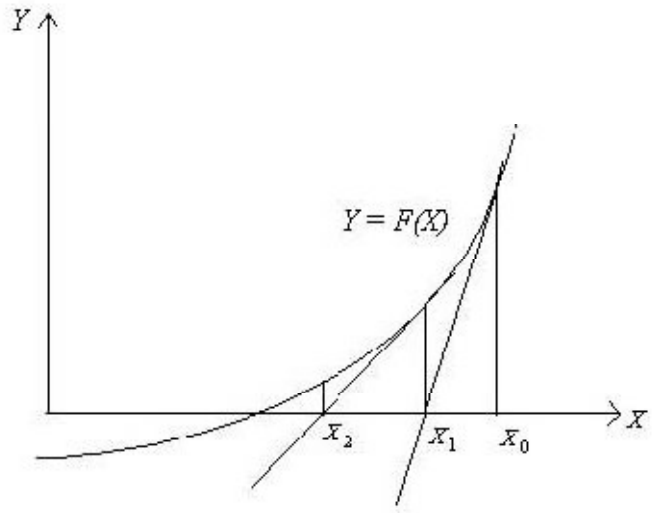

Figure 5-23: Newton method

If F is derivable in X_0, the equation of the straight line tangent to F in X_0 is:

$Y = F'(X_0)*(X - X_0) + F(X_0)$

X_1 can be found thanks to this equation by replacing X by X_1 and Y by 0:

$0 = F'(X_0)*(X_1 - X_0) + F(X_0)$

$$X_1 = X_o - \frac{F(X_0)}{F'(X_0)}$$

X_1 is nearer to the solution than X_0. The same procedure is used to find X_2. By iteration, $X_3, X_4, X_5, \ldots$ are found. The iteration is stopped when an approximation near the solution is reached.

This was the case with a simple equation. Even when a system of equations needs to be solved, the procedure is essentially the same:

In this case $F(X) = (F_1(X)...., F_6(X))$

where X,=z, y, x, α, β, γ and:

$$F_i(X) = x^2 + y^2 + z^2 + r_p^2 + r_b^2 + 2\left(r_{11}p_{ix} + r_{12}p_{iy}\right)(x - b_{ix}) + 2\left(r_{21}p_{ix} + r_{22}p_{iy}\right)\left(y - b_{iy}\right) - 2\left(xb_{ix} + yb_{iy}\right) - l_i^2 \quad (5.21)$$

The matrix is defined by**:**

$$J_{ij}(X) = \frac{dF_i}{dX_j}(X) \text{ for } \forall\{i,j\} \subset \{1,\ldots,6\} \quad (5.22)$$

$\{X^{(n)}\}_{n\geq 0}$ is defined by

$$\left\{\begin{array}{c} X^{(0)} = (x_0, y_0, z_0, \alpha_0, \beta_0, \gamma_0) \\ X^{(n+1)} = X^{(n)} - \left[J\left(X^{(n)}\right)\right]^{-1} F(X^{(n)}) \end{array}\right\} \quad (5.23)$$

This method is called the Newton-Raphson method. The approximation of the solution is found by iteration. Iterations stop when the approximation is near the solution. A convergence criterion must then be established:

Iterations stop when $|F_i(X)| < \varepsilon$ for i = 1,2,…,6

ε is chosen arbitrarily.

5.5.3 A second way to find the centre of rotation

Another advantage of this platform is that is can measure the centre of rotation of the platform. Therefore, with this device, not only can the six degrees of freedom of the elbow be measured but also the centre of rotation of the elbow during flexion. Even though the centre of rotation is assumed to move during flexion,

thanks to the platform, the exact position of the centre of rotation and the direction of the axis of rotation can be measured.

The following expression gives the relationship between v, ω and r.

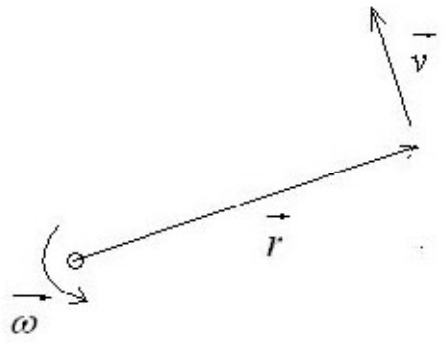

Figure 5-24: Centre of rotation

$v = \omega \wedge r$

Therefore v and ω must be calculated. The position and the orientation of the

$$\overrightarrow{v} \rightleftharpoons \begin{bmatrix} V_x \\ V_y \\ V_Z \end{bmatrix} = \begin{bmatrix} \frac{(x_{t+1} - x_t}{dt} \\ \frac{(y_{t+1} - y_t}{dt} \\ \frac{(z_{t+1} - z_t}{dt} \end{bmatrix}$$

$$\overrightarrow{\omega} \rightleftharpoons \begin{bmatrix} V_x \\ V_y \\ V_Z \end{bmatrix} = \begin{bmatrix} \frac{(\alpha_{t+1} - \alpha_t}{dt} \\ \frac{(\beta_{t+1} - \beta_t}{dt} \\ \frac{(\gamma_{t+1} - \gamma_t}{dt} \end{bmatrix}$$

platform *(x, y, z, α, β, γ)* are known; thus, the velocity v can be found thanks to *(x, y, z)* and the angular velocity ω thanks to *(α, β, γ)*.

Therefore r can be found:

- The direction of r is found, thanks to:

$$\overrightarrow{e_r} = \overrightarrow{e_v} \wedge \overrightarrow{e_\omega}$$

where e_ω and e_r are supposed perpendicular.

The norm is found by:

$$\left\| \vec{r} \right\| = \frac{\left\| \vec{v} \right\|}{\left\| \vec{\omega} \right\|}$$

The position of the centre of rotation with respect to frame {B} is thus $-r$.

5.6 Calibration of the device

To calculate directly the new length of the wire from the output voltage, the expression which links the output voltage to the length of the wire must be established. This expression must have the following form: y = aV + b

where

y= wire length (mm)

V= output voltage (V)

a and b = coefficients

To find the coefficient “a”, several measurements are taken for each device (in the measuring potentiometer, the linearity of each of them can be checked; see Figure 5-26).

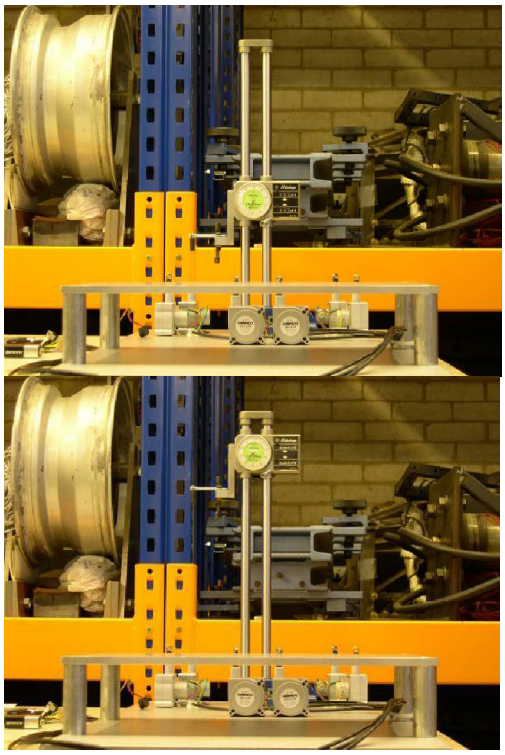

Figure 5-25: Calibration setup

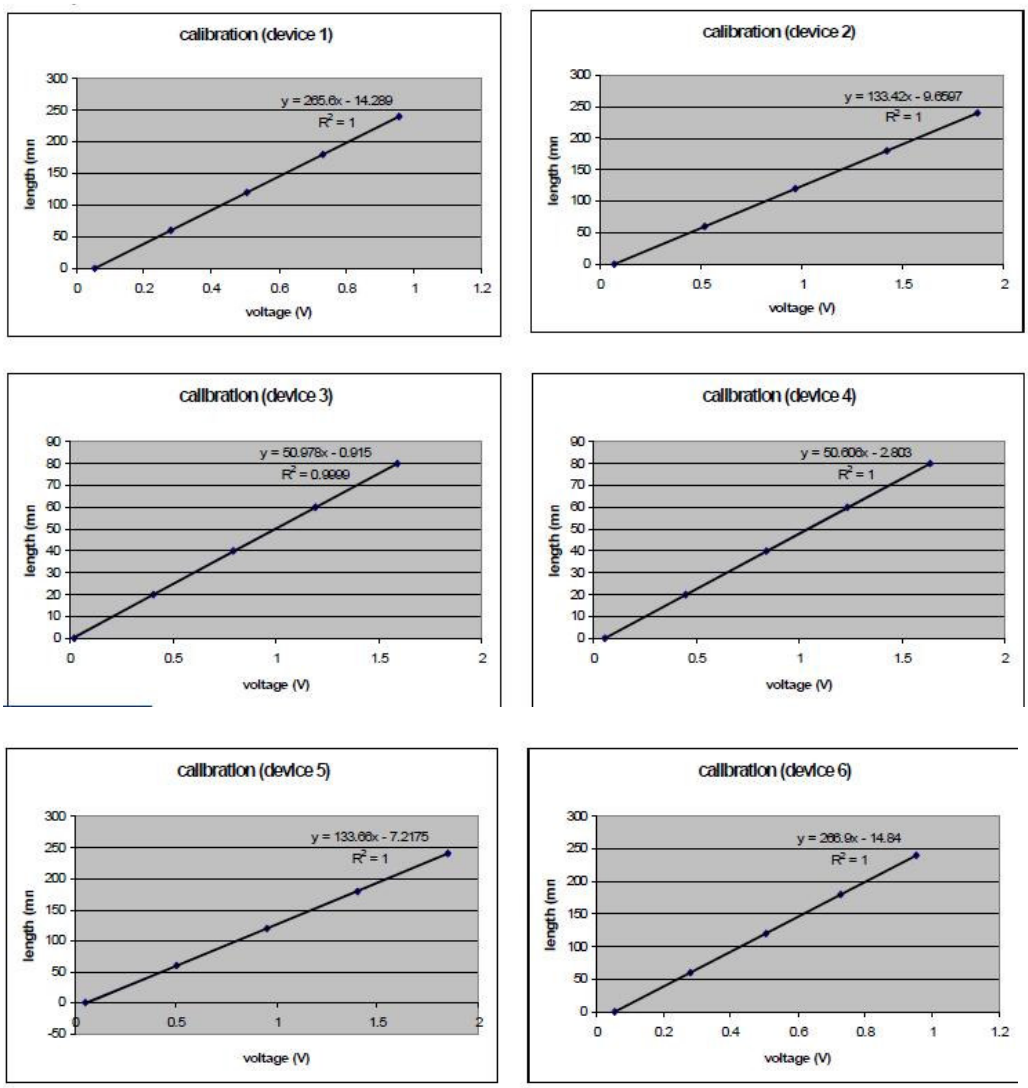

Figure 5-26: Calibration Graphs

The results show that the linearity of each device is good enough to be acceptable. Now, coefficient "b" must be found. From the expression: y = a*x + b, "b" can be isolated: b = y - a*x

To find "b", the wire length "y" and the equivalent output voltage "x" must be read at one particular point.

	Device 1	Device 2	Device 3	Device 4	Device 5	Device 6
b	68.52	64.78	61.6	60	71.72	62.14

The final expressions for each device are:

Device 1	Device 3	Device 3
y = 265.6 *x + 68.52	y = 133.42 *x + 64.78	y = 50.978 *x + 61.6

Device 4	Device 5	Device 6
y = 50.606 *x + 60	y = 133.66 *x + 71.72	y = 266.9 *x + 62.14

To put data on the computer, the "Pico" data logger (adc-11) with a 0.5% accuracy and 0.61 mV resolution is used with the software "Lab-View", as shown in Figure 5-17.

5.7 Simmechanics Model of the Stewart Platform Mechanism

Sim-Mechanics is a block type dynamic modelling tool which works under Matlab-Simulink. The Newton methodology constitutes the basis of the modelling method. Each block involves a different sub program and each program determines the motion of a modelled object.

5.7.1 Principles

Simmechanics modelling is based on the principle of creating a model with block diagrams. The advantages of modelling with Simmechanics can be summarised as follows:

The method provides a better understanding of mechanism using visual elements.

The user can build, simulate and animate the system easily.

Its disadvantages are that the user cannot observe the maths underlying behind the model of the system because the blocks hide the mathematics of the system's dynamics .

A sample Simmechanics model of a pendulum is shown in Figure 5-27.

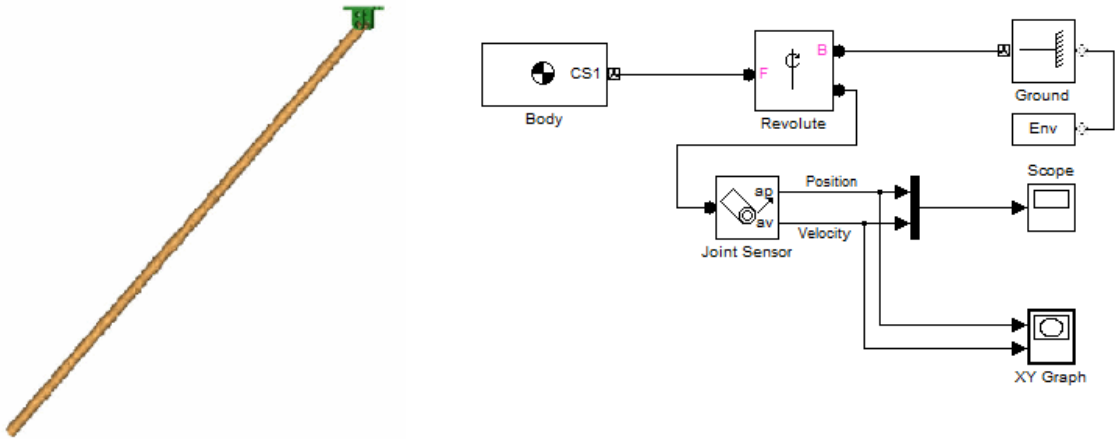

Figure 5-27: Simmechanics model of a sample pendulum system

In Figure 1, the "Body" block represents the dynamics of the body of the pendulum. The user has to enter figures for the mass of the body, the inertia matrix, main coordinate system and coordinates of limit points of the pendulum in

this dialog box, after double clicking on the "body" block. Another important block is the joint block, which is labelled "Revolute" in Figure 1. Joint blocks represent the dynamic relation of the connected bodies. The user has to enter the figures for the assumed coordinate system in the dialogue box after double clicking on the "Revolute" type joint block. The "Joint sensor" block gives real-time information about the displacement of the joint. The "Ground" block represents a fixed point in space to which the body or bodies are connected. The user has to enter the stationary points of the modelled mechanism here. The "Env" block is another important block, which handles the solution method for the modelled system, including choice of either "inverse" and "forward" dynamics. This block also includes the gravity vector which the user can modify and change. Each block has to be connected with a signal arrow which indicates the relationship between blocks. After connecting the blocks, the solver of the algorithm has to be chosen. The solver helps to solve the differential equations, which are built in the blocks.

During the simulation, the user can watch the motion of the modelled system in an animation window.

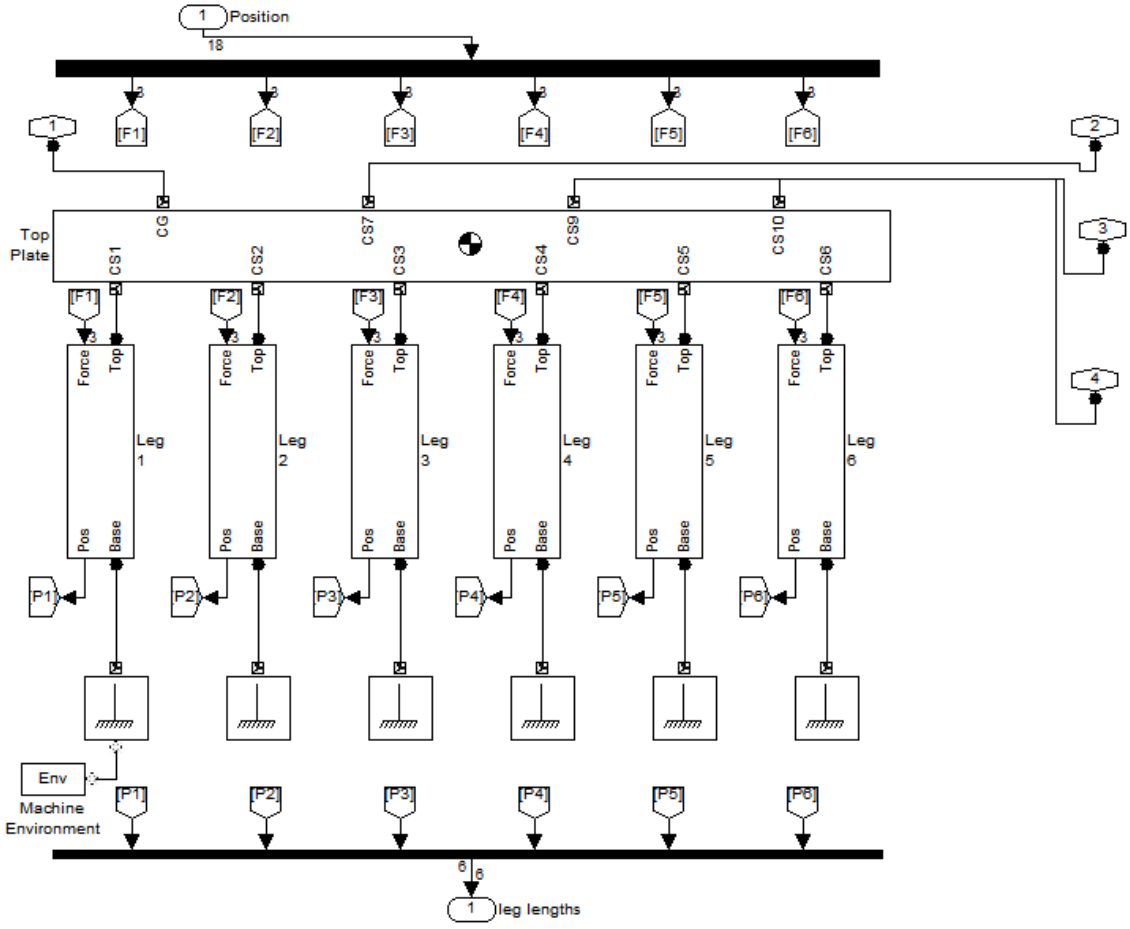

Figure 5-28: Sim-mechanics model of the Stewart Platform mechanism

Figure 5-28 shows the Simmechanics model of the Stewart Platform mechanism. The signal named "position" handles the position data of each leg. These position data are position, velocity and acceleration for each leg in turn. It is assumed that the velocity and acceleration of legs are equal to zero, because in this study the dynamic model is used only for obtaining the direct kinematic solution which means obtaining the location of the upper plate of the Stewart Platform from the lengths of the platform legs.

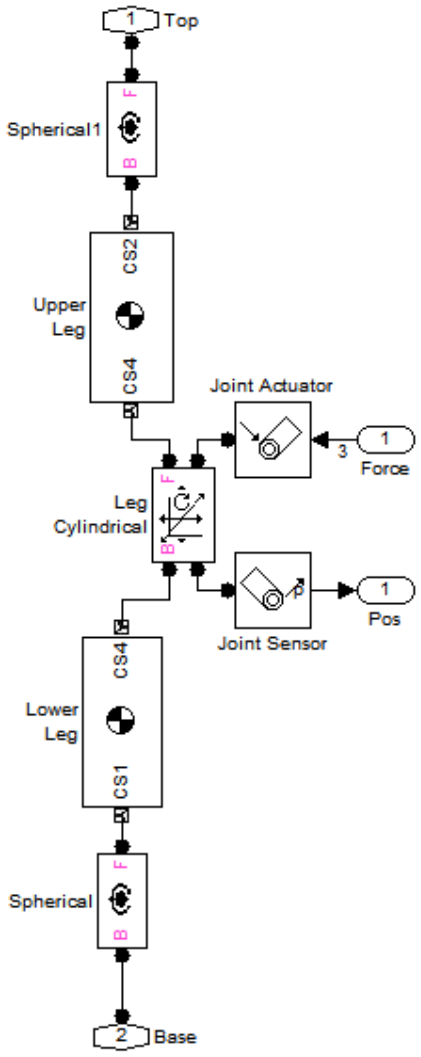

Figure 5-29: Inside of the "Leg" Block

In this project, SPM is used for measuring the position of the forearm. The leg of the Stewart Platform mechanism is shown in Figure 5-29. This block represents the potentiometer which connects the stationary and the mobile plate of the Stewart Platform mechanism. The data for the heading "position" include those potentiometer data which represent the lengths of the legs.

The Stewart Platform: as an elbow joint Laxity Measurement Device

Model and Simulation:

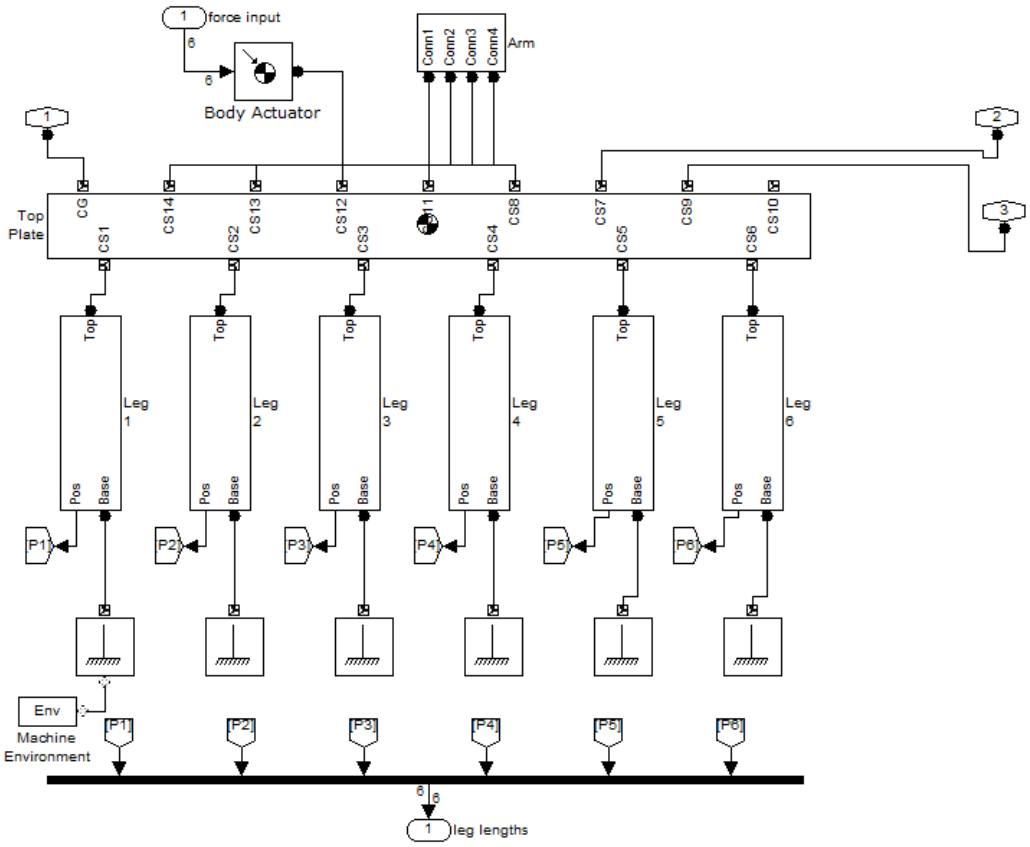

Figure 5-30: Simmechanics model of SPM

Figure 5-30 shows the Sim-mechanics model of the Stewart Platform Mechanism (SPM). In Figure 5-30, the top plate represents the mobile part of the SPM to which the fore arm is attached on it. The "Arm" Block in Figure 5-30 represents the connection between the fore arm and the mobile plate of the SPM.

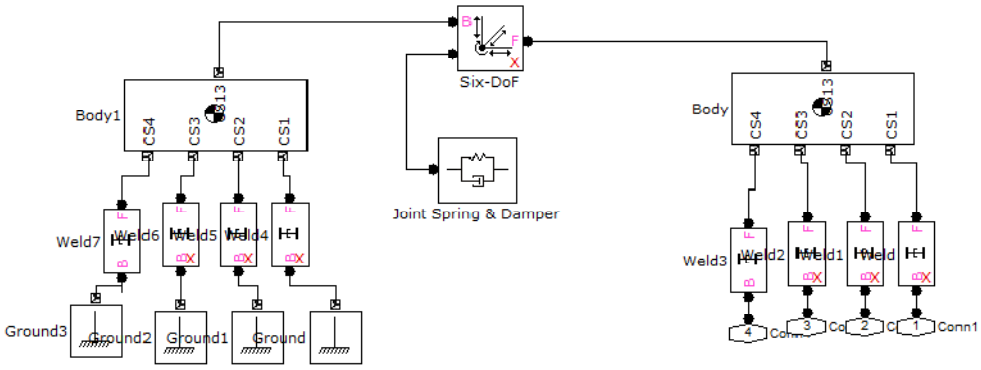

Figure 5-31: Inside the Arm Block

Figure 5-31 shows the contents of the "Arm" block. The "Body" block represents the fore arm which is securely connected to the mobile plate of the SPM by the illustrated weld joints. (weld joints were used because they were secure). The "Body1" block represents the humerus which is connected the stationary part of the experimental setup. The "Six-DoF" block represents the elbow joint. The "Joint Spring & damper" block represents the elasticity of the elbow joint. With the help of this elastic joint we can measure Centres of Rotations during motion.

Simulation 1:

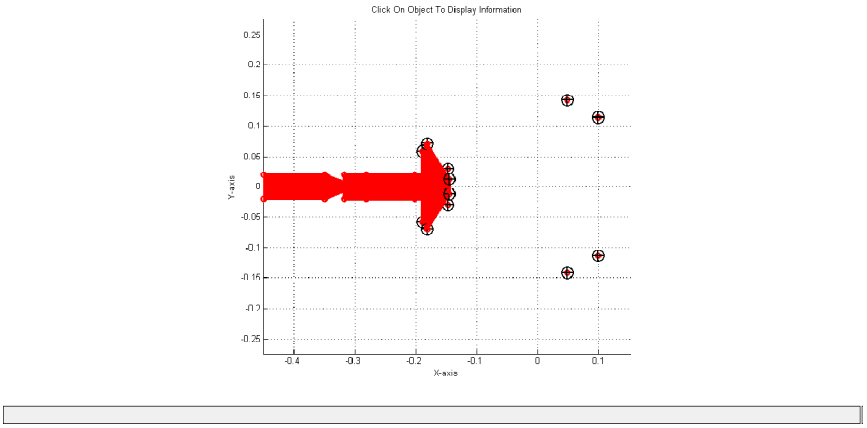

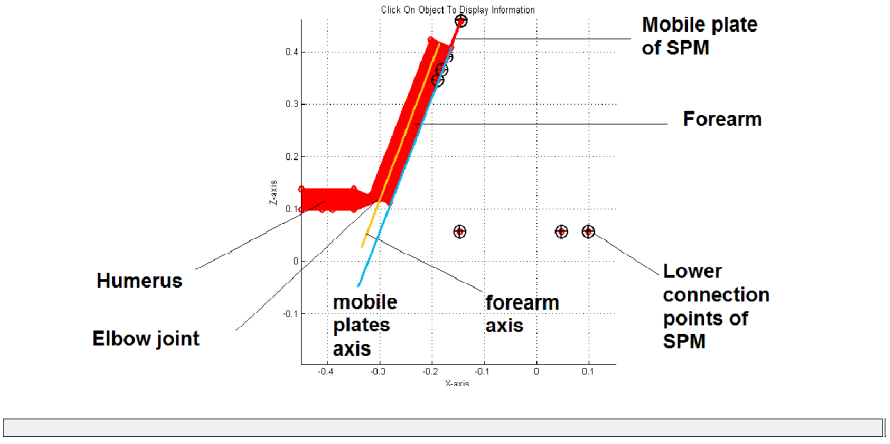

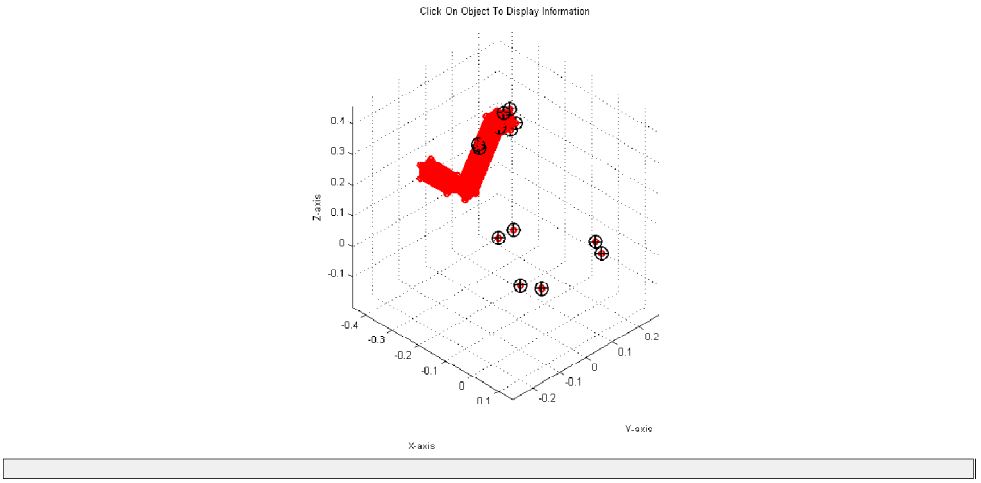

Figure 5-32: Views from Simulation

Chapter 6. Experimental Results and Discussion

6.1 Introduction

A Stewart Platform based tracking system and elbow joint measurement device was tested to measure the motion at the elbow joint when the forearm was extended and flexed. The device was tested on a number of volunteers and successfully measured a full range of motion at the elbow, giving data on the centre of rotation.

To obtain the kinematics of a joint, initially, the 6 SP cord positions were obtained from the SP sensors. Then the displacement and rotation of the links were found using the given formula (see Chapter 5). In the next step, the motion of the SP flexible plate was calculated and the centre of rotation of the construct was found. Following this, the kinematics of the elbow joint could be calculated using Matlab Simmechanics by employing the Newton Raphson and methods. Although the idea of this system is not new, this application and method of measurement are novel. The measurement method is simple and can be stopped or repeated at any time. It can be used as an additional tool to examine possible joint laxity.

Calibration was performed on the SP system to measure possible errors on the device and to identify whether these errors were random or constant. Constant errors were found and a factor was applied to the calculation method to reduce their effect. Random errors were also examined. Although the random errors were small, they might have affected the results. However this did not limit the capacity

of the device to find joint laxity, but does highlight the need to improve its accuracy.

6.2 Measuring the Angles of Flexion-Extension and Valgus-Varus

Flexion and extension motions are shown in Figure 6-1. The flexion angles are limited to about 86 degrees because the lengths of potentiometers are limited. Two subject volunteers were used to measure the elbow joint flexion-extension angle of their elbow joint. The results of the experiment are shown in the following graphs.

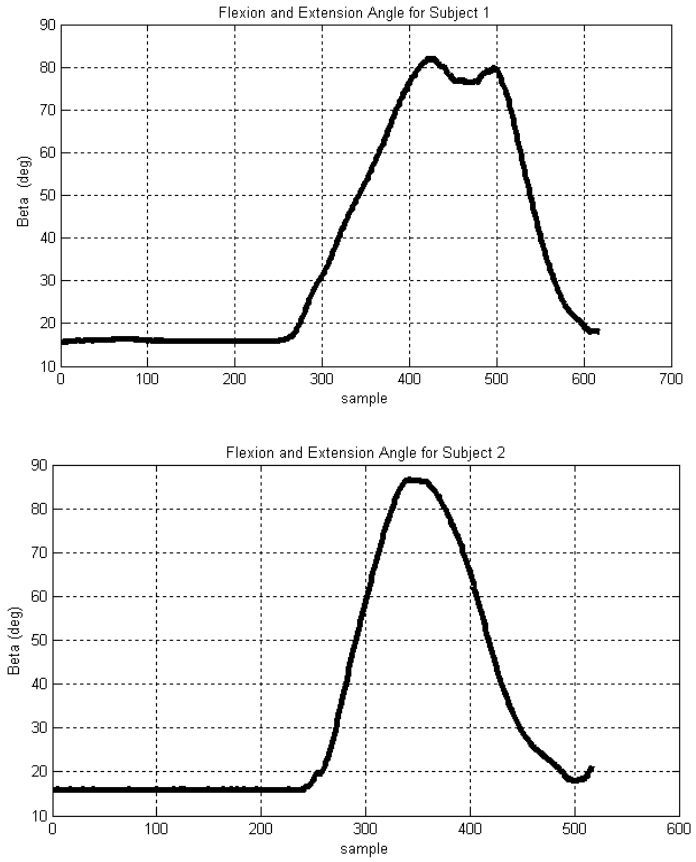

Figure 6-1: Flexion and Extension angles

The varus and valgus motions are shown in Figure 6-2. In the first graph, the subject starts with varus motion and follows it with valgus motion. Both graphs illustrate that the varus and valgus motion capacities are limited to a minimum of 5 degrees.

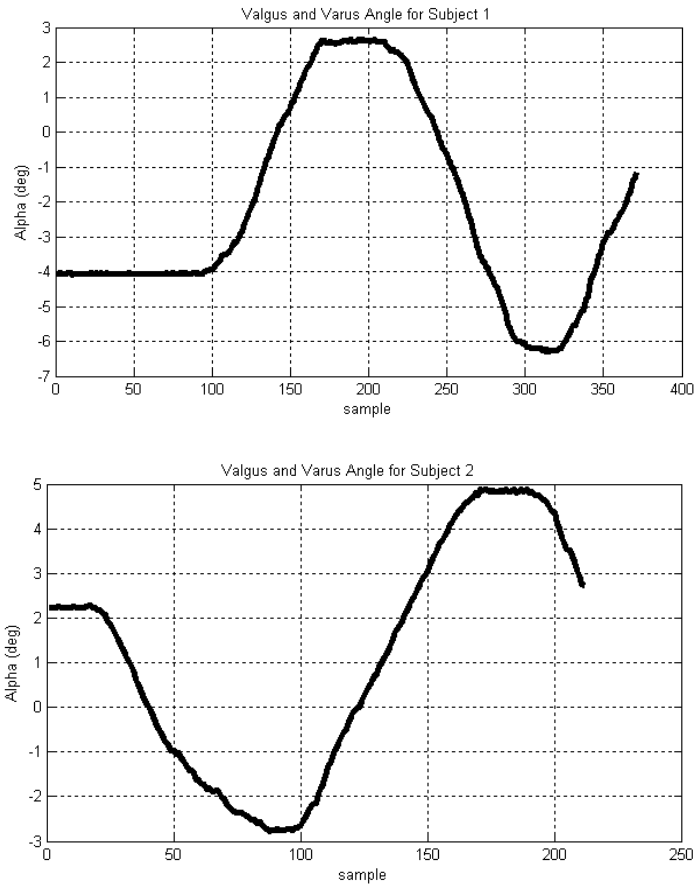

Figure 6-2: Valgus and Varus angles

6.3 Centre of Rotation (C.O. R) via angle of flexion

The result of measurement in a typical examination of both elbow joints of a 32±2 year old male is shown in Figure 6-3. As seen in the picture, the COR of the right and left elbow joints have been drawn in X,Y,Z planes against the angle of rotation. The results show that the COR for the right and left elbows are different.

However, there is no unexpected motion in their trajectory patterns in each plane and so it can be considered an intact joint with no laxity. This is not surprising, as the subject was a fit and healthy individual with no elbow injury.

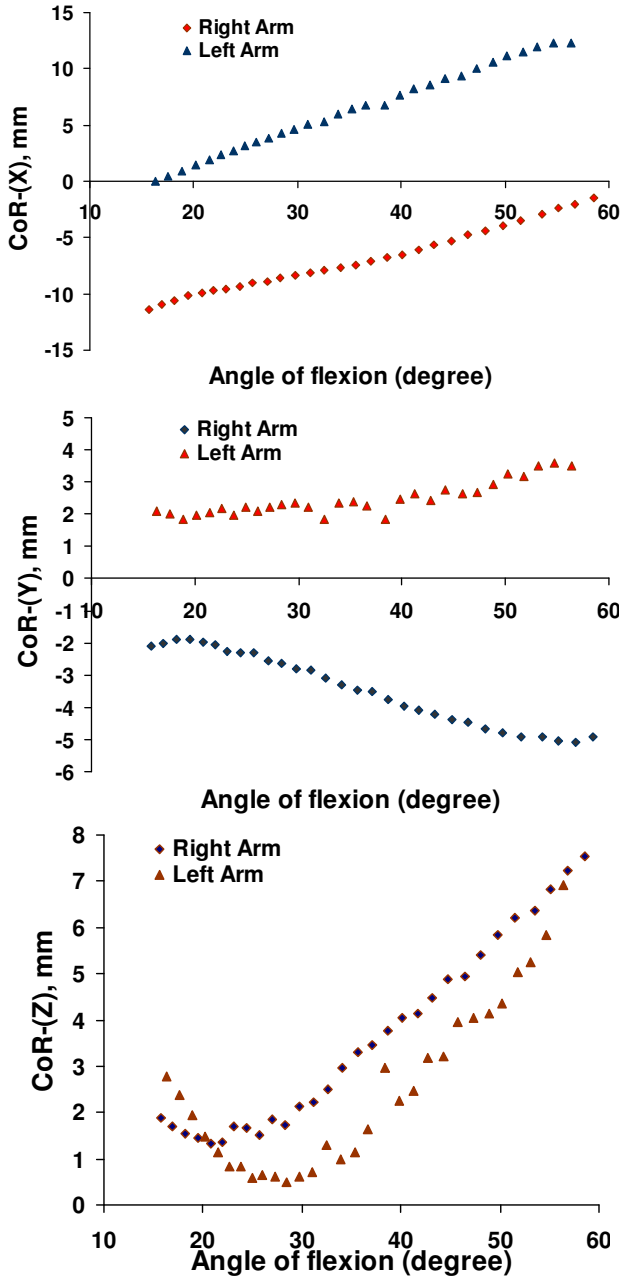

Figure 6-3: Centre of rotation (X, Y, Z) versus angle of flexion for both right and left arms.

6.4 Centre of Rotation (COR) via Valgus-varus movement

The forearms of two subjects were tested by the SPM based measurement mechanism. The motions of the SPM and centre of rotation can be seen in Figure 6-4. In this figure, the x, y, z graphs demonstrate the translational motion of the SPM mechanism. X_a, Y_a, Z_a depict the angular motions of the SPM mechanism, which are γ, β, α. The last three graphs illustrate the centre of rotation of the forearm. All the graphs in Figure 6.4 were created from the data taken from one subject during valgus and varus motions and were not created with the aim of comparison. They show that the SPM-based measuring mechanism allows all six axes to be measured.

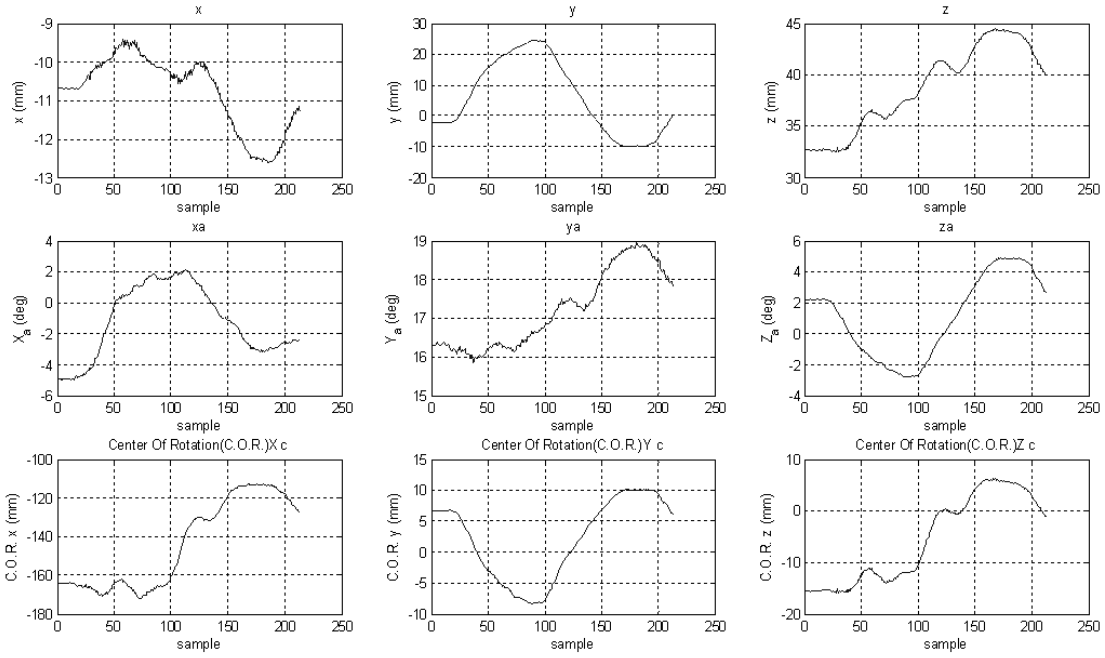

Figure 6-4: Motions of SPM and Centre of Rotation during the Vargus and Valgus motions

6.5 Angle of Varus-Valgus and joint laxity

Figure 6.5 illustrates the centre of rotation of the forearm on the YZ axis during varus and valgus motions, exposing joint laxity. Joint laxity is directly related to the bounds of the links hence this is the main reason for selecting both valgus and varus motion. Values are a little higher than expected, because fixing both the forearm and shoulder to the set up was insufficiently exact.

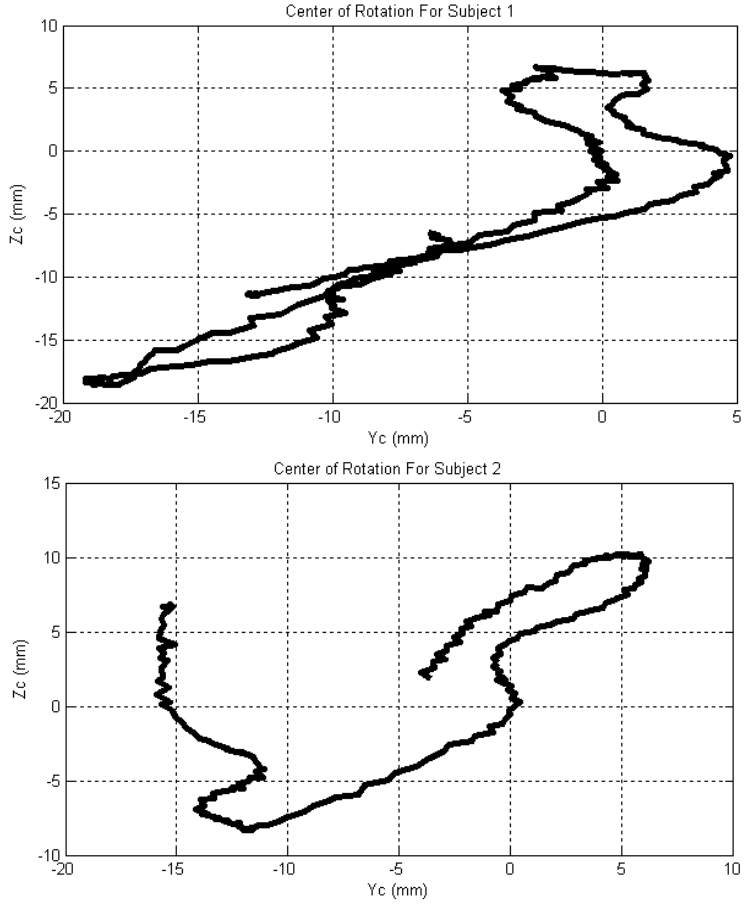

Figure 6-5: Joint Laxity and Valgus-Varus

6.6 Centre of rotation & Stewart Platform position in 3D

As discussed in Chapter 5, the output of the mechanism will be the 6 known position of the moving platform as they relate to the base platform. Then these 6 data were exchanged for 3 translational and 3 rotational degrees of freedom for the moving platform. These data were read accurately but due to some errors (to be discussed in the next chapter) we need to measure a specific sample several times and then work out an average.

To show the capacity and repeatability of our measurement with the Stewart Platform to find the centre of rotation (COR) we found the measurements for 3 different cases and then showed them in three dimension. To have reasonable and reliable data, we repeated each case five times and then we found the average results.

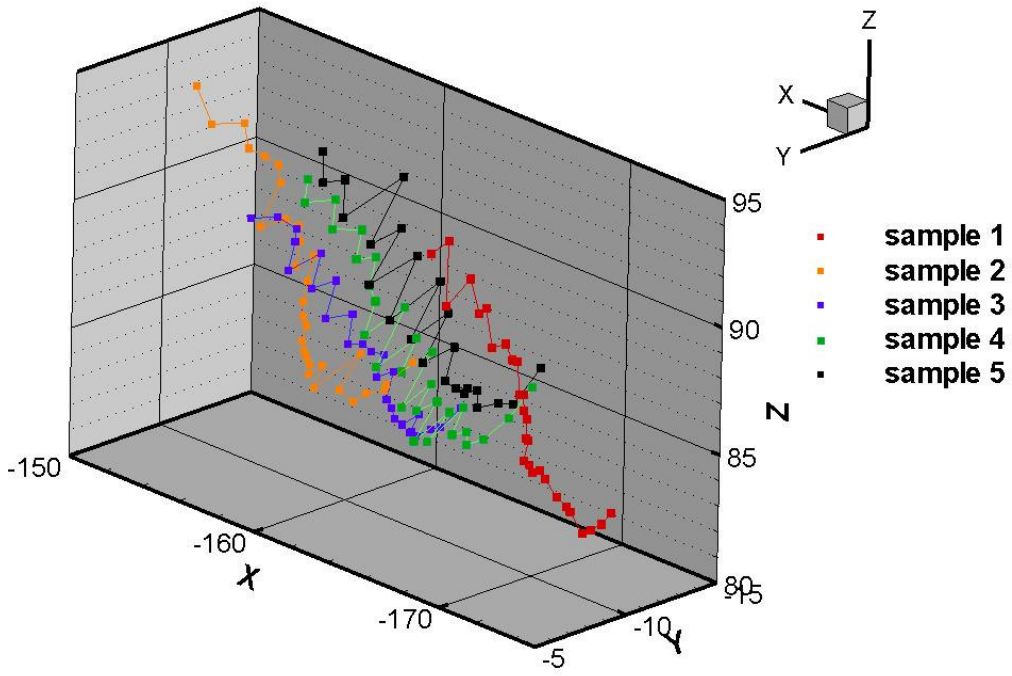

Figure 6-6: 5 samples of the centre of rotation for a case without averaging

Figure 6-6 and Figure 6-7 show the position of the COR and position of the Stewart Platform in 3D for the left hand of our first case (without averaging). As the results were collected at different speeds (the hand was not always moving at the same speed), to find an accurate average it is necessary to pay attention to the nature of the data. To find the average we used the normal method of adding the results together for every sequence of sampling and dividing by the number of samples in each sequence.

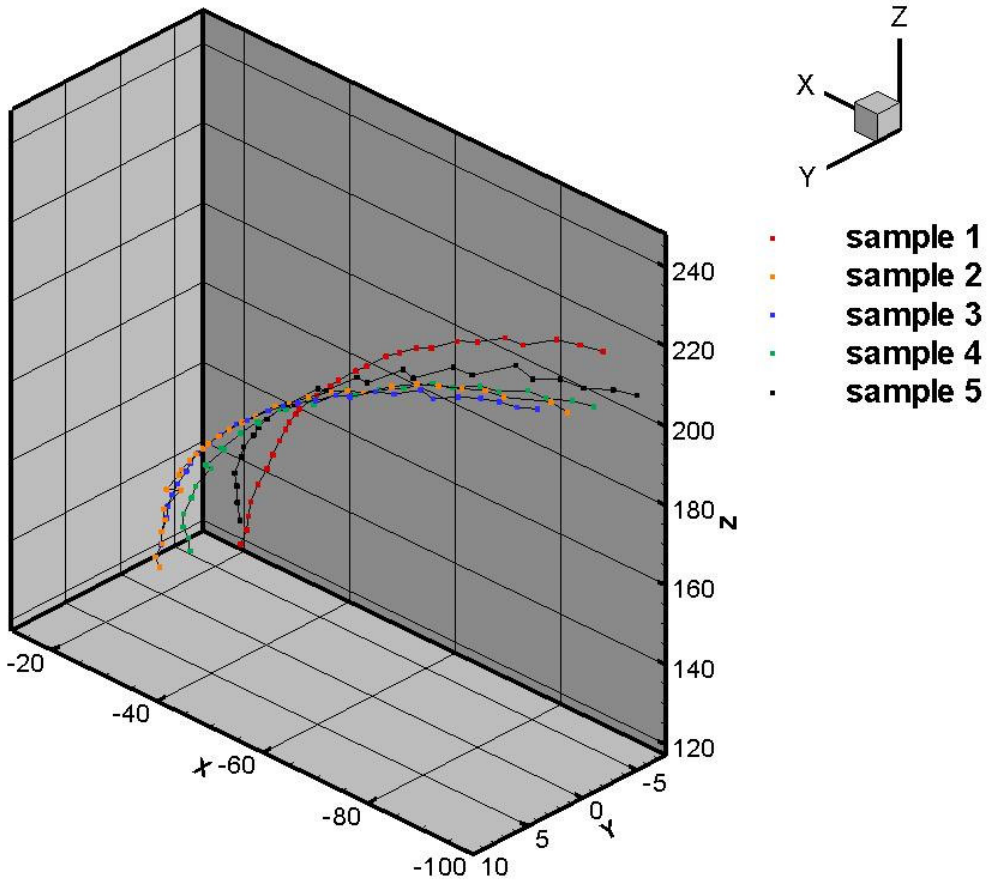

Figure 6-7: Coordinate of the SP platform Position for 5 different samples of one case

6.7 Normal averaging

In this method, the average data were plotted versus the sampling time. One of the problems of this method was to control the speed of motion of the elbow joint. The movement of the hand in each attempt was not the same as before because the subject did not control the movement of the hand by any force (the passive method). To enhance the accuracy of this method, it is always useful to check our data before averaging to make sure that they all have the same trend and we do not have any anomalous data, produced by the errors related to the sampling procedure. In Figure 6-8, the data in X direction have some offset related to each other, but as all the samples have the same trend, we do not need to move the data in x direction before averaging. The important thing about the result is that the position of the graphs in relation to each other is not important as long as they have same trend.

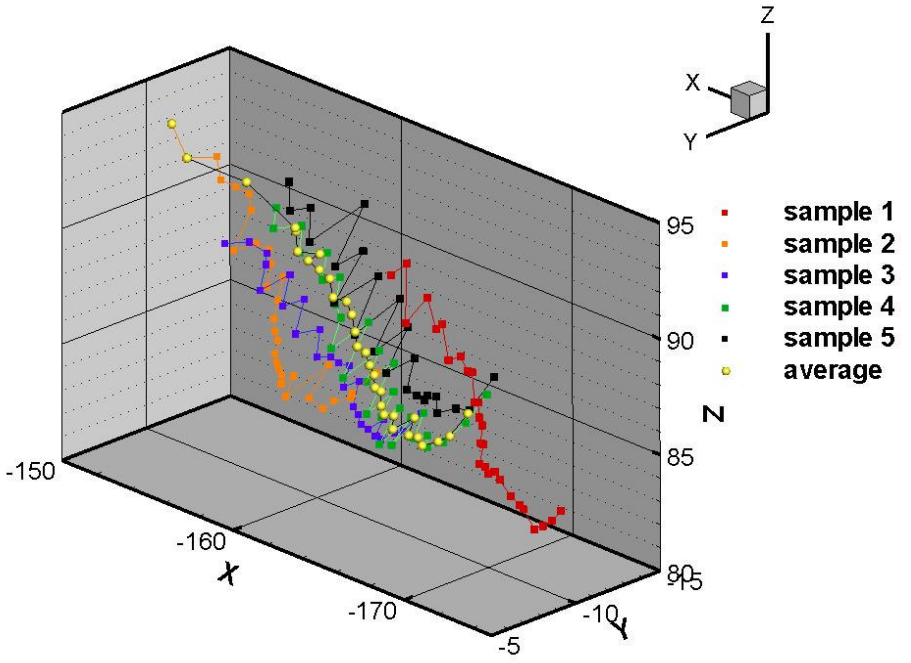

Figure 6-8: Normal averaging for 5 samples of one left hand case (COR)

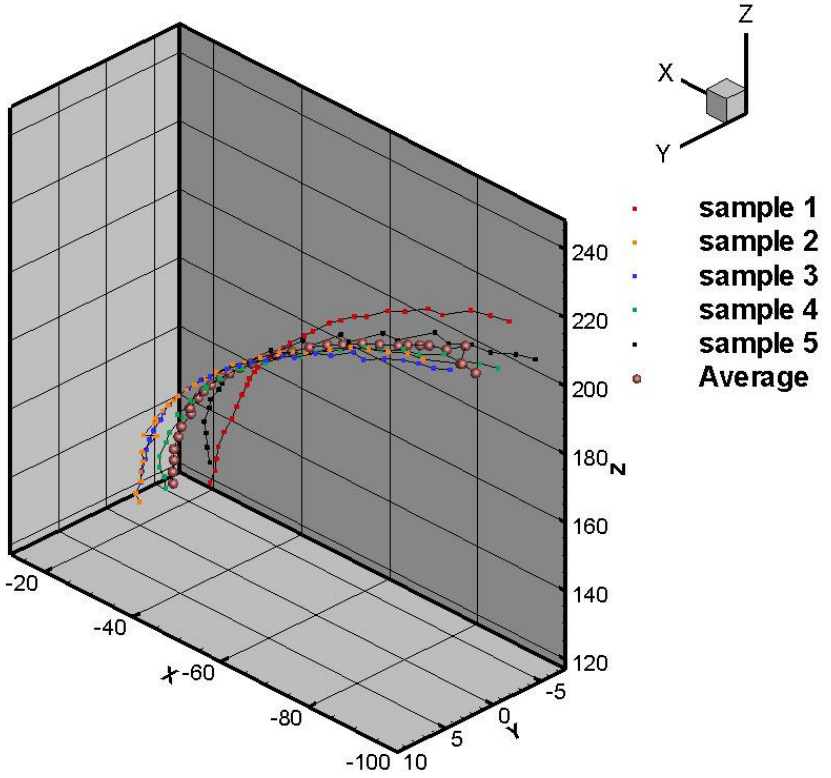

Figure 6-9: Normal averaging for 5 samples of one left hand case (SP)

6.8 Comparing average results for 3 different cases

To judge the reliability of the Stewart Mechanism in measuring different cases, we took 3 different cases with both left hand and right hand. Figure 6-10 shows the results for COR for these cases. According to the graphs, although there are clear differences between the curves of the COR for the 3 left-hand cases, the trend of the curves is near that of the others with slight offset results. The offset in the position of the results is not important, because it shows only the position of the centre of rotation according to a specific reference and this position could have been different even if the test for one hand had been repeated in the mechanism.

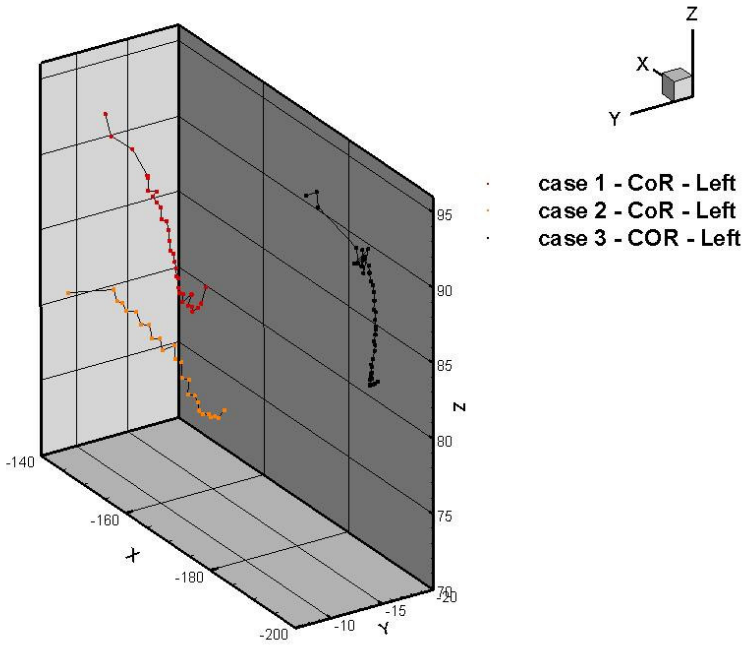

Figure 6-10: Average data of COR for 3 different cases – left hand

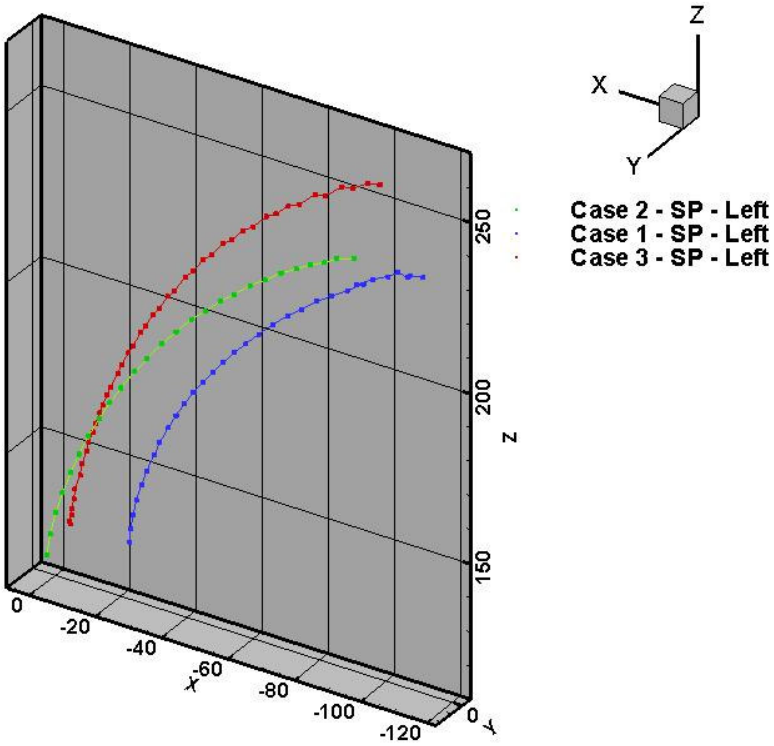

Figure 6-11: Average data of SP for 3 different cases – left hand

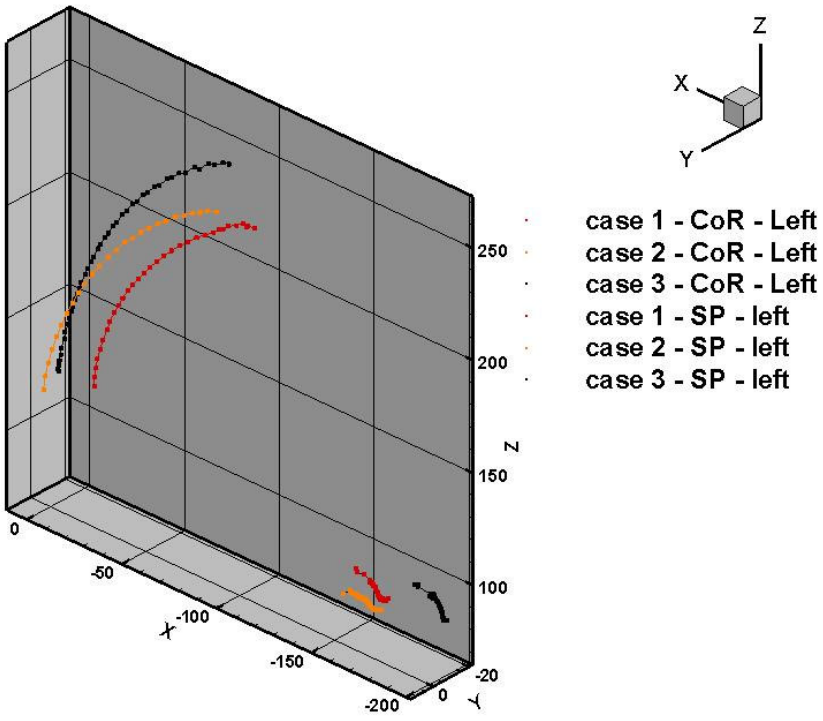

Figure 6-12: Average data of COR and SP for 3 different cases – Left hand

Figure 6-11 is the average data for 3 different cases of the left hand. The graphs show for each of these cases the position of the Stewart Platform. According to the graphs, the trends are similar but show a slight shift between them. Still, this is accepting; as we are testing three different hands of different lengths. Figure 6-12 shows all the graphs of COR and SP related to these three left-hand cases. In these figure the relation between COR and SP is important.

6.9 Comparing average results for left and right hand

In Figure 6-13, Figure 6-14 Figure 6-15, the results of the tests for the left hand and right hand for three different cases are compared.

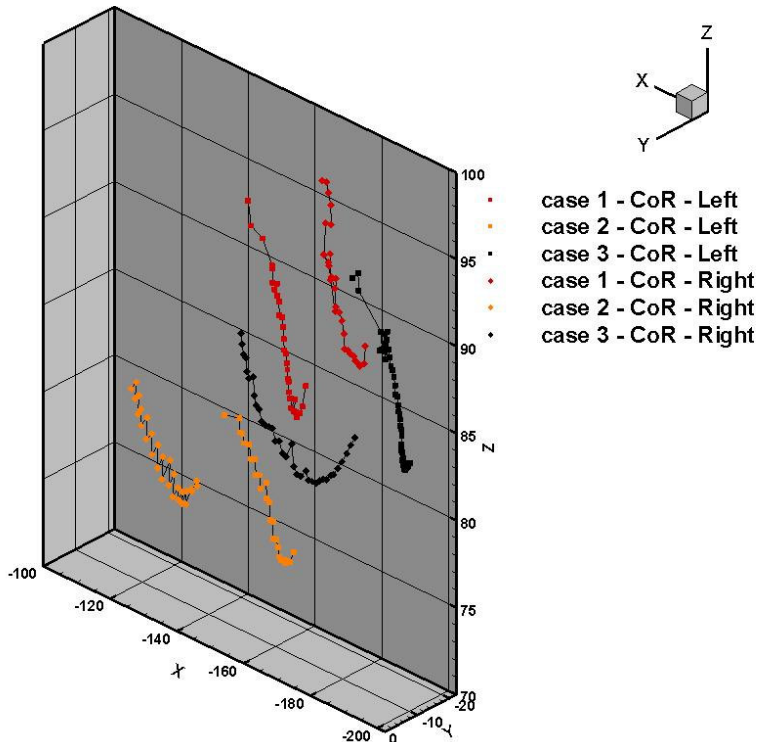

Figure 6-13: Average data of COR for 3 different cases - left and right hand

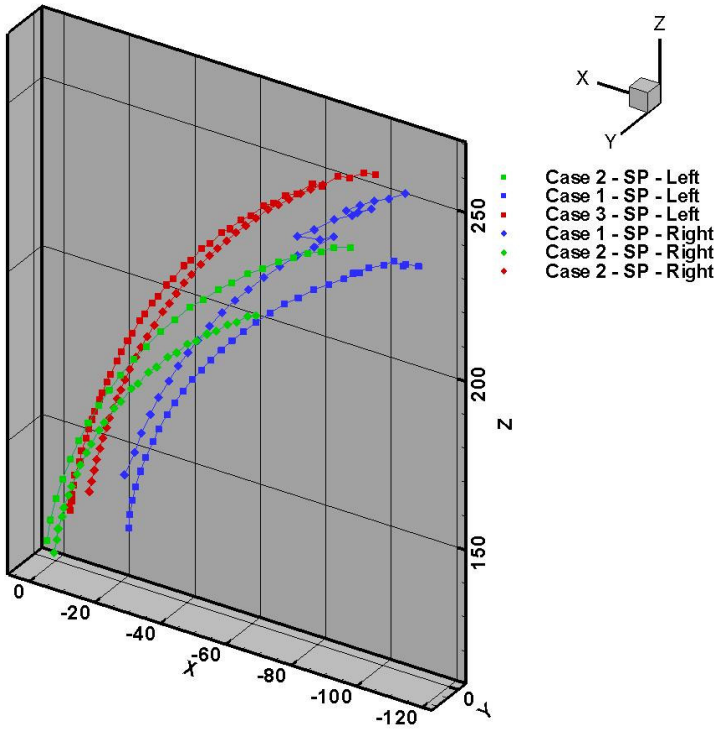

Figure 6-14: Average data of SP for 3 different cases left and right hand

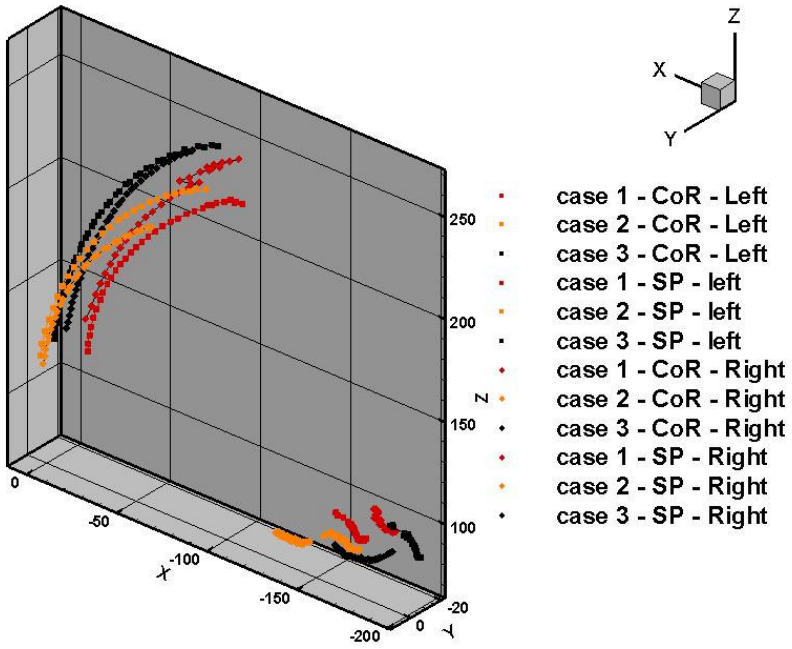

Figure 6-15: Average data-left and right hand- COR - SP- 3 cases

6.10 Screw Displacement Axis (SDA)

Woltring et al. (1985) presented an analytical model which showed the landmark position data on the definition of the finite centroid and the finite helical axis. Blankevoort et al. (1996) depicted the finite helical axes as a flexion motion, and placed markers on four human knees and tracked their movement to check the repeatability of the results. Soudan et al. (1979) classified one of the widespread methods for investigating the mechanics of human joints was the instant axis, or screw axis.

In our study we used screw coordinates to epitomize elbow motion; this will make it possible to classify elbow pathologies to identify elbow deficiencies.

The momentary transformation between each two successive frames acquired during motion was depicted when the instantaneous screw parameters was calculated. The instantaneous screw parameters (also known as twist parameters) of the elbow were used, as they provide the 6-DOF transformation of the elbow while in motion. A set of continuous twists are formed from the collection of all the instantaneous screws, which describes the motion. We also illustrate the fact that a set of instantaneous screws describes the motion of a given elbow, which forms a range of points.

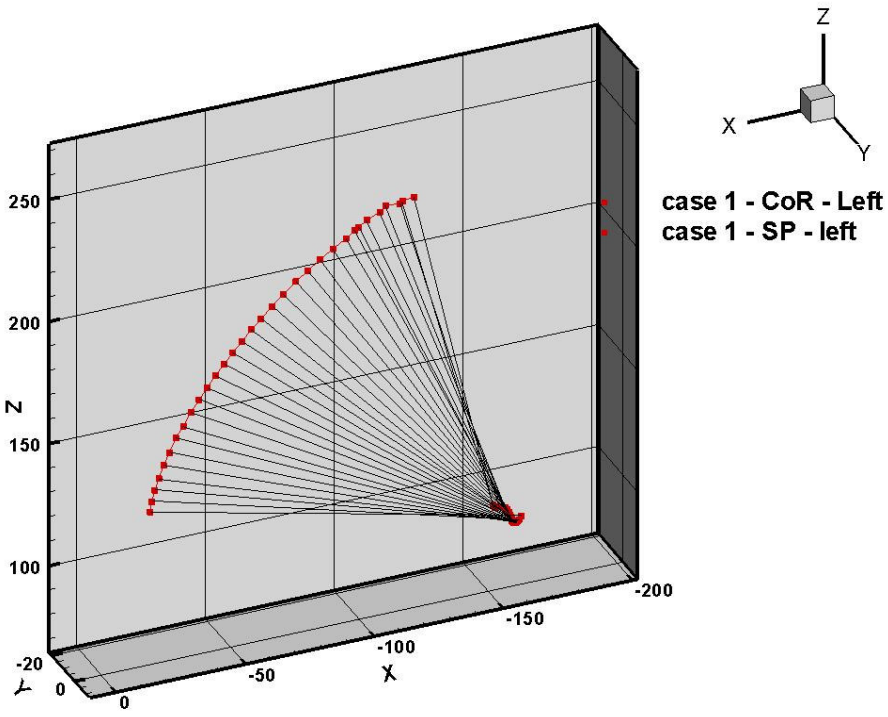

Figure 6-16: Screw Displacement for case 1 -left hand

6.11 Error analysis

A mistake is not usually an error in the scientific measurement. The terms “error” and “uncertainty” both refer to inevitable imprecision in measurement. Since we

cannot measure things with accurately high precision, it is useful to know how to evaluate the imprecision of the results. In our system the measurements of different quantities to obtain a final quantity were combined. Even if it is assumed that we know the error associated with each individual quantity, the problem is to find the errors of the combined quantity. Sometimes one of the errors is dominant in comparison with the rest of errors; at other times, the errors compensate for each other.

There are in general two types of error, random and systematic. In this part, we first define these kinds of error in general and then bring out the source of our errors and try to categorise these on the basis of the definitions. Finally we try to calculate the errors of the present system.

Random errors

Random or anomalous errors in experimental measurements are generally caused by unknown and unpredictable changes in the experiment. These changes may occur via the measuring instruments, or the environmental or physical area. The best way to tackle such errors is to repeat the test several times and take an average of the results to have more reliable findings.

Systematic Errors

Systematic errors are errors associated or caused by a flaw in the equipment or in the design of the experiment. Systematic errors are very unlikely to be found by repeating the experiment with the same equipment. This may lead to inaccurate

results. Unlike random errors, systematic errors always alter the results in one direction.

Systematic errors are much more difficult to uncover than random errors. To identify systematic errors, we need to understand the nature of the experiment and the instruments involved. When we encounter major systematic errors in our investigations, we may suspect that our measurements are biased; therefore, we should try to identify the possible sources of the systematic error.

Because in our cases we are mostly using comparison as a method, we tend to compare a healthy elbow with another which has laxity or other problems; hence, systematic errors are not very important, as these errors are found in all the experiments.

There are several areas here error could be caused in calculating the Centre of Rotation (COR) and analysing the kinematics of the elbow. Here we list them and explain how to measure and deal with these errors so as to minimize them.

6.11.1 Manufacturing errors

These are primary errors, related to the stage of manufacturing the platforms. As the position of the sensors on the base and the moving platform are used to calculate the centre of rotation and any other output from our mechanism, any errors in measuring the positions of these sensors will create systematic errors which, unfortunately, do not change when the test is repeated and influence our results.

The manufacturing errors were checked. The errors in measuring and positioning the potentiometers on the base platform and its related wires on the moving

platform would in the worst case come to about ±0.1mm (errors in measuring tools). This amount of error in comparison to the dimension of the radios of the platforms (Rp=71mm and Rb=150mm) is negligible. Moreover, the error in average would be about 0.01 % and does not affect the output results noticeably. For instance our A/D device has less than 1% error.

6.11.2 Uncertainty on the measuring sensors

There are 6 Potentiometers which measure the position of the moving platform in relation to the base platform. The supplier of these sensors claims the accuracy of these devices for full stroke to be about 0.25% (Appendix B). In our platform as we are using different lengths for the measuring wires there may be different amounts of possible error for each leg of the platform. We can use this information when we are calculating the total errors. But this is not the whole story, since we are using sensors of various lengths on the platform, which could cause some systematic errors. In addition to measuring various lengths, they introduce different levels of accuracy.

Such errors are not minimized by calibrating the potentiometers before the experiment.

Because the potentiometers could have different errors, first, because they deal with legs of different lengths and, second, because they vary in accuracy, we should consider another important issue. This is that, when we are using the Newton-Raphson method to calculate the positions and the angle of the platform, the errors prevent the moving platform from being treated as a flat plate. To

remedy this issue, in the Matlab program which we provided for calculation, we have considered a 0.01 convergence error.

Here we have calculated the error for one of the most extreme situations, to show how negligible this kind of error is in comparison to others. We have six wire potentiometers on Figure 5-8 If we consider two sensors in front of the arm's station (sensors B6 and B5 on Figure 5-10) and two others, labelled B2 and B3, in front of the platform, . In extreme conditions, the length of the wire potentiometers of B6-P6 and B5-P5 will be about 250 mm and the wire potentiometers for B2P2 and B3P3 will be about 500mm. To calculate the errors we consider the extreme conditions. According to the manufacturer's catalogue the error is about 1% of the length of the wire, with B6-P6 and B5-P5 having the same length with (1%*250) ±2.5 mm error and B2-P2 and B3-P3 (1%*500) ±5 mm error. With this amount of error, we assume that the errors in the case of the wire potentiometer of B6-P6 and B5-P5 is -2 and for that in the case of B2-P2 and B3-P3 the error is +5mm (to calculate in extreme conditions). Figure 6-17 shows schematically how the errors on the reading legs of the platform affect on the calculation of the results. The errors in this figure have been exaggerated. Changing the angle of the moving platform around the X axis becomes about 3.5 degrees less than 5% of the measured angle in the same position, which could be negligible. Changing the position of the centre of the platform in z and x direction also amounts to about 1 mm (less than 0.25% of the original measurement). These calculations show that the errors due to an error on the potentiometer and the A/D system will affect less than 5% of our results.

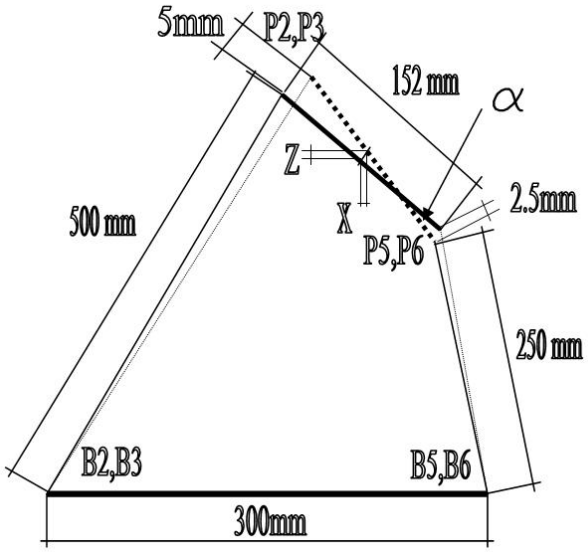

Figure 6-17: Schematic Calculation of the maximum error

6.11.3 Errors due wire length uncertainties

Length deviations of the wires due to manufacturing tolerances such as wire length differences may result in the unreliable performance of the wire-based tracking system. In general, calibration can be utilized to eliminate all systematic errors. To compensate for specific errors, some techniques for calibration have already been proposed in the literature. For example, Geng and Haynes (1994) introduced a method of compensating for the cable guide outlet shape of wire encoders. Moreover errors related to compensating for the length of the wires cannot be rectified because of their random nature. This error could be minimized by repeating the experiments and using a method of averaging.

6.11.4 Errors related to the force exerted by the device

The force exerted by the measuring device itself is another indirect source of errors. The commercial wire encoders are intended to use a powerful string tension. This is necessary to ensure that the inertia of the mechanism does not cause a wire going slack in rapid motion. If a small amount of force is used, it would reduce the maximum speed of the object to be tracked without the wires going slack. Therefore, it becomes necessary to reconcile accuracy and speed. On the other hand, if a substantially large amount of force is used, the trajectory of the tracked object could be altered by the measuring device.

6.11.5 Noise and Data Acquisition errors

The data from the potentiometers are sent through an acquisition system to the computer to store and for further calculation. The Pico data logger ACD 11 was used here to transfer data from the sensors to the computer. According to the manufacturer's handbook, the ADC-11/16 is accurate to within 1% (Appendix A). However, because of the effect of the environmental there is always some noise in the output voltage of the sensors.

To minimize these errors we always monitor the output of potentiometers to check if there is extra noise.

6.11.6 Calculation errors

As discussed earlier (Chapter 5), the output of the wire potentiometers are values for the changes in length of the wires. These parameters should be changed to displacement in 3 directions (X, Y, Z) and Rotation about 3 axis (X, Y, Z) for the

moving platform. This relationship does not have an exact analytical solution and needs some method of iteration, such as the Newton-Raphson method. Like other numerical methods, this one has its own inherent error. Error analysis for calculations is as follows:

This error analysis is inverse kinematics-based error analysis; therefore the deviation of error is investigated from the positions of SPM to the length of the legs.

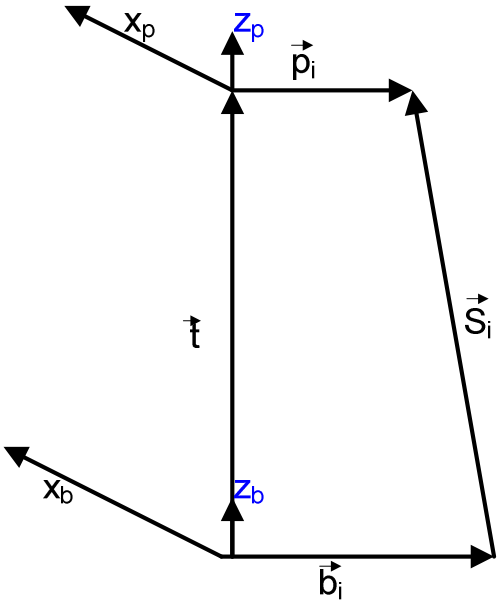

Figure 6-18: Link Length

$$^{P}\vec{p}_i = \{\vec{p}_{ix}, \vec{p}_{iy}, \vec{p}_{iz}\}^T = \{r_p.\cos(\lambda_i), r_p.\sin(\lambda_i), 0\}^T \quad (6.12)$$

$$^{B}\vec{b}_i = \{\vec{b}_{ix}, \vec{b}_{iy}, \vec{b}_{iz}\}^T = \{r_b.\cos(\Lambda_i), r_b.\sin(\Lambda_i), 0\}^T \quad (6.13)$$

$$^{B}\vec{S}_i = -^{B}\vec{b}_i + ^{B}\vec{t} + ^{B}\vec{p}_i \quad (6.14)$$

$$ {}^{B}\vec{p}_i = {}^{B}_{P}\boldsymbol{R}\,{}^{P}\vec{p}_i \tag{6.15} $$

$$ l_i = \sqrt{S_{ix}^2 + S_{iy}^2 + S_{iz}^2} \tag{6.16} $$

$$ l_i^2 = x^2 + y^2 + z^2 + r_p{}^2 + r_b{}^2 + 2(r_{11}\cdot p_{ix} + r_{12}\cdot p_{iy})(x - b_{ix}) + 2(r_{21}\cdot p_{ix} + r_{22}\cdot p_{iy})(y - b_{iy}) $$
$$ + 2(r_{31}\cdot p_{ix} + r_{32}\cdot p_{iy})(z) - 2(x\cdot b_{ix} + y\cdot b_{iy}) $$

(6.17)

For an explanations of the equations given above, see Equation (5.26) .

The error value on the leg length is:

$$ el_i^2 = ex^2 + ey^2 + ez^2 + r_p{}^2 + r_b{}^2 + 2(er_{11}\cdot p_{ix} + er_{12}\cdot p_{iy}) $$
$$ (ex - b_{ix}) + 2(er_{21}\cdot p_{ix} + er_{22}\cdot p_{iy})(ey - b_{iy}) $$
$$ + 2(er_{31}\cdot p_{ix} + er_{32}\cdot p_{iy})(ez) - 2(ex\cdot b_{ix} + ey\cdot b_{iy}) \tag{6.18} $$

Where el_i denotes the error value on leg length; ex, ey, ez values are the translational errors of SPM; r_{11}, r_{12}, r_{21}, r_{22}, r_{31}, r_{32} are the error values of elements of the rotation matrix.

Although we can calculate the leg errors from this equation, direct kinematics is the most effective way to calculate the position errors of SPM from leg errors. This is the simplest way to watch for the effects of errors.

Procedure:

We examined the error equation according to the following procedure.

- Measure the exact positions (translation and rotation) of platform. We should measure it precisely. (Let us call it "Pm")
- Obtain the positions of SPM using leg lengths (Pc).
- Get leg lengths from the LabView program (Lc).
- Find position errors. (eP=Pc-Pm)
- Measure the leg lengths by using a precise device (Lm).
- Find leg error values by extracting the leg lengths values (eLi=Lc-Lm).
- Put the values into the equation given below:

$$el_i^2 = ex^2 + ey^2 + ez^2 + r_p{}^2 + r_b{}^2 + 2(er_{11} \cdot p_{ix} + er_{12} \cdot p_{iy})$$
$$(ex - b_{ix}) + 2(er_{21} \cdot p_{ix} + er_{22} \cdot p_{iy})(ey - b_{iy})$$
$$+ 2(er_{31} \cdot p_{ix} + er_{32} \cdot p_{iy})(ez) - 2(ex \cdot b_{ix} + ey \cdot b_{iy}) \quad (6.19)$$

Finally, we find the effect of the error values of the legs in the motion of the platform. The simulations were made realised with small deviations of the mobile plate of the mechanism from 0 mm to 1 mm in translational motion and from 0 degrees to 3 degrees on the rotational axes. In the next section, we use this relationship to show the effect of skin movement.

The velocity of the error values can be calculated from the simulation data by using the discrete derivative formula which is given below:

$$\frac{\partial X}{\partial t} = \frac{X_1 - X_0}{t_1 - t_0} = \frac{X_1 - X_0}{T_s}$$

The X_1 term shows the position value of any simulation data in time t_1. T_s represents the sampling time of the simulation. In this case, the simulation time is

the same as the sampling time of the experimental setup which is 0.0156 seconds. In this situation the velocity deviations of the mobile plate are constant; they are 0.064 m/s in the translational axes and 0.367 deg/sec in the rotational axes. The velocity errors on legs are various.

The errors can be calculated by this method, but the errors were not significant in comparison to the other sources of error (check the part of 6.11.2 which deals with the calculation of errors in extreme conditions). One of the important issues is to maintain the moving platform, after calculation, as a solid object. We have to define a threshold error in calculation to maintain this issue. According to this, we define 0.01 as a stop point for calculation. This means that we continue our calculation and iteration until it reaches this point.

6.11.7 Errors related to the fixing of the hand (skin movement)

One the most important sources of error is related to the method of fixing the arm on the platform. As this is an *in vivo* test it is nearly impossible to attach the arm on the moving platform and the forearm on the fixed platform so that the subject cannot move at all. And always there is related movement between the skin and the bones which creates errors in the measurement and calculation of the centre of rotation (since this is related to the bones). To reduce such errors, we have designed some special support on both the moving and the fixed platform. Our calculations show that the most important and influential factors in error are related to this point.

To show the effect of skin movement on our results, we have used the relationship in section 6.1.6. These formulas show the relationship between the mobile

platform and the length of the leg of the potentiometer. Although skin movement is mostly along the X axis and its rotation around the Y axis, we have shown this effect for all 6 degrees of freedom. We have assumed this effect separately for each degree of freedom. The simulations are enacted with deviations of the mobile plate of the mechanism from 1mm to 10 mm in translational motion and from 0 degree to 60 degrees on the rotational axes. This assumption of error values should refer to fixation errors or should be the errors coming from the motion of the skin. Figure 6-18 to 6-23, given above, show the effect of the error on the mobile plate (because of the relationship of the skin movement to the leg lengths. The simulation code which is written in the Matlab command line is shown in Appendix D.

As we can see in Figure 6-18 the effect of 10 mm displacement on mobile platform in x direction will be about 5% change on the length of the leg for leg1. In section 6.11.2, we have calculated these errors for extreme conditions.

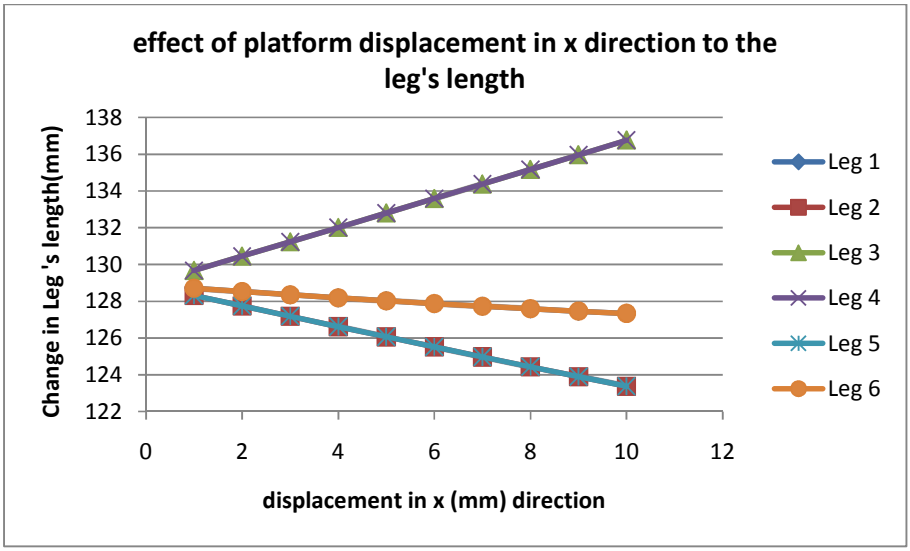

Figure 6-19: The effect of the translational movement of the mobile platform from 1 to 10 mm along x direction to the leg's length.

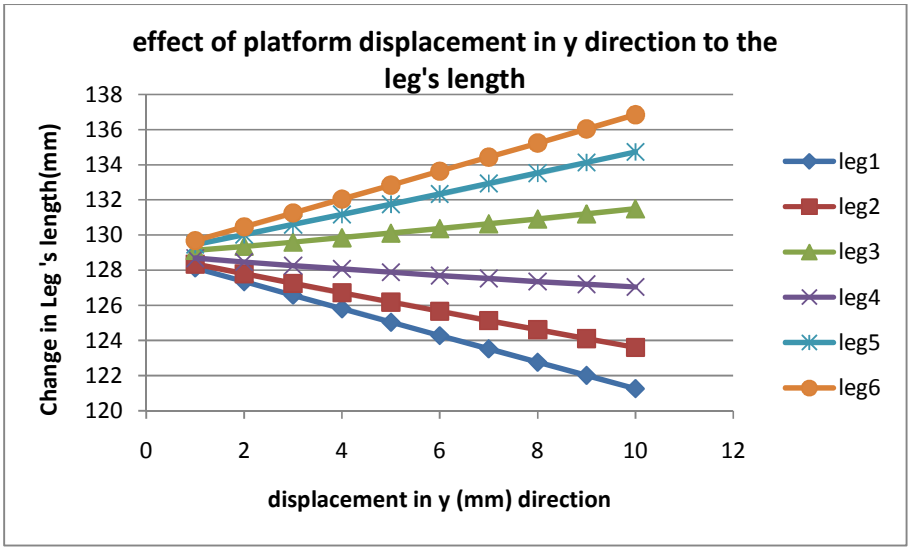

Figure 6-20: The effect of the translational movement of the mobile platform from 1 to 10 mm along y direction to the leg's length.

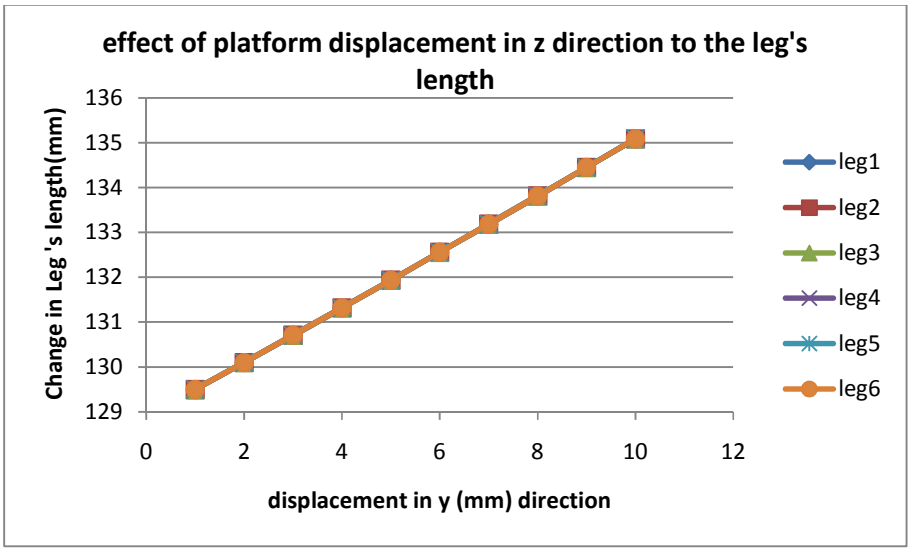

Figure 6-21: The effect of the translational movement of the mobile platform from 1 to 10 mm along z direction to the leg's length

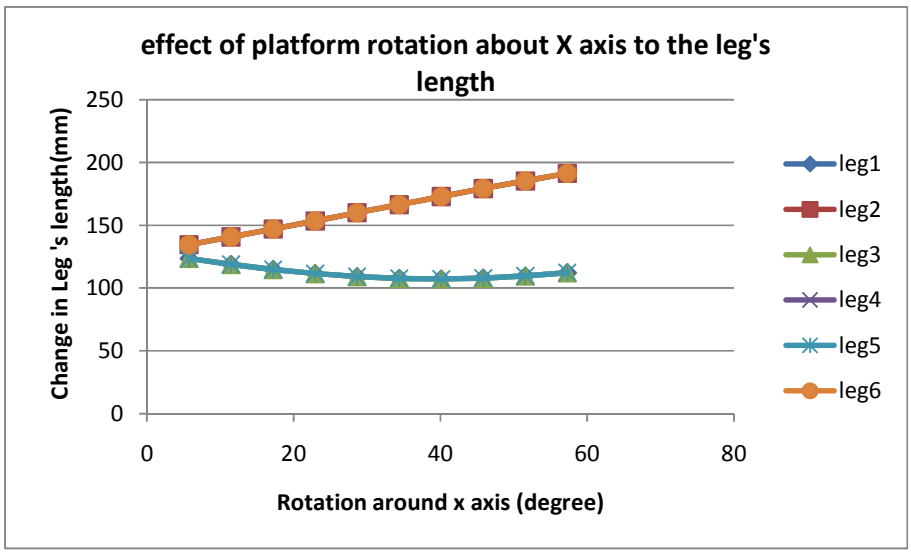

Figure 6-22: The effect of the rotational movement of the mobile platform from 0 to 60 degrees about the x axis to the leg's length.

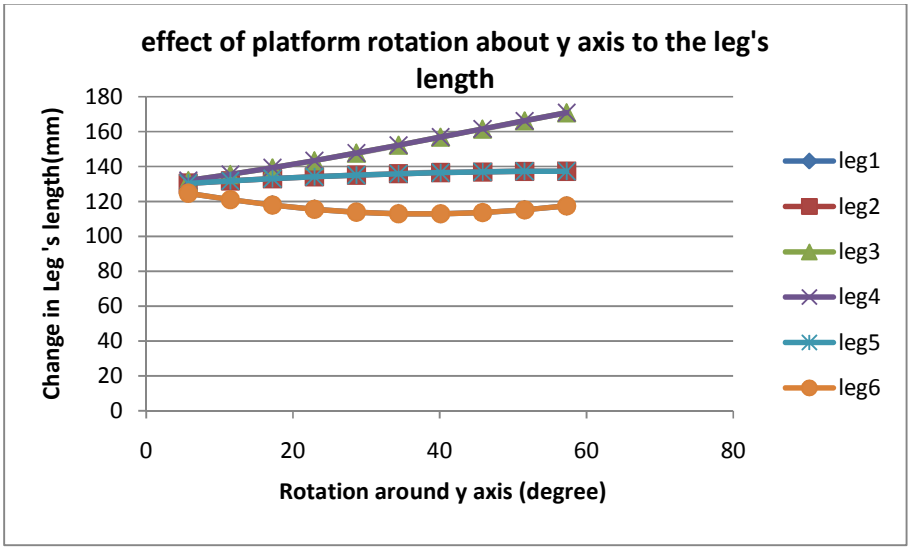

Figure 6-23: effect of rotational movement of mobile platform from 0 to 60 degree about y axis to the leg's length.

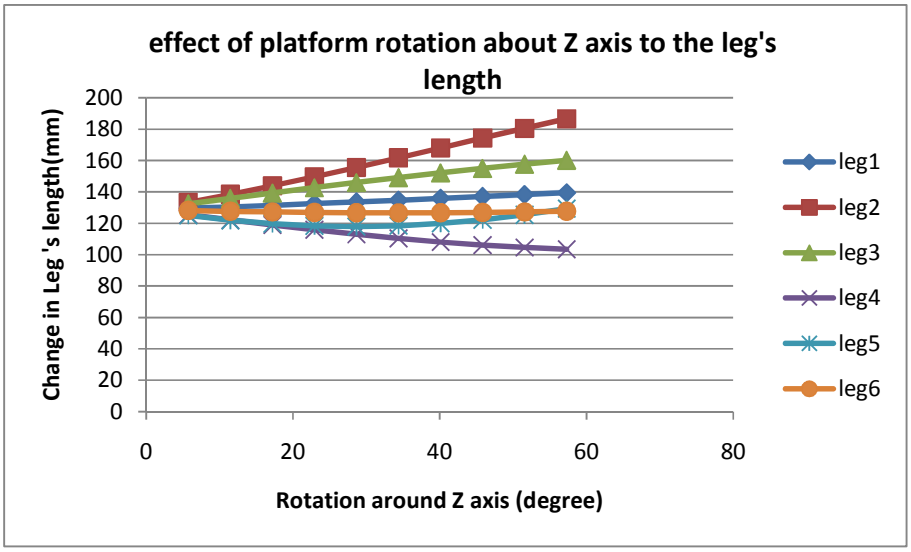

Figure 6-24: effect of the rotational movement of the mobile platform from 0 to 60 degrees about the z axis to the leg's length.

Errors related to the method of testing

This test is an active kind of test, which means that while testing, the movement of moving platform is control only by the hand and there is no complete control of the time and the exact path of the movement of the hand for each test. This is the reason why one hand could end after the test by having two different CORs. In addition, having different sampling rates makes averaging difficult and makes the test unrepeatable. To remedy these shortcomings we arranged a protocol for our testing and made those whose arms were being tested aware of its guidelines, for example, they should be clear how fast they had to move their hand and what were suitable directions of movement. Of course, this protocol shows one of the advantages of the active method. With the passive method, the hand moves with specific force and in a specific direction, but sourly the results do not represent the only elbow kinematics.

6.11.8 Minimizing the experimental errors

In the nature of errors, there are always some ways to minimize the effect of errors to the results. For instance, in the case of systematic errors, manufacturing errors could be minimized if we used appropriate and accurate tools to measure the dimensions of the platform as it is the assembled.

To control random errors, which are mostly related to the relative movement between the bones and the skin, we use the averaging method. Figure 6-8 shows the COR of one of the cases. In this method, each test is repeated at least 5 times and then the final results come from averaging the results of these iterations. Then the standard deviation of the results is calculated, but the results are accepted only when the standard deviation of the results is less than 5% of the average results. This number is calculated in a specific case of our device which we thought demonstrated extreme conditions (see section 6-11-2).

In the following we show how we can use standard deviation to minimise and show the random errors. Figure 6-25 shows five data sets and their average, including standard deviation error for these five data sets. Data set X1(COR) and some parts of data set X2(COR) are outside the standard deviation range. In Figure 6-26, the data set X1(COR) has been omitted from the calculation related to the averaging and standard deviation. And in Figure 6-26, the data set X2(COR) is omitted as well. Figures 6-28 to Figure 6-26 clearly show how the range of errors is reduced in our averaging by more than 5% when we take out the inaccurate results from our data set.

It is possible to show the same theory for the two other axes and also the 3 angles. Here we will take only those about the Z axis which has more changes than the y axis has and other three angles (we have 6 degree of freedom, 3 displacements and 3 rotations about our axes.

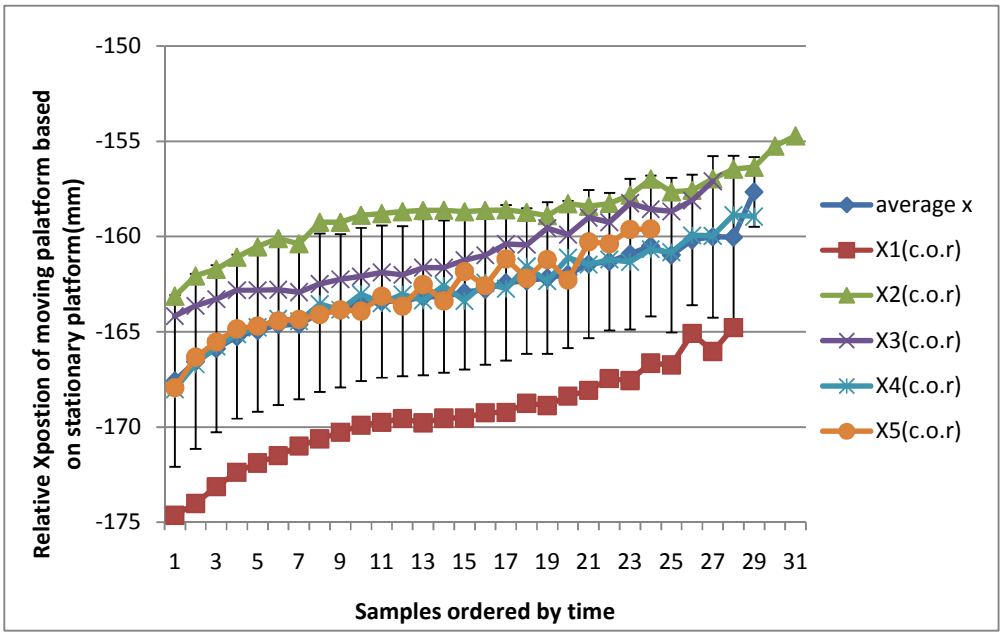

Figure 6-25: Data related to the X axis - five data sets and their average, including standard deviation

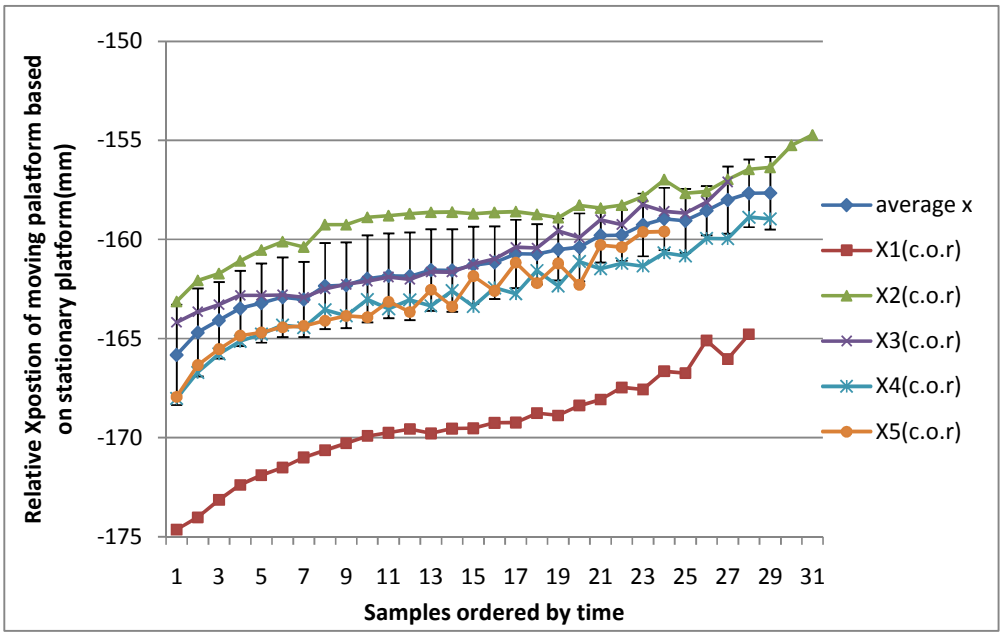

Figure 6-26: Five data sets related to the X axis, but the average and standard deviation are excluded from data set one.

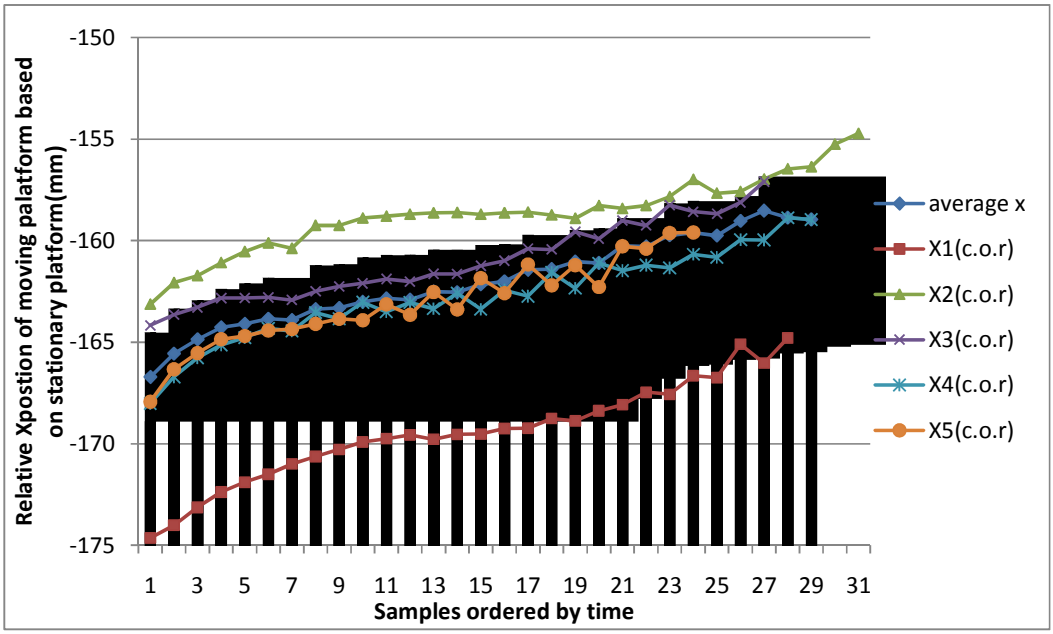

Figure 6-27: Five data sets related to the X axis, but the average and standard deviation are excluded from data sets one and two.

Figure 6-28 shows the five data sets for the z axis plus the average and standard deviations for these data sets. It can be seen in Figure 6-29 that if we exclude data set number 5 from the averaging we will improve the standard deviation by about 36% and will reduce the errors. It is possible to further improve the average and reduce the errors by omitting data set number 4.

6.12 Summary

There are different sources of error in our devices, of which the relative movement between the skin and the bones is the most important. Another important source of potential error in our calculation is the varying speed of the movement of the hand or the different number of samples between our iterations for one hand.

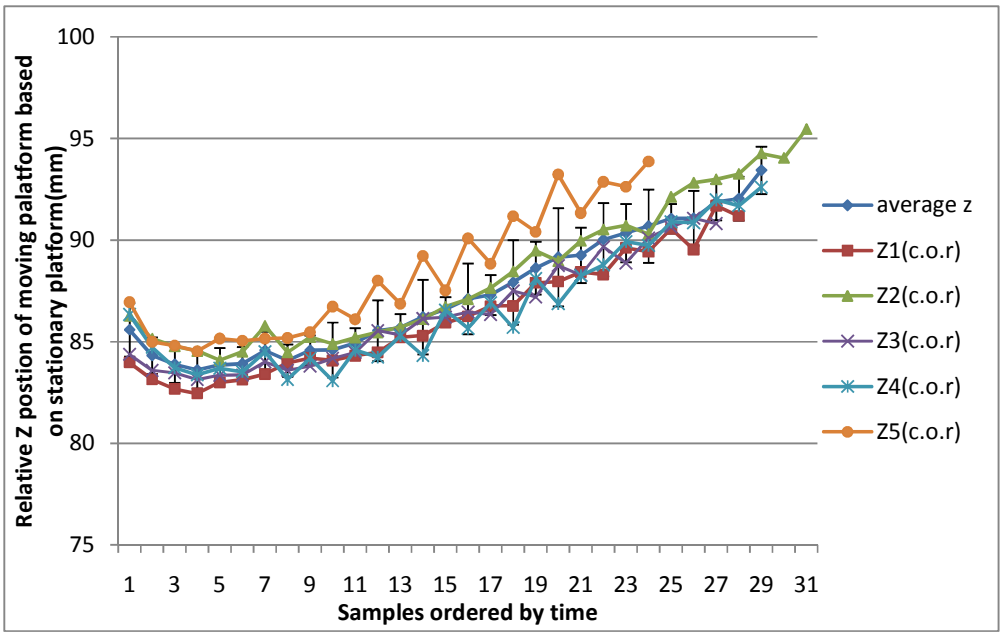

Figure 6-28: Five data sets for the axis and their average results, including standard deviation.

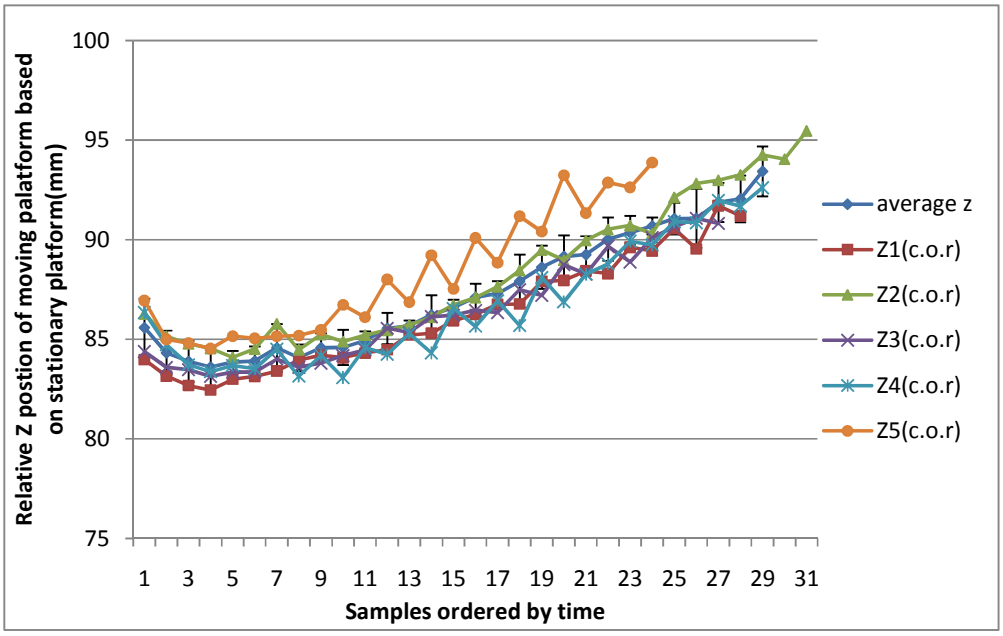

Figure 6-29: Five data sets for the Z axis but data set number five has been excluded from the average result and its standard deviation.

In addition, the free movement of the hand may be another source of error making the results unreliable.

To overcome all these problems and to have more reliable data we introduce our method for averaging data and then controlling them with standard deviation. In this method we accept only the data set results where the standard deviation falls between 5% of the average related to those results.

In addition, to obtain better results with lower standard deviation, it is recommended that the test should be performed at constant speed and along a similar path. This means that while we are testing we should ask the subjects to move their hands at a constant speed (whatever it may be) and along the same path for all iterations related to one hand.

If the standard deviation of our results is greater than 5%, then we must repeat the test and follow the two above recommendations.

Chapter 7. CONCLUSION AND SUGGESTIONS FOR FUTURE WORK

7.1 Conclusion and final remarks

- In this thesis we have used the Stewart Platform mechanism tracking system to measure elbow kinematics and to detect possible joint laxity. As this method has been designed for *in vivo* tests, it can be used for clinical applications.
- A Steward Mechanism Platform based tracking system and elbow joint measurement device was tested with basic motions of the forearm. The mechanism was tested with several subjects and succeeded in measuring all the motions of the forearm and ascertaining the centre of rotation. The tests were executed with the help of another person to ensure that the subjects made the specified motions.
- The first aim of this work was to validate the theoretical aspect of the platform. To this end, a theoretical study took place to show the capacity of the Stewart Platform mechanism to measure the six degrees of freedom of the elbow joint.
- Second an attempt was made to improve elbow motion measurements in *in vivo* conditions. The device traces the centre of the joint rotation in each incremental phase of motion to plot a trajectory for the centre of the joint.

- Moreover, the research was undertaken to develop, implement and validate software capable of computing and following the position of forearm during pronation/supination, Valgus/Varus and Flexion/Extension movements.
- From the available literature there appears to be a lack of an accurate and handy measurement of elbow laxity. This device has the potential to diagnose a lax joint if used in a clinical setting.
- This work also contributes to the fundamental understanding of the laxity in elbow movements and the ability to improve the clinical understanding of elbow function.
- Finally, the results of this work can be of benefit to a wide range of applications, including prosthetic limb design, the development of new rehabilitation strategies for those with compromised elbow function and the immediate benefit of clinically-oriented studies of medical implants.

7.2 Experimental issues

- Fixing the hand in place on the device is not necessarily the same as fixing the hand bones. Due to skin movement, there is some difference between the movement of the hand and the moment of the bones. The error of mistaking one for the other has to be considered in the final results. In this study, the relative motion between the skin and the bones was considered in the section of error analysis; however for further study it is suggested that this area should be investigated.

- Another important challenge in this device relates to the insufficient control of the forearm while measurements are being taken. This could affect the process of averaging. When one case is tested several times, a similar result is expected, but as the subject can move freely in the process of being tested, some inaccuracy in the results could be created. Equally, the forearm could move at a different speed in a different test, since the sampling rate is related to questions of time. When the rate goes up, fewer data are provided. This subject could cause important problems when averaging the results for one case. We discuss these issues in the section on error analysis, but further study in this area is still necessary.
- Comparing the affected elbow to the unaffected is important, because the centre of rotation of the joint changes when the joint is enveloped in soft tissue. This could determine whether or not to proceed with surgery to correct laxity in a symptomatic patient.
- A method of tracking elbow joint motion in three dimensions has not been depicted *in vivo*. A tracking system - the Stewart Platform mechanism, was used to measure the movement of the elbow. We aimed to develop a method of measuring, calculating and modelling elbow joint motion, which might be used to upgrade the kinematic performance of elbow implant designs. A group of volunteers with normal elbows were also studied. Using a screw axis displacement, an iterative computer model was developed. To upgrade joint implants elsewhere in the body a computer modelling has been utilized.

- We believe we have attained this with the Stewart Platform tracking system. One of the goals of this study was to develop a non-invasive tool to capture elbow motion in a way which would allow individual patterns to be compared visually over time. Computerised analysis is made after a visual inspection of the three- dimensional patterns of movement. Our procedure of data acquirement is non-invasive and not time-consuming. Even in normal volunteers, these recorded patterns can vary from person to person.
- Optimum geometric parameters for an elbow replacement design could be produced using the pooled model results of a group of individuals with normal elbows. If implanted correctly, these replacements should most closely produce an accurate replica of normal elbow kinematics, within the limits of the simple model chosen. We accept the fact that the model we chose does not completely depict elbow kinematics. Another goal was to develop a computer program, which was capable of reproducing (as closely as possible) the motion patterns which we had calculated, using a simplified geometric model. Our results so far have gone some way towards attaining this goal.
- As it stands, our method of tracking elbow motion could be suitable for clinical or surgical application. This research constructs the initial results of a new approach to the rational design of elbow implants. We feel that the measuring method described here has the potential to be used for designing a new elbow implant or improving existing elbow devices.

7.3 Future work: some recommendations

- It was challenging to attach the arm and forearm to the device. The potential for error was due to the mobility of the soft tissues. This potential error has to be considered when seeking conclusions from the data. Although special clamps were used to position the limb on the fixed and mobile platforms, improvements still have to be made. One way of reducing the error was to use both the upper limbs of each test subject, assuming that they are similar with regard to the proportion of soft tissue. This could be considered an internal control.
- In further work, a new SPM-based joint measurement device with forced feedback is suggested. This could allow more accurate and comparable data to be gathered with the help of forced feedback and linear actuators.
- As the fixation of the arm and forearm in the platform is always a controversial issue in this method, an important suggestion is to improve the fixture of the hand to the device to reduce the problems of skin movement.
- We measured our results as closely as possible, using a simplified geometric model. It has been suggested that a computer program should be developed based on measurement motion which is able to reproduce the movement patterns of the elbow. Optimum geometric parameters for an elbow replacement design could be produced using the pooled model results of a group of individuals with normal elbows. Our results so far have gone a considerable way towards achieving this goal. The fact that

the model was chosen may not exactly depict elbow kinematics is assumed and accepted.

References

Adrian, M.J. & Cooper, J.M. (1989) Biomechanics of Human Movement: Tools for Human Movement Analysis. 2nd ed. McGraw-Hill. pp. 129-150

Alrashidi M.; Yildiz, I; Alrashdan K; Esat, I; Evaluating elbow joint kinematics with the Stewart Platform Mechanism, Modelling in Medicine and Biology, BIOMED 2009, 8 th. International Conference on 26-28 May 2009, WIT Transactions on Biomedicine and Health, Vol 13, Page(s): pp.181-189

Alrashidi M.; Yildiz, I; Vanat Q.; Alrashdan K; Esat, I; Chizari, M.; Evaluating the Human Joint Laxity Using Stewart Platform Mechanism,The Atlas T3 Annual Meeting Proceedings, Page(s): pp.157-161, May 2010

M. Alrashidi, I. Yildiz, Q. Vanat, K. Alrashdan, I.I. Esat, M. Chizari, Evaluating the Elbow Joint Laxity Using Stewart Platform Mechanism: An Experimental Study, Journal of Biomechanics, Vol:43 Supplement 1, Page S73, June 2010, doi:10.1016/S0021-9290(10)70166-4

American Sport Medicine Institute (2007) Pitching biomechanics evaluation [Internet] Available from: http://www.asmi.org/asmiweb/pitching%20biomechanics%20evaluation.htm[Accessed 7th July 2008].

An, K.N. and Morrey B.F., Biomechanics of the elbow, in The elbow and its disorders. 2003, W.B. Saunders: Philadelphia. pp. 43-60.

Bain, G.I., A review of complex trauma to the elbow. Aust N Z J Surg, 1999. 69(8): pp. 578-81.

Arner, O., Ekengren K., and Von Schreeb T., Fractures of the head and neck of the radius; a clinical and roentgenographic study of 310 cases. Acta Chir Scand, 1957. 112(2): pp. 115-34.

Bain, G.I., A review of complex trauma to the elbow. Aust N Z J Surg, 1999. 69(8): pp. 578-81.

Balažic M., Recek D, Kramar D, Milfelner M. Kopač J, (2008) "Development process and manufacturing of modern medical implants with LENS technology", Department of Machining Technology Management, Faculty of Mechanical Engineering, University of Ljubljana

Beckett, K.S., et al., Variations in the normal anatomy of the collateral ligaments of the human elbow joint. J Anat, 2000. 197 Pt 3: pp. 507-11.

Blankevoort, L., Huiskes, R.and De Lange, A. "Helical axes of passive knee joint motions," *J. Biomech.*, vol. 23, no. 12, pp. 1219-1229, 1990.

Brand, P.W., Beach R.B., and Thompson D.E., Relative tension and potential excursion of muscles in the forearm and hand. J Hand Surg [Am], 1981. 6(3): pp. 209-19.

Bibb R., Eggbeer D., Williams R. (2006) Rapid manufacture of removable partial denture frameworks. Rapid Prototyp J 12(2): 95–99

Bottlang, M., Madey, S.M., Steyers, C.M., Marsh, J.L., Brown, T.D, Assessment of Elbow Joint Kinematics in Passive Motion by Electromagnetic Motion Tracking. J. Orthop Res, Vol.18:195-202, 2000

Captier, G., et al., Biometry of the radial head: biomechanical implications in pronation and supination. Surg Radiol Anat, 2002. 24(5): pp. 295-301.

Castberg, T. and Thing, E., Treatment of fractures of the upper end of the radius. Acta Chir Scand, 1953. 105(1-4): pp. 62-9.

Cherry, J.C., Use of acrylic prosthesis in the treatment of fracture of the head of the radius. J Bone Joint Surg Br, 1953. 35-B(1): pp. 70-1.

Coleman, D.A., Blair, W.F., and Shurr, D., Resection of the radial head for fracture of the radial head. Long-term follow-up of seventeen cases. J Bone Joint Surg Am, 1987. 69(3): pp. 385-92.

Conn, J. and. Wade P.A, Injuries of the Elbow: A Ten Year Review. Journal of Trauma, 1961. 1: p. 248

Dasgupta, B., Mruthyunjaya, T.S.. The Stewart Platform manipulator: a review. Mechanism and Machine Theory 35 (2000) 15-40, December 1998.Duck, T.R., G.J.W.

De Smet, A. A., Winter, T. C., Best, T. M. Bernhardt, D. T., 2002 “Dynamic Sonography with Valgus Stress to Assess Elbow Ulnar Collateral Ligament Injury in Baseball Pitchers”, keletal Radiology, Vol.31, pp. 671- 676.

Deutch, S. R., Olsen, B. S., Jensen, S. L., Tyrdal, S., Sneppen, O., 2003 “Ligamentous and Capsular Restraints to Experimental Posterior Elbow Joint Dislocation”, Scandinavian Journal of Medicine and Science in Sports, Vol. 13, pp. 311-316.

Duck, T.R., et al., Variability and repeatability of the flexion axis at the ulnohumeral joint. J Orthop Res, 2003. 21(3): pp. 399-404.

du Plessis, L. J, An optimization approach to the determination of manipulator workspaces. A thesis submitted in partial fulfillment of the requirement for the degree of Master of Engineering in the Faculty of Engineering - University of Pretoria, 1999.

Ewald, F.C., Total elbow replacement. Orthop Clin North Am, 1975. 6(3): pp. 685-96.

Esat, I., Ozada, N., (2010), “Articular Human Joint Modelling,” Robotica, Special Issue Surgical Robotics.

Galik, K., Gordon, M. and Bullough, P.G. The effect of the annular ligament on kinematics of the radial head. Synovial and osseous inflammation in failed silicone-rubber prostheses. J Bone Joint Surg Am, 1982. 64(4): pp. 574-80.

Garnier, S. ; "Investigation of the Elbow Joint Movements, Measurement of Freedom Degrees"; 2005-6, Brunel University

Geng, Z. J. and Haynes, L. S, "A 3-2-1 kinematic configuration of a Stewart Platform and its application to six degree of freedom post-measurements," Robot. Comput.-Integr. Manuf., vol. 11, no. 1, pp. 23–34, 1994.

Griffith, M., Rangaswamy, P.L, Prime, M.B., Holden T.M., Rogge, R.B., Edwards, J.M., Sebring, R.J., (2005) "Residual stresses in LENS components using neutron diffraction and contour method" Materials Science and Engineering A 399, 72-83. Hand Surg [Am], 2007. 32(8): pp. 1218-1224.

Gonzalez, R.V., et al., Development and evaluation of a musculoskeletal model of the elbow joint complex. J Biomech Eng, 1996. 118(1): pp. 32-40.

Gough, V.E. and Whitehall, S.G. Universal tyre test machine. In Proceeding 9th international technical congress F.I.S.I.T.A, Vol. 117, pp.117-137, 1962.

Hannouche D., Begue T., 1999 "Functional Anatomy of the Lateral Collateral Ligament complex of the Elbow", Surgical Radiology, Vol. 21, pp. 187-191.

Jonsson, H. and Karrholm, J. "Three-dimensional knee joint movements during step-up: evaluation after anterior cruciate ligament rupture," *J. Orthp. Res.*, vol. 12, no. 6, pp. 769-779, November 1994.

Hatzel, B, Horodyski, M, Kaminski, T W, Meister, K, Powers, M, Brunt, D; "Measurement of glenohumeral joint laxity using the KT-2000 knee ligament arthrometer: Reliability analysis" Physical Therapy in Sport 7 (2006) 137–143.

Hollander, D.A., von Walter, M., Wirtz, T., Sellei, R., Rohlfing, B.S., Paar, O., Erli, H.J., (2006) "Structural, mechanical and in vitro characterization of individually structured Ti–6Al–4V produced by direct laser forming" Biomaterials 27, 955-963.

Hollister, A.M., Gellman, H. and Waters, R.L. The relationship of the interosseous membrane to the axis of rotation of the forearm. Clin Orthop Relat Res, 1994(298): pp. 272-6.

Hotchkiss, R.N., Displaced Fractures of the Radial Head: Internal Fixation or Excision? J Am Acad Orthop Surg, 1997. 5(1): pp. 1-10.

Hotchkiss, R.N. and Weiland, A.J., Valgus stability of the elbow. J Orthop Res, 1987. 5(3): pp. 372-7.

Hunt, K.H.. Structural kinematics of in-parallel-actuated-robot-arm. ASME J. Mech., Trans. Automat. Des.,vol.105, pp.705-715,1983

Iannatsis J., Dedoussis, V., (2007).Additive fabrication technologies applied to medicine and health care: a review. Int J Adv Manuf Technology.

Jensen, S. L., Olsen, B. S., Sojberjg, J. O., 1999 "Elbow joint Kinematics After Excision of the Radial Head" Journal of Shoulder and Elbow Surgery, Vol. 8, pp. 238-241.

Jensen, S. L., Olsen, B. S., Tyrdal, S., Sojberjg, J. O., Sneppen, O., 2004 "Elbow Joint Laxity After Experimental Radial Head Excision and Lateral Collateral Ligament Rupture: Efficacy of Prosthetic Replacement and Ligament Repair", Journal of Shoulder and Elbow Surgery, Vol.14, pp. 78-84.

Jensen, S.L., et al., Laxity of the elbow after experimental excision of the radial head and division of the medial collateral ligament. Efficacy of ligament repair and radial head prosthetic replacement: a cadaver study. J Bone Joint Surg Br, 2003. 85(7): pp. 1006-10.

Jeong, J, Kim, S, and Kwak, Y., "Kinematics and workspace analysis of a parallel wire mechanism for measuring a robot pose," *Mech. Mach. Theory*, vol. 34, no. 6, pp. 825–841, 1999.

Johnson, G.W., A Follow-Up of One Hundred Cases of Fracture of the Head of the Radius with a Review of the Literature. Ulster Medicine Journal, 1952. 31: pp. 51-56.

Khan, S. F. and Dalgarno, K. W., (2007), Design of Customised Medical Implants by Layered Manufacturing, School of Mechanical and Systems Engineering, Newcastle University

King, G.J and. Johnson J.A. Screw Displacement Axes of Forearm Pro-Supination. in 47th Annual Meeting, ORS. 2001. San Francisco, California.

King, G.J., Evans, D.C. and Kellam, J.F. Open reduction and internal fixation of radial head fractures. J Orthop Trauma, 1991. 5(1): pp. 21-8.

King, G.J., et al., Metallic radial head arthroplasty improves valgus stability of the elbow. Clin Orthop, 1999(368): pp. 114-25.

Knight, D.J., et al., Primary replacement of the fractured radial head with a metal prosthesis. J Bone Joint Surg Br, 1993. 75(4): pp. 572-6.

Kupper, J.C., Ramage, B. L., Corr, D.T., Hart, D.A., Ronsky, J.L., Measuring knee joint laxity: A review of applicable models and the need for new approaches to minimize variability. Clinical Biomechanics 22 (2007) 1–13, www.Elsevier.com/locate/ clinbiomech.

Liew, V.S., et al., The effect of metallic radial head arthroplasty on radiocapitellar Ring, D., J. Quintero, and J.B. Jupiter, Open reduction and internal fixation of fractures of the radial head. J Bone Joint Surg Am, 2002. 84-A(10): pp. 1811-5.

López de Lacalle, L.N., Lamikiz, A., Celaya,A., (2002) "Simulation of plasma assisted milling of heat resistant alloys" International Journal of Simulation Modelling 1/1, 5-15

Magnusen, J. P., DESIGN AND FABRICATION OF AN ELBOW MOTION SIMULATOR, Thesis for fulfillment of the requirements for the degree of Master of Science in Mechanical Engineering, University of Pittsburgh 2004.

Melhorn, J. M.: Cumulative trauma disorders and repetitive strain injuries.The future. *Clin. Orthop.,* 351: 107-126, 1998

Mihata, T., Safran, M. R., McGarry, M. H., Abe, M. and Lee, T. Q., Elbow Valgus Laxity May Result in an Overestimation of Apparent Shoulder External Rotation During Physical Examination, Am J Sports Med 2008 36: 978 originally published online February 13, 2008, DOI: 10.1177/0363546507313086

Mihata, T., Safran, M. R., McGarry, M.H., Abe, M., Lee, T.Q., Elbow Valgus Laxity May Result in an Overestimation of Apparent Shoulder External Rotation During Physical Examination, The American Journal of Sports Medicine, 2008 36: 978 originally published online February 13, 2008, http://ajs.sagepub.com/content/36/5/978.

Mikic, Z.D. and Vukadinovic, S.M. Late results in fractures of the radial head treated by excision. Clin Orthop Relat Res, 1983(181): pp. 220-8.

Milovanović J., Trajanović, M., (2007) Medical Applications Of Rapid Prototyping, FACTA UNIVERSITATIS Series: Mechanical Engineering Vol. 5, No 1, pp. 79 - 85

Moro, J.K., et al., Arthroplasty with a metal radial head for unreconstructible fractures of the radial head. J Bone Joint Surg Am, 2001. 83-A(8): pp. 1201-11.

Morrey, B.F. and Chao, E.Y.: Passive Motion of the Elbow Joint. J. Bone and Joint Surg., 58:501-508, 1976.

Morrey, B.F., Chao, E.Y., and Hui, F.C., Biomechanical study of the elbow following excision of the radial head. J Bone Joint Surg Am, 1979. 61(1): pp. 63-8.

Morrey, B.F., Askew, L.J., and Chao, E.Y., A biomechanical study of normal functional elbow motion. J Bone Joint Surg Am, 1981. 63(6): pp. 872-7.

Morrey, B.F. and An K.N., Articular and ligamentous contributions to the stability of the elbow joint. Am J Sports Med, 1983. 11(5): pp. 315-9.

Morrey, B.F. and An, K.N., Functional anatomy of the ligaments of the elbow. Clin Orthop Relat Res, 1985(201): pp. 84-90.

Morrey, B.F., Tanaka, S., and An, K.N., Valgus stability of the elbow. A definition of primary and secondary constraints. Clin Orthop, 1991(265): pp. 187-95.

Morrey, B.F., Complex instability of the elbow. Instr Course Lect, 1998. 47: pp. 157-64.

Morrey, B.F., Radial head fracture, in The elbow and its disorders. 2000, W.B. Saunders: Philadelphia. pp. 341-364.

Murray, R., Fractures of the head and neck of the radius. Br. J. Surg, 1940. 28: pp. 106.

Nijhof, E. Jan and Gabriel, D.A. Maximum isometric arm forces in the horizontal plane. J Biomech, 2006. 39(4): pp. 708-16.

Nurul Wahida Binti Mat Aron. 'The development of camera imaging software to investigate elbow joint laxity using new design arm device'', Brunel University thesis.

Olsen, B.S., et al., Lateral collateral ligament of the elbow joint: anatomy and kinematics. J Shoulder Elbow Surg, 1996. 5(2 Pt 1): pp. 103-12.

O`Driscoll, S. W., Bell, D. F., Morrey, B. F., 1991 "Posterolateral rotatory instability of the Elbow", Journal of Bone and Joint Surgery, Vol. 73, pp. 440-446.

O`Driscoll, S. W., Horii, E., Morrey, B. F., Carmichael, S.W., 1992 "Anatomy of the Ulnar Part of the Lateral Collateral Ligament of the Elbow", Clinical Anatomy, Vol.5, pp. 296-303.

Olsen, B. S., Sojberjg, J. O., Dalstra, M., Sneppen, O., 1996 "Kinematics of the Lateral Ligamentous Constraints of the Elbow joint", Journal of Shoulder and Elbow Surgery, Vol. 5, pp. 333-341.

Olsen, B. S., Vaesel, M. T., Sojbjerg, J. O., Helmig, P., Sneppen, O., 1996 "Lateral Collateral Ligament of the elbow Joint: Anatomy and Kinematics", Journal of Shoulder and Elbow Surgery, Vol. 5, pp. 103-112.

Olsen, B. S., Sojberjg, J. O., Nielsen, K. K., Vaesel, M. T., Dalstra, M., Sneppen, O., 1998 "Posterolateral Elbow Joint Instability: The Basic Kinematics", Journal of Shoulder and Elbow Surgery, Vol. 7, pp.19-29.

Ozada, N, and Esat, I., (2007) "HUMAN JOINT MODELING" Brunel University, Department of Mechanical Engineering.

Pomianowski, S., et al., Contribution of monoblock and bipolar radial head prostheses to valgus stability of the elbow. J Bone Joint Surg Am, 2001. 83-A(12): pp. 1829-34.

Pribyl, C.R., et al., The effect of the radial head and prosthetic radial head replacement on resisting valgus stress at the elbow. Orthopedics, 1986. 9(5): pp. 723-6.

Ring, D., Jupiter, J.B., and Zilberfarb, J., Posterior dislocation of the elbow with fractures of the radial head and Coronoid. J Bone Joint Surg Am, 2002. 84-A(4): pp. 547-51.

Safran, M. R., Mcgarry, M. H., Shin, S., Han, S., Lee, T. Q., 2005 " Effects of Elbow Flexion and Forearm Rotations on Valgus Laxity of the Elbow", Journal of Bone and Joint Surgery, Vol. 87, No.9.

Safran, M. R., 2007 "Comparison of Elbow Valgus Laxity Using Radiographic and Non- Radiographic Objective Measurements", 6th Biennial ISOKAS Congress.

Sauers, E L, Borsa, P A, Herling, D E, Stanley, R D, "Instrumented measurement of glenohumeral joint laxity: reliability and normative data" Knee Surg, Sports Traumatol, Arthrosc (2001) 9 :34–41

Sampath, G., et al. Design and development of an active marker based system for analysis of 3-D pediatric foot and ankle motion. in Engineering in Medicine and Biology Society, 1998. Proceedings of the 20th Annual International Conference of the IEEE. 1998.

Shultz, S. J., Shimokochi, Y., Nguyen A. D., Schmitz, R. J., Beynnon, B. D., Perrin, D. H., Measurement of Varus–Valgus and Internal–External Rotational Knee Laxities In Vivo—Part I: Assessment of Measurement Reliability and Bilateral Asymmetry, Published online 24 April 2007 in Wiley InterScience (www.interscience.wiley.com). DOI 0.1002/jor.20397.

Sojbjerg, J.O., Ovesen, J., and Gundorf, C.E., The stability of the elbow following excision of the radial head and transection of the annular ligament. An experimental study. Arch Orthop Trauma Surg, 1987. 106(4): pp. 248-50.

Soudan, K. Van Audekercke, R. and Martens, M. "Methods, difficulties and inaccuracies in the study of human joint kinematics and pathokinematics by the instant axis concept. Example: the knee joint," *J. Biomech.*, vol. 12, no. 1, pp. 27-33, 1979.

Stewart, D., "A platform with six degrees of freedom," Proc. Inst. Mech. Eng., Vol.180, partI(15), 1965-1966, pp.371-386.

Swanson, A.B., Jaeger, S.H., and La Rochelle, D., Comminuted fractures of the radial head. The role of silicone-implant replacement arthroplasty. J Bone Joint Surg Am, 1981. 63(7): pp. 1039-49.

Tanaka, S., An, K.N., Morrey, B.F.: Kinematics and Laxity of Ulnohumeral Joint under Varus-Valgus Stress. J. Musculoskel Res 2:45-54, 1998.

Tengvall, P., Lundstrom, I., (1992) "Physico-chemical considerations of titanium as a biomaterial" Clinical Materials 9, pp 115-134.

Thomas, T.T., Fractures of the head of the radius. Univ. Pa. Med. Bull., 1905. 18: pp. 184-221.

Tomaino, M.M., et al., Reconstruction of the interosseous ligament of the forearm reduces load on the radial head in cadavers. J Hand Surg [Br], 2003. 28(3): pp. 267-70.

Trousdale, R.T., et al., Radio-ulnar dissociation. A review of twenty cases. J Bone Joint Surg Am, 1992. 74(10): pp. 1486-97.

Vangsness, C.T., Jr., et al., The origin of the long head of the biceps from the scapula and glenoid labrum. An anatomical study of 100 shoulders. J Bone Joint Surg Br, 1994. 76(6): pp. 951-4.

Van Riet, R.P., et al., The noncircular shape of the radial head. J Hand Surg [Am], 2003. 28(6): pp. 972-8.

Van Riet, R.P., et al., The effect of the orientation of the noncircular radial head on elbow kinematics. Clin Biomech (Bristol, Avon), 2004. 19(6): pp. 595-9.

Van Zuylen, E.J., van Velzen, A., and Denier van der Gon, J.J., A biomechanical model for flexion torques of human arm muscles as a function of elbow angle. J Biomech, 1988. 21(3): pp. 183-90.

Veeger, H.E.J., Yu, B., and An, K.N, Orientation of Axes in the Elbow and Forearm for Biomechanical Modeling. in First Conference of the International Shoulder Group. 1997: Maastricht, Delft.

Wagner, C. H., 1977 "Determination of the Rotary Flexibility of the Elbow Joint", European Journal of Applied Physiology, Vol. 37, pp. 47-59.

Waugh, A, Grant, A, 'Ross and Wilson Anatomy and physiology in Health and Illness' Churchill Livingstone 2001.

Weiss, A.-P., C. and H. Hastings II, The Anatomy of the Proximal Radioulnar Joint. Journal of Shoulder and Elbow Surgery, 1992. 1(4): pp. 193-199.

Wohlers, T. (2007) "State of the Industry" Annual Worldwide Progress Report, Wohlers Associates, Fort Collins,USA, ISBN 0-9754429-3-7

Woltring, H. J., Huiskes, R. de Lange, A. and Veldpaus, F. E. "Finite centroid and helical axis estimation from noisy landmark measurements in the study of human joint kinematics," *J. Biomech.*, vol. 185, pp. 379-389, 1985.

Yasser A. Hosni, (2000) "Contribution of CAD-CAM and Reverse Engineering Technology to the Biomedical Field" Proceedings, MDP7 Conference Proceedings, Cairo, Egypt

Yasser, A. Hosni1, Ola Harrysson, (2002)"Design and Manufacturing of Customized Implants" Industrial Engineering and Management Systems

Some related sites:

Optomec company, http://www.optomec.com, access 12.01.2011 5.23 pm

CT-scan, http://www.google.co.uk/imgres, access 28.02.2011 7.28 pm

MRI, http://www.google.co.uk/imgres, access 28.02.2011 7.28 pm.

PARALLEMIC, http://www.parallemic.org/reviews/review007.html , accessed 28/02/2010.

Appendixes

Appendix A

Screw displacement Axis Theory

We want to determine the screw displacement parameters for a spatial displacement. These parameters consist of:

φ_ = the angle of rotation about the screw axis

$d_{\parallel}$ = the translation along the screw axis

ω = a unit vector parallel to the screw axis

ρ = a vector to a point on the screw axis

Assume that we have a rigid body which contains three non-colinear points: P, Q, R. Let P_6, Q_6, and R_6 denote the positions of the points in the body before displacement. Let P_1, Q_1, and R_1 be the position of these points after a screw displacement.

Solution:

To determine the screw parameters from the displacement of these three points, we solve the following three simultaneous equations:

$$P_1 - P_0 = \tan(\frac{\phi}{2})\ \vec{\omega} \times (P_1 + P_0 - 2\vec{\rho}) + d^{\parallel}\vec{\omega} \qquad \textbf{(6.1)}$$

$$Q_1 - Q_0 = \tan(\frac{\phi}{2})\ \vec{\omega} \times (Q_1 + Q_0 - 2\vec{\rho}) + d^{\parallel}\vec{\omega} \qquad \textbf{(6.2)}$$

$$R_1 - R_0 = \tan(\frac{\phi}{2})\ \vec{\omega} \times (R_1 + R_0 - 2\vec{\rho}) + d^{\parallel}\vec{\omega} \qquad \textbf{(6.3)}$$

Where, each equation is the Rodriguez displacement equation for the points P, Q, and R respectively.

Step 1: Subtract Equation (3) from Equations (1) and (2):

$(P_1 - P_6) - (R_1 - R_6) = \tan(\varphi/2) \times \omega \times [(P_1 + P_6) - (R_1 + R_6)]$ (6.4)

$(Q_1 - Q_6) - (R_1 - R_6) = \tan(\varphi/2) \times \omega \times [(Q_1 + Q_6) - (R_1 + R_6)]$ (6.5)

Form the cross product of $[(Q_1 - Q_6) - (R_1 - R_6)]$ with Equation (6.5):

$[(Q_1 - Q_6) - (R_1 - R_6)] \times [(P_1 - P_6) - (R_1 - R_6)]$

$= \tan(\varphi/2) [(Q_1 - Q_6) - (R_1 - R_6)] \times \{\omega \times [(P_1 + P_6) - (R_1 + R_6)]\}$ (6.6)

Note: from Equation (5), we know that $[(Q_1-Q_6)-(R_1-R_6)]$ is perpendicular to ω, since it results from the cross produce of a vector with ω. Therefore, the right hand side of Equation (6) will be a vector proportional to ω

We can use the vector identity $a \times (b \times c) = (a \cdot c)\, b - (a \cdot b)\, c$ to simplify Equation (6):

$[(Q_1 - Q_6) - (R_1 - R_6)] \times [(P_1 - P_6) - (R_1 - R_6)]$

$= \tan(\varphi/2) [(Q_1 - Q_6) - (R_1 - R_6)] \cdot [(P_1 + P_6) - (R_1 + R_6)]\, \omega$ (6.7)

We can solve Equation (7) for $\tan(\varphi/2)\, \omega$:

$\tan(\varphi/2)\omega = [(Q_1 - Q_6) - (R_1 - R_6)] \times [(P_1 - P_6) - (R_1 - R_6)] / [(Q_1 - Q_6) - (R_1 - R_6)] \cdot [(P_1 + P_6) - (R_1 + R_6)]$ (6.8)

Thus, the rotation angle, $\tan(\varphi/2)$, can be computed as the norm to the vector in Equation (8), while ω is the normalized vector of Equation (6.8).

Step 2: Now take the cross product of ω with Equation (6.1) and use the above vector cross product identity:

$$\begin{aligned} \vec{\omega} \times (P_1 - P_0) &= \vec{\omega} \times [\tan(\tfrac{\phi}{2})\, \vec{\omega} \times (P_1 + P_0 - 2r\vec{h}o) + d^{\parallel}\vec{\omega}] \\ &= \tan(\tfrac{\phi}{2})\ [[\vec{\omega} \cdot (P_1 + P_0)]\vec{\omega} - (P_0 + P_1) - 2(\vec{\omega} \cdot \vec{\rho})\vec{\omega} + 2\rho] \end{aligned} \qquad (6.9)$$

Note that ρ $- (\omega \cdot \rho)\omega = \rho_{\perp}$, where $\rho_{\perp}$ is the component of ρ which is perpendicular to ω.

That is, while ρ is a vector from the origin of the reference frame to any point on the screw axis, ρ┼ is the shortest vector to the point on the screw axis closest to the origin of the reference frame. Equation (9) can then be solved for ρ┼:

$$\vec{\rho}_{\perp} = \frac{1}{2}\left[\frac{\vec{\omega} \times (P_1 - P_0)}{\tan\frac{\phi}{2}} - (\vec{\omega} \cdot (P_1 + P_0))\vec{\omega} + P_0 + P_1\right] \qquad (6.10)$$

Step 3:

Finally, we can use Equation (1), (2), or (3) to find d‖:

$$d^{\parallel} = \vec{\omega} \cdot (P_1 - P_0) = \vec{\omega} \cdot (Q_1 - Q_0) = \vec{\omega} \cdot (R_1 - R_0) \qquad (6.11)$$

Appendix B

Data logger – Data Acquisition

Introduction

A data logger is an electronic device used to record measurements over time. Pico data loggers require no power supply and simply plug into a parallel, serial or USB port on a PC or Laptop.

By connecting suitable sensors, Pico data acquisition products can be used to measure temperature, pressure, relative humidity, light, resistance, current, power, speed, vibration ….

Pico data loggers are supplied complete with Pico-Log software. This powerful flexible data acquisition software allows researchers to collect, analyze and display data. With Pico-Log, the data is viewable both during and after data collection, in both spreadsheet and graphical format. If required, the data can also be exported to other applications.

Pico Data Acquisition Products

Model	Channels	Humidity	Temperature	Sampling Rate	Voltage Ranges	Resolution	PC Connection
USB TC-08	8		Thermocouple		±70 mV	20 bits	USB
TH-03	3		-30° - 70° C			0.003° C	Serial

PT-104	4		PT-100 Sensor		0-2.5 V	24 bits	Serial
HumidiProbe	1	0-100% RH	0-70° C			0.01°C, 0.03%RH	USB
ADC 10	1			20kS/s	0-5 V	8 bits	Parallel
ADC 12	1			15kS/s	0-5 V	12 bits	Parallel
ADC 40	1			20kS/s	±5 V	8 bits	Parallel
ADC 42	1			15kS/s	±5 V	12 bits	Parallel
ADC 11/10	11			20kS/s	0-2.5 V	10 bits	USB
ADC 11/12	11			20kS/s	0-2.5 V	12 bits	USB
ADC 16	8			1.5 S/s	±2.5 V	16 bits	parallel
ADC 20	4 differential or 8 single-ended				±1250 mV, ±2500 mV	20 bits	USB
ADC 24	8 differential or 16 single-ended +4 Digital I/O				±39mV to ±2500mV in 7 ranges	24 bits	USB

Note: Quoted sampling rates are for single channel operation

USB ADC-11/10 and ADC-11/12

A data acquisition device with up to 11 input channels

Large number of channels

No power supply required

Digital output for control

Data acquisition software included

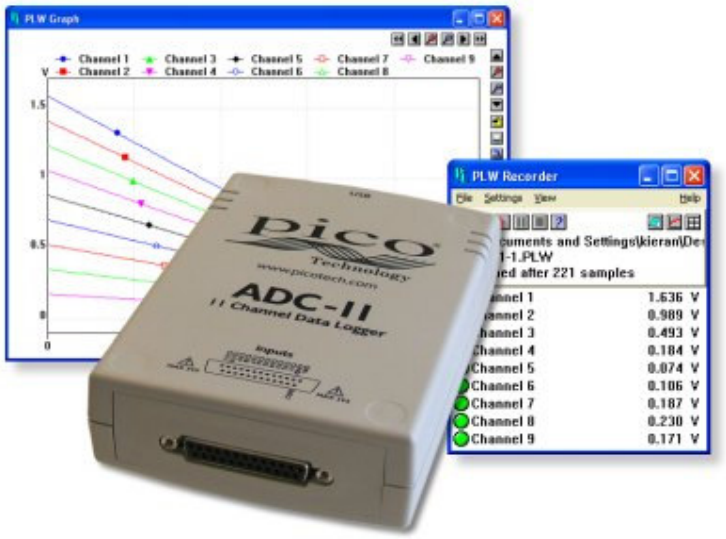

.

Resolution and Accuracy

Two different versions of the ADC-11 are available: the ADC-11/10 features 10- bit resolution, whilst the ADC-11/12 has 12--bit resolution, making it suitable for detecting very small signal changes.

With data acquisition the accuracy of measurements is paramount, which is why the ADC-11/10 is accurate to within 1%, and the ADC-11/12 to within 0.5 %.

USB connection

The USB interface makes the ADC-11 easy to connect to any modern laptop or desktop PC and allows up to 4 units to connect to one PC making up to 44 channels of data acquisition available at very low cost per channel.

Terminal block

To simplify the connection of the sensors, a terminal block is available for the ADC-11. This connects to the input of the ADC-11 and provides screw terminals to allow quick connection and disconnection of the sensors.

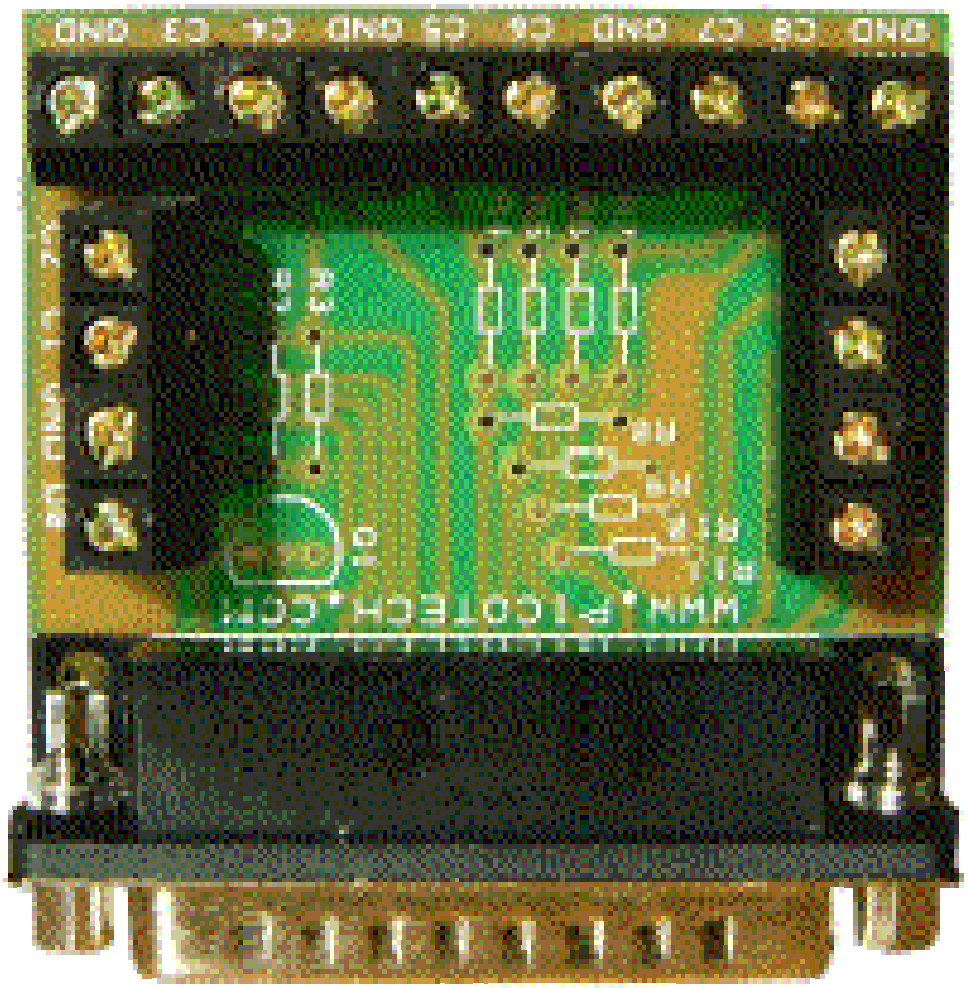

No need for power supplies or batteries

The ADC-11 is powered directly by the PC, eliminating the need for batteries or a separate power supply, and making it ideal for acquiring data with a portable device.

Control alarms and other devices

The ADC-11 data loggers include digital outputs — these can be used to control alarms or other devices. Additionally these outputs can also be used to power sensors such as thermistors (outputs can be controlled using the programming API but cannot be controlled using Pico-Log).

Data acquisition software

All products in the Pico data logger range come complete with Pico-Log — this powerful, but flexible, data acquisition software allows researchers to collect, manipulate, analyse, display and export data.

Low cost data acquisition

The Pico ADC-11 data loggers are data acquisition products capable of measuring a large number of channels at low cost solution and require no power supply. They can connect to both USB and parallel ports, and come complete with data acquisition software.

Specifications

	ADC-11/10 (PP241 OR PP239)	ADC-11/12 (PP240 OR PP242)
Number of channels	11	
Digital outputs (3.3 V)	2	2
Sampling rate #	20 kS/s	20 kS/s
Input type	Unipolar - single ended	
Voltage ranges	0 to 2.5 V	
Input connector	D25 Female	
AC/DC coupling	DC coupled	
Overload protection	±30 V	
Accuracy	1 %	0.5 %

	ADC-11/10 (PP241 OR PP239)	ADC-11/12 (PP240 OR PP242)
Input impedance	>1 MΩ	
Resolution	10 bits	12 bits
Environmental	20-30 °C for quoted accuracy, 0 to 70 °C overall. 20-90 %RH	
PC connection	USB 1.1	
Power supply	Powered directly from the PC	
Supplied software	PicoScope 5 (oscilloscope, spectrum analyser, meter) PicoLog (data logger) Software Development Kit Software is supplied on CD and is compatible with 32-bit editions of Windows XP (SP2) and Vista.	
Language support (software)	**PicoLog**: English **PicoScope 5**: English, French, German, Spanish and Czech	
Language support (documentation)	**User's guide**: English **Installation guide**: English, French, German, Italian, Spanish, Swedish, Dutch, Danish	

[#] Sampling rates are divisible by the number of channels in use.

Appendix C

Potentiometer

Ranges: Up to 50 inches
Precision Potentiometric Output
Low Cost • Fast Delivery

SP1

Handy Mounting Bracket
Mounts easily and quickly in several directions

Designed for Cable Misalignment
Long cable life, even when installation isn't perfect

Polycarbonate Enclosure
Withstands impacts and chemicals

CE **"Free-Release" Tolerant**
Greatly reduces damage due to mis-handling of cable

The Celesco SP1 String Pot is a compact, economical and durable device that utilizes a flexible cable, a spring-loaded spool, and a potentiometer to detect and measure linear position.

The SP1 is designed for tight spaces, high-cycle applications and generously allows cable misalignment. With 4 different measurement ranges and handy mounting brackets, the SP1 is a perfect solution for many applications, from light industrial to OEM.

Specification Summary:

GENERAL

Full Stroke Range Options	0-4.75, 0-12.5, 0-25, 0-50 inches
Output Signal	voltage divider (potentiometer)
Accuracy	±0.25 to ±1.00% *see ordering information*
Repeatability	± 0.05% full stroke
Resolution	essentially infinite
Measuring Cable	0.019-in. dia. nylon-coated stainless steel
Enclosure Material	polycarbonate
Sensor	plastic-hybrid precision potentiometer
Weight	3 oz. (w/o mounting bracket) max.

ELECTRICAL

Input Resistance	10K ohms, ±10%
Power Rating, Watts	2.0 at 70°F derated to 0 at 250°
Recommended Maximum Input Voltage	30 V (AC/DC)
Output Signal Change Over Full Stroke Range	94% ±4% of input voltage

ENVIRONMENTAL

Enclosure	IP 50
Operating Temperature	0° to 160°F (-18° to 71°C)
Vibration	up to 10 G's to 2000 Hz maximum

Output Signal

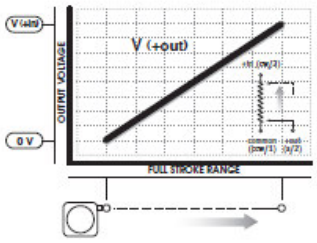

Ordering Information:

Item Number:	SP1-4	SP1-12	SP1-25	SP1-50
full stroke range:	4.75 in.	12.5 in.	25 in.	50 in.
accuracy (% of f.s.):	1.00%	0.25%	0.25%	0.25%
potentiometer cycle life:	2.5M cycles	500K cycles	500K cycles	250K cycles
cable tension (±25%):	7 oz.	7 oz.	7 oz.	7 oz.
max. cable acceleration:	15 G	15 G	15 G	15 G

celesco
celesco.com • info@celesco.com

Celesco Transducer Products, Inc.
20630 Plummer Street • Chatsworth, CA 91311
tel: 800.423.5483 • +1.818.701.2750 • fax: +1.818.701.2799

Installation Information:

Outline Drawing (w/o bracket):

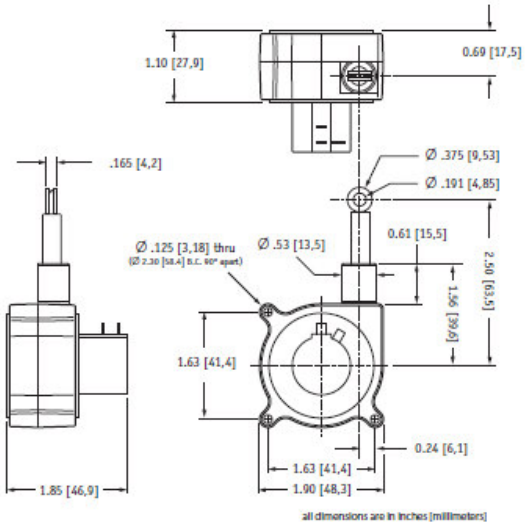

Electrical Connection:

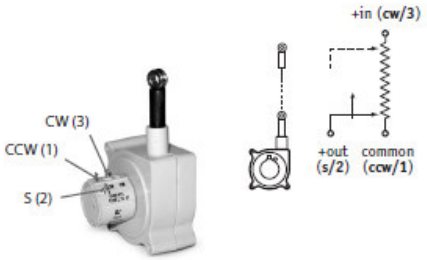

Mounting Options:

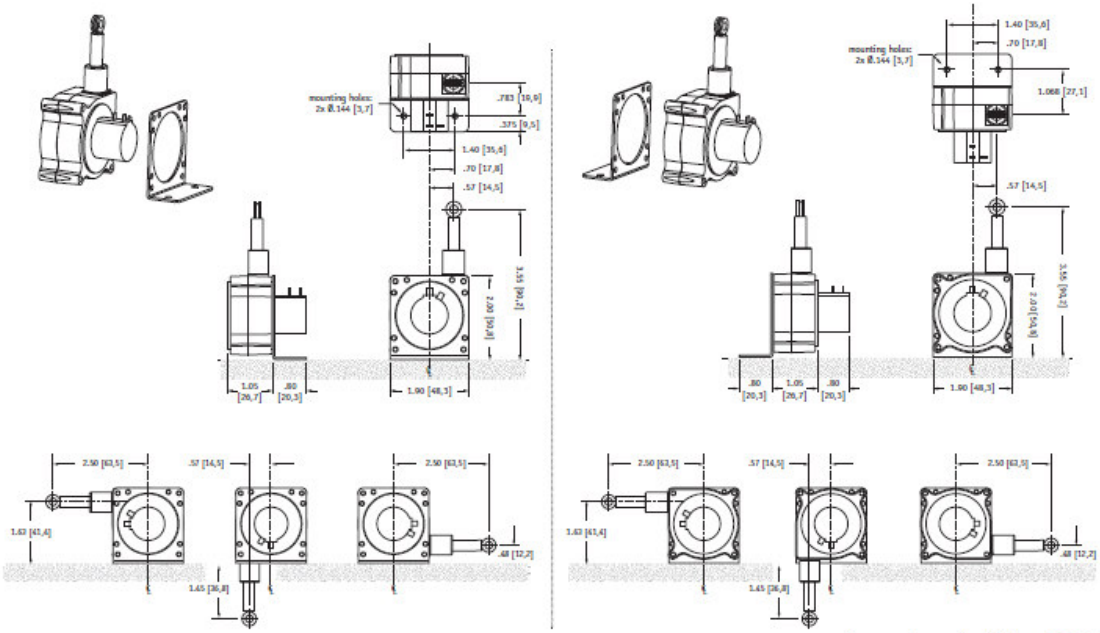

Appendix D

MATLAB Program

The MATLAB program transfers 6 wire lengths of the potentiometers to 6 degrees of movement (3 displacements along x, y, z) and 3 rotations (around x, y, z)).

```
clear all
L=xlsread('length2');
L(1,:)=[];
temps=L(:,1);
L(:,1)=[];
% Platform radius
Rp=71;
Rb=150;
% Angle tetaB and tetaP
tetaB=pi/8;
tetaP=9*pi/16;
% Sensors positions
for i=0:2
gama(2*i+1)=(pi/3)*(2*i+1)-tetaB/2;
lambda(2*i+1)=(pi/3)*(2*i+1)-tetaP/2;
end
for i=1:3
gama(2*i)=gama(2*i-1)+tetaB;
lambda(2*i)=lambda(2*i-1)+tetaP;
end
for i=1:6
P(i,:)=Rp*[cos(lambda(i)) sin(lambda(i)) 0];
B(i,:)=Rb*[cos(gama(i)) sin(gama(i)) 0];
end
% calculation of the transformation of rotation matrix
x(:,1)=[0; 0; 76.7; 0; 0; 0];
dim=size(L);
nb_echant=dim(1);
L=L';
for j=1:nb_echant
err=0.01;
ind=0;
while ind~=6
R=[cos(x(4,j))*cos(x(5,j))             cos(x(4,j))*sin(x(5,j))*sin(x(6,j))-
sin(x(4,j))*cos(x(6,j))
cos(x(4,j))*sin(x(5,j))*cos(x(6,j))+sin(x(4,j))*sin(x(6,j));
sin(x(4,j))*cos(x(5,j))
sin(x(4,j))*sin(x(5,j))*sin(x(6,j))+cos(x(4,j))*cos(x(6,j))
sin(x(4,j))*sin(x(5,j))*cos(x(6,j))-cos(x(4,j))*sin(x(6,j));
-sin(x(5,j)) cos(x(5,j))*sin(x(6,j)) cos(x(5,j))*cos(x(6,j))];
for i=1:6
f(i,j)=x(1,j)*x(1,j)+x(2,j)*x(2,j)+x(3,j)*x(3,j)+Rp*Rp+Rb*Rb+2*(R(1,1)*P(i,
1)+R(1,2)*P(i,2))*(x(1,j)-B(i,1))+2*(R(2,1)*P(i,1)+R(2,2)*P(i,2))*(x(2,j)-
B(i,2))+2*(R(3,1)*P(i,1)+R(3,2)*P(i,2))*x(3,j)-
2*(x(1,j)*B(i,1)+x(2,j)*B(i,2))-L(i,j)*L(i,j);
J(i,1)=[2*x(1,j)+2*(R(1,1)*P(i,1)+R(1,2)*P(i,2))-2*B(i,1)];
J(i,2)=[2*x(2,j)+2*(R(2,1)*P(i,1)+R(2,2)*P(i,2))-2*B(i,2)];
```

```
J(i,3)=[2*x(3,j)+2*(R(3,1)*P(i,1)+R(3,2)*P(i,2))];
J(i,4)=[2*(x(1,j)-B(i,1))*(-sin(x(4,j))*cos(x(5,j))*P(i,1)+(-
sin(x(4,j))*sin(x(5,j))*sin(x(6,j))-
cos(x(4,j))*cos(x(6,j)))*P(i,2))+2*(x(2,j)-
B(i,2))*(cos(x(4,j))*cos(x(5,j))*P(i,1)+(cos(x(4,j))*sin(x(5,j))*sin(x(6,j)
)-sin(x(4,j))*cos(x(6,j)))*P(i,2))];
J(i,5)=[2*(x(1,j)-B(i,1))*(-
cos(x(4,j))*sin(x(5,j))*P(i,1)+cos(x(4,j))*cos(x(5,j))*sin(x(6,j))*P(i,2))+
2*(x(2,j)-B(i,2))*(-
sin(x(4,j))*sin(x(5,j))*P(i,1)+sin(x(4,j))*cos(x(5,j))*sin(x(6,j))*P(i,2))+
2*x(3,j)*(-cos(x(5,j))*P(i,1)-sin(x(5,j))*sin(x(6,j))*P(i,2))];
J(i,6)=[2*(x(1,j)-
B(i,1))*(cos(x(4,j))*sin(x(5,j))*cos(x(6,j))+sin(x(4,j))*sin(x(6,j)))*P(i,2
)+2*(x(2,j)-B(i,2))*(sin(x(4,j))*sin(x(5,j))*cos(x(6,j))-
cos(x(4,j))*sin(x(6,j)))*P(i,2)+2*x(3,j)*cos(x(5,j))*cos(x(6,j))*P(i,2)];
end
diff=inv(J);
x(:,j)=x(:,j)-diff*f(:,j);
for i=1:6
f(i,j)=x(1,j)*x(1,j)+x(2,j)*x(2,j)+x(3,j)*x(3,j)+Rp*Rp+Rb*Rb+2*(R(1,1)*P(i,
1)+R(1,2)*P(i,2))*(x(1,j)-B(i,1))+2*(R(2,1)*P(i,1)+R(2,2)*P(i,2))*(x(2,j)-
B(i,2))+2*(R(3,1)*P(i,1)+R(3,2)*P(i,2))*x(3,j)-
2*(x(1,j)*B(i,1)+x(2,j)*B(i,2))-L(i,j)*L(i,j);
end
ind=0;
for k=1:6
if (abs(f(k,j))<err)

ind=ind+1;
end
end
end
x(:,j+1)=x(:,j);
end
x(:,nb_echant+1)=[];
fprintf('\n\n');
fprintf(' deplacement\n\n');
fprintf('translation \n');
fprintf('\t along x : %g \n',x(1,nb_echant)-x(1,1));
fprintf('\t along y : %g \n',x(2,nb_echant)-x(2,1));
fprintf('\t along z : %g \n',x(3,nb_echant)-x(3,1));
fprintf('\n');
fprintf('rotation \n');
fprintf('\t alpha : %g \n',x(4,nb_echant)-x(4,1));
fprintf('\t beta : %g \n',x(5,nb_echant)-x(5,1));
fprintf('\t gama : %g \n',x(6,nb_echant)-x(6,1));
fprintf('\n');
% calcualtion of the centre of rotation
% Calcul des vitesses
for t=1:(nb_echant-1)
dt(t)=temps(t+1)-temps(t);
end
for j=1:(nb_echant-1)
for i=1:6
v(i,j)=(x(i,j+1)-x(i,j))/dt(j);
end
end
% Matrices
time=0;
```

```
ind=0;
pos(1,:)=x(1,:);
pos(2,:)=x(2,:);
pos(3,:)=x(3,:);
for j=1:(nb_echant-1)
omeg=[v(6,j); v(5,j); v(4,j)];
vit=[v(1,j); v(2,j); v(3,j)];
omega=sqrt(v(4,j)*v(4,j)+v(5,j)*v(5,j)+v(6,j)*v(6,j));
vitesse=sqrt(v(1,j)*v(1,j)+v(2,j)*v(2,j)+v(3,j)*v(3,j));
if (omega~=0 & vitesse~=0)
time=time+1;
ind=ind+1;
h=vitesse/omega;
p(1)=omeg(2)*vit(3)-omeg(3)*vit(2);
p(2)=omeg(3)*vit(1)-omeg(1)*vit(3);
p(3)=omeg(1)*vit(2)-omeg(2)*vit(1);
h=h/sqrt(p(1)*p(1)+p(2)*p(2)+p(3)*p(3));
r(:,ind)=h*p(:);
if (isnan(r(1,ind)) | isnan(r(2,ind)) | isnan(r(3,ind)) | isinf(r(1,ind)) |
isinf(r(2,ind)) | isinf(r(3,ind)) )
ind=ind-1;
else
temps2(ind)=temps(time);
end
c(:,ind)=pos(:,time)+r(:,ind);
end
end
r=c;
% Recording of the results
a=2;
fprintf('\n\n');
while (a~=1)
disp('entrer le nom du repertoire');
nom = input('','s');
a=mkdir(nom);
if (a~=1)
disp('ce repertoire existe deja');
end
end
L=L';
long=[temps,L];
noml=[nom,'\','L_',nom,'.xls'];
save(noml, 'long','-ASCII','-TABS')
x=x';
resultat=[temps,x];
nomdep=[nom,'\','deplmt_',nom,'.xls'];
save(nomdep, 'resultat','-ASCII','-TABS')
r=r';
nomrot=[nom,'\','centre_',nom,'.xls'];
save(nomrot, 'r','-ASCII','-TABS')
```

Appendix E

Matlab program to find the Centre of Rotation (C.o.R)

```
clear all;
load('fkhal5.mat');
a=size(z);n=1;kl=0;
for h=1:3:a(1,1)*5/5
    if beta(h)>0.25
        kl=kl+1;
        X(kl)=x(h);
        Z(kl)=z(h);
        Y(kl)=y(h);
        B(kl)=beta(h);
        A(kl)=alpha(h);
    end
end
a=size(Z);
for h=1:a(1,2)-1
    n=n+1;
    if (cos(B(n))*sin(B(n-1))-sin(B(n))*cos(B(n-1)))~=0
    m1(h)=tan(B(n-1));
    m2(h)=tan(B(n));
    pb(h)=B(n)*180/pi;
    r2(h)=(sin(B(n-1))*(X(n)-X(n-1))+cos(B(n-1))*(Z(n-1)-
Z(n)))/(cos(B(n))*sin(B(n-1))-sin(B(n))*cos(B(n-1)));
    r1(h)=(Z(n-1)-Z(n)+r2(h)*sin(B(n)))/sin(B(n-1));
    r=mean(r1);

    end
end
n=1;
for h=1:a(1,2)-1
    n=n+1;
    if (cos(B(n))*sin(B(n-1))-sin(B(n))*cos(B(n-1)))~=0

    xc(h)=X(n-1)-r*cos(B(n-1));
    zc(h)=Z(n-1)-r*sin(B(n-1));
    yc(h)=Y(n-1)-r*sin(A(n-1));
    end
end

plot3(X*1000,Y*1000,Z*1000,'r*');hold;plot3(xc*1000,yc*1000,zc*1000,'+');gr
id;hold off;
title('3d view');
xlabel('X (mm)');ylabel('Y (mm)');zlabel('Z (mm)');
legend('SP motion','C.O.R');
figure;
subplot(1,2,1);
plot(X*1000,Y*1000,'r*');hold;plot(xc*1000,yc*1000,'+');grid;hold off;
title('X-Y view');xlabel('X (mm)');ylabel('Y (mm)');
legend('SP motion','C.O.R');
subplot(1,2,2);
plot(X*1000,Z*1000,'r*');hold;plot(xc*1000,zc*1000,'+');grid;hold off;
title('X-Z view');xlabel('X (mm)');ylabel('Z (mm)');
legend('SP motion','C.O.R');
```

```
figure;
plot(pb,xc*1000);grid;xlabel('flexion   angle   (degree)');ylabel('C.O.R   X
(mm)');
figure;
plot(pb,zc*1000);grid;xlabel('flexion   angle   (degree)');ylabel('C.O.R   Z
(mm)');
figure;
plot(pb,yc*1000);grid;xlabel('flexion   angle   (degree)');ylabel('C.O.R   Y
(mm)');
X=X'*1000;
Y=Y'*1000;
Z=Z'*1000;
xc=xc'*1000;
yc=yc'*1000;
zc=zc'*1000;
pb=pb';
DAT_sp=[X Y Z];
DAT_cor=[xc yc zc pb];
save('kha_l5.mat','DAT_sp','DAT_cor');
```

The Matlab code for position error simulation

```
clear all;
j=1;
Rp=75;
Rb=150;
tetaB=pi/8;
tetaP=9*pi/16;
for i=0:2
    gama(2*i+1)=(pi/3)*(2*i+1)-tetaB/2;
    lambda(2*i+1)=(pi/3)*(2*i+1)-tetaP/2;
end
for i=1:3
    gama(2*i)=gama(2*i-1)+tetaB;
    lambda(2*i)=lambda(2*i-1)+tetaP;
end
for i=1:6
    P(i,:)=Rp*[cos(lambda(i)) sin(lambda(i)) 0];
    B(i,:)=Rb*[cos(gama(i)) sin(gama(i)) 0];
end

for h=1:1:10
x(:,1)=[0;0;76.7;0;0;h/10];
          R=[cos(x(4,j))*cos(x(5,j)) cos(x(4,j))*sin(x(5,j))*sin(x(6,j))-
sin(x(4,j))*cos(x(6,j))
cos(x(4,j))*sin(x(5,j))*cos(x(6,j))+sin(x(4,j))*sin(x(6,j));
          sin(x(4,j))*cos(x(5,j))
sin(x(4,j))*sin(x(5,j))*sin(x(6,j))+cos(x(4,j))*cos(x(6,j))
sin(x(4,j))*sin(x(5,j))*cos(x(6,j))-cos(x(4,j))*sin(x(6,j));
          -sin(x(5,j))            cos(x(5,j))*sin(x(6,j))
cos(x(5,j))*cos(x(6,j))];
       x_t=[x(1,1) x(2,1) x(3,1)];
for i=1:6
    S(i,:)=-B(i,:)+x_t+(R*(P(i,:)'))';
    L(i,h)=sqrt((S(i,1)^2)+(S(i,2)^2)+(S(i,3)^2));
```

```
end
POSx(h)=(h/10)*180/pi;
end
save('Skin_X_az_L.mat','POSx','L');
```

The Matlab code for velocity error simulation

```
clear all;
j=1;
Rp=75;
Rb=150;
tetaB=pi/8;
tetaP=9*pi/16;
t=0.0156;
for i=0:2
    gama(2*i+1)=(pi/3)*(2*i+1)-tetaB/2;
    lambda(2*i+1)=(pi/3)*(2*i+1)-tetaP/2;
end
for i=1:3
    gama(2*i)=gama(2*i-1)+tetaB;
    lambda(2*i)=lambda(2*i-1)+tetaP;
end
for i=1:6
    P(i,:)=Rp*[cos(lambda(i)) sin(lambda(i)) 0];
    B(i,:)=Rb*[cos(gama(i)) sin(gama(i)) 0];
end

for h=1:1:10

x(:,1)=[0;0;76.7;0;0;h/10];
          R=[cos(x(4,j))*cos(x(5,j)) cos(x(4,j))*sin(x(5,j))*sin(x(6,j))-
sin(x(4,j))*cos(x(6,j))
cos(x(4,j))*sin(x(5,j))*cos(x(6,j))+sin(x(4,j))*sin(x(6,j));
          sin(x(4,j))*cos(x(5,j))
sin(x(4,j))*sin(x(5,j))*sin(x(6,j))+cos(x(4,j))*cos(x(6,j))
sin(x(4,j))*sin(x(5,j))*cos(x(6,j))-cos(x(4,j))*sin(x(6,j));
          -sin(x(5,j))            cos(x(5,j))*sin(x(6,j))
cos(x(5,j))*cos(x(6,j))];
       x_t=[x(1,1) x(2,1) x(3,1)];
for i=1:6
    S(i,:)=-B(i,:)+x_t+(R*(P(i,:)'))';
    L(i,h)=sqrt((S(i,1)^2)+(S(i,2)^2)+(S(i,3)^2));
end
POSx(h)=(h/10)*180/pi;
end
k=1;
for h=1:1:9
   k=k+1;
   VELx(h)=(POSx(k)-POSx(h))/(1000*t);
   for i=1:6
       L_dot(i,h)=(L(i,k)-L(i,h))/(1000*t);
   end
end
save('vel_X_az_L.mat','VELx','L_dot');
```

Appendix F

Data

To validate or study we ran the test several times in the last stage and 3 different cases were repeated 5 times for the right and left hand to compare the kinematics of the shoulder for different elbow joints. In total this came to 30 times.

In this part we consider our first case, for which we had already used our Matlab program to transfer the results to 3 displacements and 3 rotations for the x, y, z axes.

COR results - Case: 1 – hand: left – Iteration: 1

X(cor)	Y(cor)	Z(cor)
-167.5808993	-11.21139781	85.58646264
-166.5550039	-11.17142087	84.32406834
-165.8893546	-11.15773591	83.89136559
-165.2545594	-10.85131542	83.60885959
-164.9441193	-10.90998281	83.85890577
-164.6308947	-10.67973437	83.91521405
-164.620625	-11.03869965	84.57088984
-164.0012153	-10.37861825	84.0727719
-163.8982275	-10.54286692	84.5782403
-163.569975	-10.29904763	84.59340904
-163.4153939	-10.28535658	84.93739384
-163.3954319	-10.29484412	85.54746158
-163.1863505	-10.15500262	85.68449892
-163.1551152	-10.1477234	86.2178257
-162.9374916	-10.10452584	86.58774751
-162.7788799	-10.02485848	87.10975912
-162.4262784	-9.889164733	87.3017862
-162.3379976	-9.845687121	87.9206408
-162.17805	-9.821928764	88.61999917
-161.9906727	-9.700715853	89.15665568
-161.4503876	-9.441922669	89.25255557
-161.3173988	-9.390197014	90.0289597
-160.9226735	-9.171979331	90.3517541
-160.496035	-8.942715367	90.68746833

-160.9782463	-9.142393524	91.05847339
-160.1841003	-8.636130705	91.07160837
-160.0161317	-8.706498376	91.87140535
-160.0401397	-8.639833229	92.04791375
-157.6606256	-8.174604562	93.43376092
-155.2545767	-7.092301699	94.04371213
-154.7236175	-6.743258562	95.45997349

COR results - Case results: 1 – hand: left – Iteration: 2

X(cor)	Y(cor)	Z(cor)
-163.1301739	-10.31486	86.27919985
-162.0673535	-9.94337771	85.15677578
-161.7210478	-10.2642038	84.77639678
-161.085054	-9.87788781	84.54551499
-160.5378025	-9.74589361	84.09375868
-160.110873	-9.40726829	84.51158066
-160.3814985	-10.2813296	85.78206272
-159.2465958	-8.88702251	84.47779955
-159.2563527	-9.33776418	85.23889024
-158.8869177	-8.97416522	84.89257475
-158.7992198	-9.07990428	85.20807315
-158.6978574	-9.00194141	85.46304355
-158.6324673	-8.9594096	85.7159242
-158.6180874	-8.85563883	86.11072326
-158.7008055	-8.96715374	86.72232969
-158.6333389	-8.85211685	87.09806882
-158.596297	-8.85164712	87.64787817
-158.734618	-8.94791138	88.45985736
-158.898637	-9.10366055	89.48520567
-158.2749575	-8.75501426	88.9675019
-158.415684	-8.82774592	89.96679908
-158.2700193	-8.87629913	90.51966835
-157.8326245	-8.5973834	90.71678814
-156.9825538	-8.08459335	90.30173278
-157.663648	-8.45385913	92.13008811
-157.5810528	-8.43483605	92.82398048
-156.9673118	-8.25895208	92.99129889
-156.4640146	-7.87888056	93.26139177
-156.3641515	-7.72653728	94.26024444
-155.2545767	-7.0923017	94.04371213
-154.7236175	-6.74325856	95.45997349

COR results - Case results: 1 – hand: left – Iteration: 3

X (cor)	Y(c.o.r)	Z(cor)
-164.1765912	-11.88790568	84.38129234
-163.6459303	-11.37507457	83.58958932
-163.2896121	-11.22523959	83.47134897
-162.8223132	-10.89561677	83.13641211
-162.8206533	-10.66544602	83.35398855
-162.7949202	-10.57137558	83.36084579
-162.9234806	-10.93352879	84.00454114
-162.4917511	-10.44964658	83.59626275
-162.256788	-10.26590741	83.80060406
-162.0998809	-10.25972288	84.18642424
-161.8912133	-10.18853167	84.47566079
-162.0154835	-10.40152493	85.55095826
-161.6372201	-9.863762032	85.33459806
-161.643738	-10.23446327	86.13650728
-161.2389935	-9.977195623	86.20908721
-160.9856383	-9.759777285	86.45687833
-160.3916415	-9.549100877	86.33882281
-160.4336465	-9.717346062	87.49781622
-159.564058	-9.123140799	87.20058845
-159.9058723	-9.325768355	88.74601436
-159.0063328	-8.92565058	88.27792472
-159.247854	-9.140823962	89.66732696
-158.2505951	-8.363914328	88.87670869
-158.5770864	-8.380204145	90.10245017
-158.677977	-8.350425195	90.64260731
-158.1120801	-7.867592322	91.07268413
-157.0935712	-7.468840351	90.80999435

Cor results - Case results: 1 – hand: left – Iteration: 4

X(cor)	Y(cor)	Z(cor))
-168.0219036	-11.88486547	86.34301678
-166.7075437	-11.98881521	84.72404528
-165.7697405	-11.57618617	83.724431
-165.136267	-11.29971543	83.37494142
-164.7722169	-11.65039584	83.69077981
-164.3168654	-11.33318582	83.5228617
-164.4460512	-11.767328	84.50592208
-163.5419249	-10.78508047	83.14792845
-163.8477286	-11.645333	84.18433485
-163.0307029	-10.55710155	83.08497046
-163.4982828	-11.31237181	84.58013927

-163.0472761	-10.66192723	84.24001643
-163.3502598	-11.10279392	85.29353262
-162.5902095	-10.28132485	84.32023639
-163.3787249	-11.09057349	86.54869399
-162.4360668	-10.41649579	85.65537963
-162.7375284	-10.89298649	86.92638028
-161.5678408	-9.901307789	85.69808162
-162.3434289	-10.63220486	88.10307049
-161.1106124	-9.694812988	86.87780871
-161.4804188	-9.883657324	88.2587127
-161.2133439	-9.838596789	88.7829489
-161.3380254	-10.00081527	89.91989313
-160.6691654	-9.612150889	89.73515775
-160.8283284	-9.729420409	90.9027824
-159.9461082	-9.01878712	90.85216063
-159.9685306	-9.111327026	91.98207301
-158.8748313	-8.544415133	91.69312835
-158.9570997	-8.622671849	92.60727739

COR results - Case results: 1 – hand: left – Iteration: 5

X(cor))	Y(cor)	Z(cor))
-167.9366	-12.4268	86.94731
-166.3364	-12.5834	84.99711
-165.5322	-12.5834	84.8077
-164.8495	-12.1471	84.53316
-164.699	-12.2554	85.1584
-164.428	-11.8439	85.04608
-164.3558	-12.1041	85.15639
-164.0948	-11.6888	85.18854
-163.8521	-11.3788	85.46841
-163.9207	-11.7607	86.7255
-163.138	-10.8604	86.10839
-163.654	-11.6517	88.00642
-162.5297	-10.812	86.86366
-163.3833	-11.4643	89.21782
-161.8443	-10.3189	87.52572
-162.5881	-10.9831	90.08988
-161.1737	-9.82358	88.84132
-162.1965	-10.4834	91.17893
-161.2072	-9.83548	90.40823
-162.2846	-10.4778	93.23222
-160.2749	-9.24353	91.33009

-160.3894	-9.19348	92.86841
-159.6256	-8.77496	92.6262
-159.5992	-8.7395	93.86527

X(COR) results – average left hand – Case 1

X(cor)	X(cor)2	X(cor)3	X(cor)4	X(cor)5	x(cor)avg
-174.6392	-163.13017	-164.17659	-168.0219	-167.93662	-167.5809
-174.0178	-162.06735	-163.64593	-166.70754	-166.33641	-166.555
-173.1341	-161.72105	-163.28961	-165.76974	-165.53224	-165.88935
-172.3796	-161.08505	-162.82231	-165.13627	-164.84955	-165.25456
-171.8909	-160.5378	-162.82065	-164.77222	-164.69902	-164.94412
-171.5038	-160.11087	-162.79492	-164.31687	-164.42801	-164.63089
-170.9963	-160.3815	-162.92348	-164.44605	-164.3558	-164.62062
-170.631	-159.2466	-162.49175	-163.54192	-164.0948	-164.00122
-170.2782	-159.25635	-162.25679	-163.84773	-163.8521	-163.89823
-169.9117	-158.88692	-162.09988	-163.0307	-163.92068	-163.56998
-169.7503	-158.79922	-161.89121	-163.49828	-163.13797	-163.41539
-169.5625	-158.69786	-162.01548	-163.04728	-163.65401	-163.39543
-169.7821	-158.63247	-161.63722	-163.35026	-162.52972	-163.18635
-169.5403	-158.61809	-161.64374	-162.59021	-163.38325	-163.15512
-169.5247	-158.70081	-161.23899	-163.37872	-161.84427	-162.93749
-169.2513	-158.63334	-160.98564	-162.43607	-162.58807	-162.77888
-169.2322	-158.5963	-160.39164	-162.73753	-161.17371	-162.42628
-168.7574	-158.73462	-160.43365	-161.56784	-162.19645	-162.338
-168.8769	-158.89864	-159.56406	-162.34343	-161.2072	-162.17805
-168.3774	-158.27496	-159.90587	-161.11061	-162.28456	-161.99067
-168.0746	-158.41568	-159.00633	-161.48042	-160.27487	-161.45039
-167.4663	-158.27002	-159.24785	-161.21334	-160.38943	-161.3174
-167.5665	-157.83262	-158.2506	-161.33803	-159.62562	-160.92267
-166.6522	-156.98255	-158.57709	-160.66917	-159.5992	-160.49603
-166.743	-157.66365	-158.67798	-160.82833		-160.97825
-165.0972	-157.58105	-158.11208	-159.94611		-160.1841
-166.0351	-156.96731	-157.09357	-159.96853		-160.01613
-164.7816	-156.46401		-158.87483		-160.04014
	-156.36415		-158.9571		-157.66063
	-155.25458				-155.25458
	-154.72362				-154.72362

Y(COR) results – average left hand – Case 1

Y (cor)	Y (cor) (2	Y (cor) 3	Y (cor)4	Y (cor)5	y(cor)avg
-9.542593	-10.31486	-11.887906	-11.884865	-12.426765	-11.211398
-9.966479	-9.9433777	-11.375075	-11.988815	-12.583358	-11.171421
-10.13968	-10.264204	-11.22524	-11.576186	-12.583369	-11.157736
-10.03621	-9.8778878	-10.895617	-11.299715	-12.147147	-10.851315
-10.23273	-9.7458936	-10.665446	-11.650396	-12.255444	-10.909983
-10.2429	-9.4072683	-10.571376	-11.333186	-11.843945	-10.679734
-10.10718	-10.28133	-10.933529	-11.767328	-12.104132	-11.0387
-10.08256	-8.8870225	-10.449647	-10.78508	-11.688786	-10.378618

-10.08652	-9.3377642	-10.265907	-11.645333	-11.378809	-10.542867
-9.943587	-8.9741652	-10.259723	-10.557102	-11.760661	-10.299048
-9.985596	-9.0799043	-10.188532	-11.312372	-10.860379	-10.285357
-9.757171	-9.0019414	-10.401525	-10.661927	-11.651656	-10.294844
-10.03708	-8.9594096	-9.863762	-11.102794	-10.811966	-10.155003
-9.902902	-8.8556388	-10.234463	-10.281325	-11.464288	-10.147723
-10.16881	-8.9671537	-9.9771956	-11.090573	-10.318898	-10.104526
-10.11277	-8.8521168	-9.7597773	-10.416496	-10.983128	-10.024858
-10.32851	-8.8516471	-9.5491009	-10.892986	-9.8235773	-9.8891647
-10.17849	-8.9479114	-9.7173461	-9.9013078	-10.483383	-9.8456871
-10.41516	-9.1036605	-9.1231408	-10.632205	-9.8354768	-9.8219288
-10.2502	-8.7550143	-9.3257684	-9.694813	-10.477782	-9.7007159
-10.32903	-8.8277459	-8.9256506	-9.8836573	-9.2435268	-9.4419227
-9.90178	-8.8762991	-9.140824	-9.8385968	-9.1934847	-9.390197
-10.12282	-8.5973834	-8.3639143	-10.000815	-8.7749613	-9.1719793
-9.897132	-8.0845934	-8.3802041	-9.6121509	-8.7394965	-8.9427154
-10.03587	-8.4538591	-8.3504252	-9.7294204		-9.1423935
-9.223307	-8.434836	-7.8675923	-9.0187871		-8.6361307
-9.986874	-8.2589521	-7.4688404	-9.111327		-8.7064984
-9.496204	-7.8788806		-8.5444151		-8.6398332
	-7.7265373		-8.6226718		-8.1746046
	-7.0923017				-7.0923017
	-6.7432586				-6.7432586

Y(COR) results – average left hand – Case 1

Z (cor)	Z (cor)	Z (cor)	Z (cor)	Z (cor)	z(cor)avg
83.98149	86.2792	84.381292	86.343017	86.947311	85.5864626
83.15282	85.156776	83.589589	84.724045	84.997114	84.3240683
82.67695	84.776397	83.471349	83.724431	84.807703	83.8913656
82.45427	84.545515	83.136412	83.374941	84.533155	83.6088596
82.9976	84.093759	83.353989	83.69078	85.158398	83.8589058
83.1347	84.511581	83.360846	83.522862	85.046077	83.9152141
83.40554	85.782063	84.004541	84.505922	85.156386	84.5708898
83.95333	84.4778	83.596263	83.147928	85.188541	84.0727719
84.19896	85.23889	83.800604	84.184335	85.468411	84.5782403
84.07758	84.892575	84.186424	83.08497	86.725496	84.593409
84.31471	85.208073	84.475661	84.580139	86.108385	84.9373938
84.47687	85.463044	85.550958	84.240016	88.00642	85.5474616
85.21478	85.715924	85.334598	85.293533	86.86366	85.6844989
85.30384	86.110723	86.136507	84.320236	89.217823	86.2178257
85.93291	86.72233	86.209087	86.548694	87.525718	86.5877475
86.24859	87.098069	86.456878	85.65538	90.089882	87.1097591
86.75453	87.647878	86.338823	86.92638	88.84132	87.3017862
86.76852	88.459857	87.497816	85.698082	91.178929	87.9206408

87.9029	89.485206	87.200588	88.10307	90.408228	88.6199992
87.95974	88.967502	88.746014	86.877809	93.232216	89.1566557
88.42925	89.966799	88.277925	88.258713	91.330088	89.2525556
88.30644	90.519668	89.667327	88.782949	92.86841	90.0289597
89.61918	90.716788	88.876709	89.919893	92.626197	90.3517541
89.43273	90.301733	90.10245	89.735158	93.865272	90.6874683
90.55842	92.130088	90.642607	90.902782		91.0584734
89.53761	92.82398	91.072684	90.852161		91.0716084
91.70226	92.991299	90.809994	91.982073		91.8714054
91.18922	93.261392		91.693128		92.0479138
	94.260244		92.607277		93.4337609
	94.043712				94.0437121
	95.459973				95.4599735

SP results - Case results: 1 – hand: left – Iteration: 1

X (sp)	Y(sp)	Z(sp)
-23.04	-5.82814	123.7774
-23.6442	-6.08302	127.3548
-24.1163	-6.02377	131.2539
-24.9535	-5.82003	135.6668
-26.123	-5.91047	140.5974
-27.6728	-6.00557	145.4136
-29.2445	-5.75533	150.2819
-31.152	-5.45057	155.449
-33.3648	-4.94398	160.4929
-35.481	-4.23159	164.6655
-37.7208	-3.75939	168.7791
-39.843	-3.07848	172.4477
-42.224	-2.98598	176.2915
-44.3914	-2.4412	179.6637
-46.7851	-2.59083	183.4062
-49.2687	-2.08698	187.096
-52.1391	-2.29592	190.943
-55.0352	-1.86454	194.6262
-58.582	-1.93022	199.2629
-62.3044	-1.39276	203.3485
-66.2955	-0.99084	207.6225
-70.7506	-0.20256	211.6438
-75.7868	-0.13746	216.6724
-80.8709	0.461142	220.6105
-86.1194	0.484814	224.9677
-91.4157	1.402905	227.8744

-97.1879	1.098791	232.5074
-102.384	1.466442	234.9688
-107.961	2.066406	237.8271

SP results - Case results: 1 – hand: left – Iteration: 2

X (sp)	Y(sp)	Z(sp)
-19.1201	-0.29082	123.2493
-19.2599	0.175141	126.5299
-20.1839	0.003112	130.3058
-20.9863	0.440046	134.3254
-22.1715	0.707733	138.5039
-23.4238	1.406066	143.0123
-25.4733	0.850639	148.2758
-27.003	2.880369	152.4286
-29.182	2.771932	157.2553
-31.1169	3.530813	160.9222
-33.1392	3.733556	164.6766
-35.0196	4.018694	167.9821
-36.9308	4.362915	171.1231
-39.0054	4.888593	174.4198
-41.2984	4.969951	177.9493
-43.7306	5.25374	181.454
-46.5596	5.423214	185.3897
-49.8255	5.782613	189.6749
-53.385	5.679484	194.2352
-57.0964	6.208579	197.9106
-61.167	6.442178	202.4318
-65.5636	6.455443	206.7574
-69.844	7.050472	210.5654
-74.4104	7.764196	213.9445
-79.4186	7.629481	218.5555
-84.0687	7.550435	222.0587
-88.9202	7.934743	225.1854
-93.8864	8.209435	228.1307
-99.0117	8.539302	231.4331
-103.661	9.086728	233.4849
-112.613	9.080692	238.0516
-116.945	9.677591	239.0277

SP results - Case results: 1 – hand: left – Iteration: 3

X (sp)	Y(sp)	Z(sp)
-17.5777	-1.18298	126.81
-18.6578	-0.75667	131.2326
-19.9258	-0.57767	135.7995
-21.4079	0.065983	140.5243
-23.52	0.68398	145.6978
-25.9572	1.375365	150.9394
-28.5873	1.826939	156.4283
-31.3759	2.84475	161.6991
-34.5075	3.692053	167.2963
-37.9941	4.292766	173.0075
-41.2817	4.829278	177.9892
-44.9354	5.14882	183.4472
-48.7598	6.00534	188.0483
-52.6805	5.977607	192.9936
-56.387	6.426331	197.1031
-60.2919	6.956373	201.1399
-64.4961	7.358203	205.0631
-68.9114	7.657252	209.6252
-73.0749	8.363414	212.9426
-78.0208	8.444742	217.5337
-82.4173	8.855413	220.2837
-87.1537	8.707967	224.1807
-91.5179	9.672516	226.1289
-96.0337	9.548855	229.3136
-100.247	9.541291	231.6294
-104.497	9.879425	233.9603
-108.399	10.13836	235.4482
-112.608	10.32198	237.9923

SP results - Case results: 1 – hand: left – Iteration: 4

X (sp)	Y(sp)	Z(sp)
-20.6327	-2.35689	125.3414
-20.9481	-2.03005	129.4305
-21.8353	-1.12365	133.997
-23.1461	-0.53686	138.902
-24.7613	-0.49768	144.0348
-26.5791	0.017746	148.8893
-29.135	-0.16992	154.7582
-31.3771	1.380938	159.1541

-34.1727	1.037428	164.3645
-36.6522	2.503491	168.3665
-39.669	2.215876	173.5226
-42.1692	3.381799	177.1538
-45.1698	3.337249	181.6151
-48.0038	4.58781	184.8908
-51.4493	4.323608	190.0681
-54.5594	5.257725	193.3916
-58.351	5.031531	198.0476
-62.1869	6.419184	201.3177
-66.9609	5.766455	207.0427
-71.2113	6.917438	210.0142
-75.6248	6.916731	214.2479
-80.6011	7.08538	218.1898
-85.7151	6.931151	222.3043
-90.5473	7.421984	225.1138
-95.6385	7.366372	228.7242
-100.428	7.958814	231.2161
-105.449	7.739426	234.3622
-109.986	8.296278	236.1036
-114.898	8.257802	238.5635
-119.595	8.56716	240.6369

SP results - Case results: 1 – hand: left – Iteration: 5

X (sp)	Y(sp)	Z(sp)
-20.961	-6.76775	127.1392
-21.6643	-6.18245	132.822
-23.1364	-5.42295	139.0355
-25.001	-4.32945	145.0279
-27.6637	-3.64007	151.7809
-30.5174	-2.47208	157.7453
-33.8252	-1.81109	163.7629
-37.1652	-0.61699	169.4862
-40.8882	0.402733	175.4523
-45.0766	0.626657	182.0844
-48.8034	2.348101	186.8299
-53.7503	1.94841	193.5451
-58.3286	3.395926	198.0363
-63.5359	3.105485	204.3166
-68.1443	4.425784	207.682
-73.9243	3.920386	214.009
-78.7932	5.34081	217.0235

-84.7351	4.532844	222.3924
-90.0704	5.432692	225.1553
-96.8203	4.684618	230.8246
-101.949	5.61603	232.0971
-107.528	5.777607	235.777
-112.912	6.2501	237.6608
-118.313	6.130505	240.5372
-123.084	6.280857	242.4468

X(SP) results – average left hand – Case 1

X (sp)	X (sp)2	X (sp)3	X (sp)4	X (sp)5	x(sp)avg
-23.04	-19.1201	-17.5777	-20.6327	-20.961	-20.266303
-23.6442	-19.2599	-18.6578	-20.9481	-21.6643	-20.834876
-24.1163	-20.1839	-19.9258	-21.8353	-23.1364	-21.839543
-24.9535	-20.9863	-21.4079	-23.1461	-25.001	-23.098966
-26.123	-22.1715	-23.52	-24.7613	-27.6637	-24.847896
-27.6728	-23.4238	-25.9572	-26.5791	-30.5174	-26.83004
-29.2445	-25.4733	-28.5873	-29.135	-33.8252	-29.253041
-31.152	-27.003	-31.3759	-31.3771	-37.1652	-31.614636
-33.3648	-29.182	-34.5075	-34.1727	-40.8882	-34.423043
-35.481	-31.1169	-37.9941	-36.6522	-45.0766	-37.264164
-37.7208	-33.1392	-41.2817	-39.669	-48.8034	-40.1228
-39.843	-35.0196	-44.9354	-42.1692	-53.7503	-43.14352
-42.224	-36.9308	-48.7598	-45.1698	-58.3286	-46.282574
-44.3914	-39.0054	-52.6805	-48.0038	-63.5359	-49.523411
-46.7851	-41.2984	-56.387	-51.4493	-68.1443	-52.812824
-49.2687	-43.7306	-60.2919	-54.5594	-73.9243	-56.354958
-52.1391	-46.5596	-64.4961	-58.351	-78.7932	-60.067801
-55.0352	-49.8255	-68.9114	-62.1869	-84.7351	-64.138824
-58.582	-53.385	-73.0749	-66.9609	-90.0704	-68.414628
-62.3044	-57.0964	-78.0208	-71.2113	-96.8203	-73.090648
-66.2955	-61.167	-82.4173	-75.6248	-101.949	-77.490766
-70.7506	-65.5636	-87.1537	-80.6011	-107.528	-82.319354
-75.7868	-69.844	-91.5179	-85.7151	-112.912	-87.155118
-80.8709	-74.4104	-96.0337	-90.5473	-118.313	-92.035008
-86.1194	-79.4186	-100.247	-95.6385	-123.084	-96.901482
-91.4157	-84.0687	-104.497	-100.428		-95.102321
-97.1879	-88.9202	-108.399	-105.449		-99.988991
-102.384	-93.8864	-112.608	-109.986		-104.71624
-107.961	-99.0117		-114.898		-107.29013
	-103.661		-119.595		-111.6281
	-112.613				-112.61274
	-116.945				-116.94546

Y(SP) results – average left hand – Case 1

Y(sp)	Y(sp)2	Y(sp)3	Y(sp)4	Y(sp)5	y(sp)avg
-5.828140331	-0.29082	-1.18298	-2.35689	-6.76775	-3.2853157
-6.083017511	0.175141	-0.75667	-2.03005	-6.18245	-2.9754097
-6.023771801	0.003112	-0.57767	-1.12365	-5.42295	-2.6289867
-5.820032257	0.440046	0.065983	-0.53686	-4.32945	-2.0360629
-5.910470432	0.707733	0.68398	-0.49768	-3.64007	-1.7313003
-6.005570226	1.406066	1.375365	0.017746	-2.47208	-1.1356938
-5.755332487	0.850639	1.826939	-0.16992	-1.81109	-1.0117535
-5.450567414	2.880369	2.84475	1.380938	-0.61699	0.2076995
-4.943984388	2.771932	3.692053	1.037428	0.402733	0.5920322
-4.231591055	3.530813	4.292766	2.503491	0.626657	1.3444272
-3.759394712	3.733556	4.829278	2.215876	2.348101	1.8734833
-3.07847797	4.018694	5.14882	3.381799	1.94841	2.2838492
-2.985980096	4.362915	6.00534	3.337249	3.395926	2.8230898
-2.441204161	4.888593	5.977607	4.58781	3.105485	3.2236582
-2.590829095	4.969951	6.426331	4.323608	4.425784	3.5109689
-2.086978395	5.25374	6.956373	5.257725	3.920386	3.860249
-2.295924749	5.423214	7.358203	5.031531	5.34081	4.1715665
-1.864540855	5.782613	7.657252	6.419184	4.532844	4.5054704
-1.93022169	5.679484	8.363414	5.766455	5.432692	4.6623647
-1.392761115	6.208579	8.444742	6.917438	4.684618	4.9725232
-0.990839814	6.442178	8.855413	6.916731	5.61603	5.3679024
-0.202561478	6.455443	8.707967	7.08538	5.777607	5.5647672
-0.137463464	7.050472	9.672516	6.931151	6.2501	5.9533553
0.461142298	7.764196	9.548855	7.421984	6.130505	6.2653363
0.484814223	7.629481	9.541291	7.366372	6.280857	6.260563
1.402905308	7.550435	9.879425	7.958814		6.6978949
1.098791065	7.934743	10.13836	7.739426		6.7278303
1.466441933	8.209435	10.32198	8.296278		7.0735349
2.066406445	8.539302		8.257802		6.2878369
	9.086728		8.56716		8.8269437
	9.080692				9.080692
	9.677591				9.677591

Z(SP) results – average left hand – Case 1

Z(sp)	Z(sp)2	Z(sp)3	Z(sp)4	Z(sp)5	z(sp)avg
123.7774	123.2493	126.81	125.3414	127.1392	125.26348
127.3548	126.5299	131.2326	129.4305	132.822	129.47393
131.2539	130.3058	135.7995	133.997	139.0355	134.07836
135.6668	134.3254	140.5243	138.902	145.0279	138.8893
140.5974	138.5039	145.6978	144.0348	151.7809	144.12295
145.4136	143.0123	150.9394	148.8893	157.7453	149.19995
150.2819	148.2758	156.4283	154.7582	163.7629	154.70142
155.449	152.4286	161.6991	159.1541	169.4862	159.64341
160.4929	157.2553	167.2963	164.3645	175.4523	164.97225
164.6655	160.9222	173.0075	168.3665	182.0844	169.80922
168.7791	164.6766	177.9892	173.5226	186.8299	174.35947
172.4477	167.9821	183.4472	177.1538	193.5451	178.91516
176.2915	171.1231	188.0483	181.6151	198.0363	183.02283
179.6637	174.4198	192.9936	184.8908	204.3166	187.2569

183.4062	177.9493	197.1031	190.0681	207.682	191.24175
187.096	181.454	201.1399	193.3916	214.009	195.4181
190.943	185.3897	205.0631	198.0476	217.0235	199.29339
194.6262	189.6749	209.6252	201.3177	222.3924	203.52728
199.2629	194.2352	212.9426	207.0427	225.1553	207.72774
203.3485	197.9106	217.5337	210.0142	230.8246	211.9263
207.6225	202.4318	220.2837	214.2479	232.0971	215.33662
211.6438	206.7574	224.1807	218.1898	235.777	219.30974
216.6724	210.5654	226.1289	222.3043	237.6608	222.66637
220.6105	213.9445	229.3136	225.1138	240.5372	225.90392
224.9677	218.5555	231.6294	228.7242	242.4468	229.26474
227.8744	222.0587	233.9603	231.2161		228.77737
232.5074	225.1854	235.4482	234.3622		231.87582
234.9688	228.1307	237.9923	236.1036		234.29884
237.8271	231.4331		238.5635		235.94123
	233.4849		240.6369		237.06089
	238.0516				238.05157
	239.0277				239.02765

Average Results – Case 1 – SP and COR

	x(sp)avg	y(sp)avg	z(sp)avg	x(cor)avg	y(cor)avg	z(cor)avg
1	-20.266303	-3.2853157	125.263484	-167.5808993	-11.211398	85.5864626
2	-20.834876	-2.9754097	129.473926	-166.5550039	-11.171421	84.3240683
3	-21.839543	-2.6289867	134.078359	-165.8893546	-11.157736	83.8913656
4	-23.098966	-2.0360629	138.889301	-165.2545594	-10.851315	83.6088596
5	-24.847896	-1.7313003	144.122946	-164.9441193	-10.909983	83.8589058
6	-26.83004	-1.1356938	149.199951	-164.6308947	-10.679734	83.9152141
7	-29.253041	-1.0117535	154.701425	-164.620625	-11.0387	84.5708898
8	-31.614636	0.2076995	159.643405	-164.0012153	-10.378618	84.0727719
9	-34.423043	0.5920322	164.972254	-163.8982275	-10.542867	84.5782403
10	-37.264164	1.3444272	169.80922	-163.569975	-10.299048	84.593409
11	-40.1228	1.8734833	174.359473	-163.4153939	-10.285357	84.9373938
12	-43.14352	2.2838492	178.915163	-163.3954319	-10.294844	85.5474616
13	-46.282574	2.8230898	183.022834	-163.1863505	-10.155003	85.6844989
14	-49.523411	3.2236582	187.256898	-163.1551152	-10.147723	86.2178257
15	-52.812824	3.5109689	191.241746	-162.9374916	-10.104526	86.5877475
16	-56.354958	3.860249	195.418102	-162.7788799	-10.024858	87.1097591
17	-60.067801	4.1715665	199.293392	-162.4262784	-9.8891647	87.3017862
18	-64.138824	4.5054704	203.527283	-162.3379976	-9.8456871	87.9206408
19	-68.414628	4.6623647	207.72774	-162.17805	-9.8219288	88.6199992
20	-73.090648	4.9725232	211.926297	-161.9906727	-9.7007159	89.1566557
21	-77.490766	5.3679024	215.336623	-161.4503876	-9.4419227	89.2525556
22	-82.319354	5.5647672	219.309737	-161.3173988	-9.390197	90.0289597
23	-87.155118	5.9533553	222.666373	-160.9226735	-9.1719793	90.3517541
24	-92.035008	6.2653363	225.903921	-160.496035	-8.9427154	90.6874683
25	-96.901482	6.260563	229.264744	-160.9782463	-9.1423935	91.0584734
26	-95.102321	6.6978949	228.777372	-160.1841003	-8.6361307	91.0716084
27	-99.988991	6.7278303	231.875823	-160.0161317	-8.7064984	91.8714054

28	-104.71624	7.0735349	234.298842	-160.0401397	-8.6398332	92.0479138
29	-107.29013	6.2878369	235.941231	-157.6606256	-8.1746046	93.4337609
30	-111.6281	8.8269437	237.060886	-155.2545767	-7.0923017	94.0437121
31	-112.61274	9.080692	238.05157	-154.7236175	-6.7432586	95.4599735
32	-116.94546	9.677591	239.027654			